FATE, TRANSPORT, AND RETENTION OF VIRUSES, BACTERIA, AND NANOPARTICLES IN SATURATED POROUS MEDIA

SALINI SASIDHARAN

Master of Science (Biotechnology), Bachelor of Science (Biotechnology)

Thesis Submitted as a Requirement in Full for the Degree of Doctor of Philosophy

in the School of the Environment, Faculty of Science and Engineering

Flinders University of South Australia, Australia

14 April 2016

Supervisors: Dr Saeed Torkzaban

Prof Peter G. Cook

Dr Vadakattu V.S.R Gupta

Prof Howard Fallowfield

SUMMARY

The main objective of this thesis was to gain a fundamental understanding of the mechanisms involved in the fate, transport and retention of colloidal particles such as viruses, bacteria, and nanoparticles in saturated porous media. Laboratory scale systematic column and batch experiments were conducted by employing sand or biochar as the saturated porous media. Bacteriophages (ΦX174, PRD1, and MS2) and *Escherichia coli* were used as surrogates for pathogenic viruses and bacteria, respectively. Negatively charged carboxyl-methylated latex nanoparticles (50 and 100 nm) were employed as model-engineered nanoparticles. The effects of water solution chemistries on colloid transport were investigated; specifically, pH (5.8–7.2), ionic strength (1–60 mM), ion type (Na^+ and Ca^{2+}), temperature (4 and 20 °C), and physical factors including flow velocity (0.1–20 m d^{-1}), and solid grain surface physical (surface roughness) and chemical (metal oxides) heterogeneity. All the experiments were conducted in saturated packed columns to simulate the natural aquifer environment.

Long-term colloid deposition experiments were conducted in order to determine the solid surface area that contributed to the attachment of colloids (S_f) at various physiochemical conditions. Colloid transport in saturated porous media was described by utilising a one-dimensional form of the advection-dispersion transport model that accounts for colloid interaction with the solid-water interfaces (SWI). Results clearly indicated that colloid retention in porous media and the value of S_f increased with decreasing colloidal size, colloid input concentration, pH of the electrolyte solution, pore water velocity, increasing ionic strength, and concentration of multivalent ions in the electrolyte solution. Simulation of the observed breakthrough concentrations (BTCs) using Hydrus-1D modelling showed

I

that nanosized-colloids (nanoparticles and viruses) required a two-site kinetic model (site 1, which represents an initial delay due to the presence of highly favourable attachment sites, and site 2, which represents a sharp rise where blocking is present) to produce a good fit for the BTCs obtained from the column experiments.

This was the first study to examine the effect of temperature on virus and nanoparticle attachment in a saturated packed column transport experiment. Systematic experiments were conducted and the BTCs were fitted using the Hydrus-1D model to determine the fitted parameters. Theoretical simulations and mathematical solutions were employed to quantify the extended Derjaguin-Landau-Verwey-Overbeek (XDLVO) interaction energy between a colloid and a heterogeneous (presence of surface roughness and positive charge) collector surfaces. This study established that the increase in attachment rate coefficient (k_{att}) with an increase in temperature (4 to 20 °C) at moderate IS (10–30 mM) was a function of single-collector efficiency (η) and sticking efficiency (α), and, therefore, a function of S_f.

The removal efficiency of various plant-based biochar materials for viruses has not previously been addressed. Batch experiments conducted with various types of biochar showed negligible attachment of viruses and bacteria to the biochar surface. Transport experiments conducted using biochar-amended sand columns showed enhanced transport of viruses and enhanced deposition of bacteria. However, elimination of the fine fraction of biochar (< 60 μm) particles in biochar-amended sand columns significantly reduced the bacteria retention. This study demonstrated that biochar plays a role in microbe (bacteria) retention via straining, by alteration of pore size distribution, and not via attachment. However, the straining mechanism

does not result in virus removal due to their considerably smaller size.

This research acknowledged that the colloid retention in saturated porous media and the value of S_f is determined by the coupled physio-chemical processes that strongly depend on colloid size, temperature, solution chemistry, and system hydrodynamics. Results from the actual column experiments and theoretical simulations have clearly shown that nanoscale chemical and physical heterogeneities on both collector and colloid surface determine the XDLVO interaction energy at the interfacial scale. Therefore, modelling colloid transport through saturated porous media and quantifying the interaction energy at interfacial scale will require non-traditional approaches to account for the aforementioned factors that are not addressed by classical DLVO calculations.

IV

DECLARATION

I certify that this thesis does not incorporate without acknowledgement any material previously submitted for a degree or diploma in any university, and that to the best of my knowledge and belief it does not contain any material previously published or written by another person except where due reference is made in the text.

Name: <u>Salini Sasidharan</u>

Date: <u>14 April 2016</u>

CO-AUTHORSHIP

Salini Sasidharan is the primary author on all chapters in this thesis. Co-authors

listed on published chapters provided intellectual supervision and editorial support.

ACKNOWLEDGEMENTS

happiest and difficult times of my entire Ph.D. process, and without his love and

support, I would be lost. As my gratitude, I would love to dedicate this thesis to

him.

"Saraswathi Namastubhyam Varade Kamarupini

Vidyarambham Karishyami Siddhir Bhavatu Me Sada"

I offer the deepest respect and great admiration to divine mother the Goddess
Saraswathi, who fulfils my desires, provides excellence in my education,
nourishes my intellect, and helps me in my efforts to gain knowledge and other
noble goals.

TABLE OF CONTENT

LIST OF TABLES

LIST OF FIGURES

8

CHAPTER 1

Introduction

Process in Saturated Porous media

Chapter 1

1.1   Motivation

Seventy per cent of the Earth's surface is covered by water, and of this amount 97.5% is 'salt water' and only 2.5% is 'freshwater' (Rowell, 2006). Freshwater is defined as the water that contains less than 500 mg L^{-1} total dissolved solids (Hem, 1985). However, 68.9% of this freshwater, enclosed in ice glaciers and permanent snow cover, soil moisture, and groundwater aquifers, is considered inaccessible to humans (Gleick, 1993). Approximately 1% of the freshwater is available to humans for direct use, which is in the form of lakes, rivers, and accessible groundwater resources (Palaniappan and Gleick, 2008).

Globally, the agriculture sector consumes the largest amount of freshwater (70%) followed by industry, and domestic usage (Brown, 2000). Even though the total freshwater on the earth's surface has remained the same over centuries, the uneven distribution of water, growing population, and increased water demand have caused serious problems for the accessibility and availability of freshwater (Diop et al., 2002). Providing potable water for communities in developing nations is expensive and difficult (Earth Policy Institute, 2006). According to the Population Action International, based on the United Nations medium population projection, the rapid growth in population, resilience to climate change, the decline in agriculture production, and water scarcity would create many challenges for the existence of many countries in the world (Engelman, 1997). By 2025, 2.8 billion people in 48 countries would face severe water scarcity or stress. Forty countries out of these 48 countries are in Africa and West Asia. By 2050, about 4 billion people from 54 countries i.e., about 40% of the projected population of 9.4 billion would face water stress and scarcity (Diop et al., 2002; Simpson, 2009). Therefore, there is an urgent need for alternative sources of freshwater, and developing

economic and effective water reclamation, recycling, reuse, and preservation techniques for the survival of our future generations.

1.2   Background

Due to the increased demand for freshwater, many nations across the globe are exploring groundwater as a major freshwater source for domestic and agricultural purposes (Bhattacharya et al., 2008; Harrington and Cook, 2014). In Australia, groundwater is a major water resource, meeting more than 30% of the total water consumption and contributing to agricultural, mining and industrial development to produce national economic growth worth $34 billion a year (Simmons, 2015). However, groundwater may become contaminated with pathogenic microorganisms from contaminated water, e.g., infiltration from septic tanks, leaking sewage pipes, land manure application, industrial wastewater outlets, and managed aquifer recharge of stormwater, surface water or recycled wastewater (Schijven and Hassanizadeh, 2000).

Nanotechnology is rapidly growing and leading to the mass-scale production and widespread application of nanoparticles (NPs) (Wang et al., 2012). According to the US National Nanotechnology Initiative, particles with dimensions between 1 and 100 nm in size are classified as NPs (Petosa et al., 2012). During their production, application and disposal, the NPs inevitably enter the subsurface environment and may lead to groundwater contamination (Wiesner et al., 2006). Because of their potential toxicity, they pose a great health risk to humans, animals and ecosystems (Wang et al., 2012).

1.3   Safe Drinking Water

According to the World Health Organization (WHO), waterborne diseases are

the primary cause of diseases and death in the world (WHO, 2011). Millions of people around the globe are suffering due to insufficient access to safe drinking water. Every year 3.4 million people die (mainly young children under the age of five) by drinking contaminated water, and due to lack of sanitation (WHO, 2011). Lack of public health protection in water supply raises health concerns not only in developing countries but also in developed countries. In March 1999, outbreaks of *Salmonella Saintpaul* with 28 cases of gastroenteritis among 200 workers were reported in Queensland, Australia (Taylor et al., 2000) and a recent *Salmonella Anatum* outbreak associated with salad leaf products was thought to have originated from a faecal-contaminated irrigation water source (DHHS, 2016; Perrott, 2016). In the United States, 764 waterborne disease outbreaks related to drinking water were reported from 1971 to 2002, which resulted in 575,457 cases of illness and 79 deaths (Reynolds et al., 2008). 89 cases of the waterborne gastrointestinal disease, largely caused by *Cryptosporidium* and *Campylobacter* sps, affecting 4321 people, were reported in England and Wales during the period of 1992 to 2003 (Smith et al., 2006).

Most of the waterborne diseases are caused by contact with or consumption of water contaminated by human, animal or bird faeces or urine, containing pathogenic microorganisms, include viruses, bacteria, and protozoa (Gleick, 2002). Information on major waterborne pathogens, the diseases caused by them, host organisms, infectious dose, the major route of exposure, and modes of transmission are given in Table 1. Pathogenic viruses and bacteria are detected in wells and drinking water supplies due to the improper management of waste disposal, septic tank, wastewater treatment plants, and landfills (Zhuang and Jin, 2008). The nature of interaction of viruses and bacteria in groundwater and the subsurface

Table 1. Major waterborne pathogens

Responsible pathogen	Diseases	Reservoir	Infectious dose	Route of exposure	Mode of transmission
Bacteria					
Vibrio cholerae	Cholera	Aquatic environments, shell stocks, humans	High (10^3 to 10^8 cells)	Gastrointestinal	Waterborne
Clostridium botulinum	Botulism	Humans, fishes, cows, dogs, minks	0.001 µg toxin/kg body weight	Gastrointestinal	Water/foodborne
Salmonella typhi	Typhoid	Humans	Medium (10^3 to 10^5)	Gastrointestinal	Water/foodborne
Legionella sp.	Legionellosis	Natural environment	Very Low (1 cell)	Respiratory	Recreational water
Shigella dysenteriae	Shigellosis	Humans and primates	Very Low (< 10 cells)	Gastrointestinal	Water/foodborne
Campylobacter jejuni	Dysentery	Poultry, cattle, birds, puppies, kittens, swine	Low (< 500 cells)	Gastrointestinal	Waterborne
Escherichia coli	Dysentery	Cattle, deer, goats, sheep, humans	Low (10^1 to 10^2 cells)	Gastrointestinal	Waterborne
Viruses					
Norovirus	Dysentery	Humans, pigs, cattle, mice	Very Low (< 10 virions)	Gastrointestinal	Waterborne
Rotavirus	Dysentery	Humans and experimentally infected animals	Very Low (< 10 virions)	Gastrointestinal	Waterborne
Hepatitis A	Jaundice	Humans, Chimpanzees, non-human primates	Very Low (10 to 100 virions)	Gastrointestinal	Waterborne
Adenovirus[‡]	Pharyngoconjunctival fever	Humans	Very Low (5 to 150 virions)	Respiratory	Recreational water
Poliovirus	Poliomyelitis	Humans	Very Low (1 TO 10 $TCID_{50}$) [§]	Gastrointestinal	Waterborne
Coxsackievirus	Dysentery	Human, monkey, mouse	Low (15 to 5 $TCID_{50}$)	Gastrointestinal	Waterborne
Parasites					
Cryptosporidium	Cryptosporidiosis	Humans, animals, fishes, amphibians, reptiles	Very Low (1 to 5 oocytes)	Gastrointestinal	Water/foodborne
Giardia lamblia	Giardiasis	Humans, animals, primates, rodents, cattle	Very Low (< 10 cysts)	Gastrointestinal	Water/foodborne
Entamoeba histolytica	Amoebiasis	Humans and non-human primates	Medium (> 10^3 organisms)	Gastrointestinal	Water/foodborne

[§]$TCID_{50}$ = 50% Tissue Culture Infective Dose; [‡]DNA virus

(Department of Health and Human Services) (Centers for Disease Control and Prevention) (Public Health Agency of Canada, 2011)Massachusetts water recourse Authority, 2013)(Katz and Plotkin, 1967; Schmid-Hempel and Frank, 2007; Ward et al., 1986)

environment have a large impact on the quality of drinking water (Attinti et al., 2010).

1.4. Major Techniques for Water Recycling and Purification

Increasing water pollution, global warming, climate change, and the global water crisis have made renewable and sustainable water recycling a popular area of research in the past few decades (Levine and Asano, 2004). Water purification can be achieved by passing the contaminated water through various treatment procedures in order to convert it to reusable water for irrigation, livestock, industrial, household, or drinking water purposes (Shannon et al., 2008). Development of these methods depends on sources of water pollution, the water resource, and the end-use purpose (Eslamian, 2015).

1.4.1. Disinfection

Disinfectants are chemical agents used to remove viruses, bacteria, and other organisms from drinking water (Richardson and Postigo, 2012). The most common water disinfectant is Chlorine, which effectively destroys many biological agents in water (NRC, 1980). However, free chlorine is ineffective in controlling pathogens such as *Cryptosporidium parvum, Giardia,* and *Mycobacterium avium* (Li et al., 2008a; Shannon et al., 2008). Other major disinfection methods include ozone (Am Water Works Res et al., 1991), ultraviolet (UV) (Song et al., 2016), hydrogen peroxide (Asghar et al., 2015; Malato et al., 2016; Martin et al., 2015), fluoridation (Spellman, 2013) and more (Glaze et al., 1987). Both UV and ozone are very effective in controlling *C. parvum* oocysts (Morita et al., 2002). However, some viruses (e.g., adenovirus) are resistant to both UV and combined chlorine disinfection (Shannon et al., 2008; Sirikanchana, 2007). The weakness of various

disinfection technique is low penetrative power of UV in turbid water, decreasing resistivity, presence of DNA repairing enzymes (UV damages) in microbes, and incapability to remove particles, colloids, or ions from water (Fiessinger et al., 1981; Hassen et al., 2000). Moreover, disinfection by-products (DBPs) such as carcinogenic bromate ion can be formed by ozone, and combined with chlorine it can form unregulated DBPs such as haloacetonitriles and iodoacetic acid (Krasner et al., 2006; Muellner et al., 2007; Shannon et al., 2008). Therefore, a disinfection method will be only effective if it can provide a barrier against all pathogens by inactivating viruses, large bacteria, and protozoa without the extensive use of chemicals and production of DBPs (Shannon et al., 2008).

1.4.2. Desalination

Desalination refers to a reduction in salinity used for the production of freshwater from seawater or brackish water sources such as saline aquifers and rivers (Elimelech and Phillip, 2011). The major desalination technologies include membrane filtration via reverse osmosis (RO) and thermal distillation (Zhou and Tol, 2005). RO is an effective method to remove all types of contaminants such as colloidal particles, pyrogens, microorganisms, and dissolved inorganic and monovalent ions (Greenlee et al., 2009). The drawback of the RO technique is that the production capacity is limited to a few gallons day^{-1} (Greenlee et al., 2009). Thermal distillation is inefficient in terms of energy use, corrosion of equipment, and high maintenance (NWC, 2008). Therefore, desalination of all types is considered as an expensive and energy intensive process, which typically requires pre and post-processing, waste (brine) management, maintenance, and transportation from the plant location (Greenlee et al., 2009; Shannon et al., 2008; Veerapaneni et al., 2007).

1.4.3. Reclamation, Recycling, and Reuse

Wastewater reclamation, recycling, and reuse has gained a lot of research interest and public acceptance in recent years as an alternative method to expensive and energy intensive desalination techniques (Dolnicar and Schäfer, 2009) (Asano and Levine, 1996). The comparison study by Côté et al., on the cost of producing water from secondary effluent and from seawater for a 38,000 $m^3 d^{-1}$ plant showed a 50% greater capital cost for a desalination plant than a recycling and reuse plant (Côté et al., 2004). Municipal wastewater treatment consists of a series of pre and post treatment techniques before releasing it for end-use (Mujeriego and Asano, 1999). The level of post-treatment required depends upon the end-use purpose such as discharge to surface water, restricted irrigation, industrial application, direct or indirect potable use (NRC, 2012). Some of these post-treatment techniques include:

1.4.3.1. *Membrane Bioreactors*

Membrane bioreactors (MBR) use micro or ultrafiltration membranes to remove suspended solid material produced by the biological process to produce a clarified and disinfected water (Judd, 2010). The major obstacle for the efficient application of MBR is membrane fouling (Drioli and Giorno, 2010). Additionally, the effluent water from micro MBR may contain dissolved species and colloids that act to foul membranes on RO in the post-treatment process (Shannon et al., 2008). A significant amount of research is going on to improve membrane quality to reduce fouling, develop membranes with specific polymer coating for improved nutrient recovery, and nanofiltration membrane to produce high-quality effluent (Nguyen et al., 2012; Shannon et al., 2008).

1.4.3.2. *Ion Exchange*

Industrial wastewater contains a significant amount of heavy metals such as Pb,

Hg, Cr, Ni, Cd, Cu, and Zn, and pose a threat to human and aquatic life (Rengaraj et al., 2001). Ion exchange resins are insoluble cross-linked polymers that contain acidic or basic functional groups which are capable of exchanging mobile counter-ions present in the surrounding solution (Helfferich, 1962; Hughes, 2004). This technique is effective in removing dissolved inorganics efficiently, however, ineffective in removing colloidal particles, pyrogens, or bacteria (Dabrowski et al., 2004; Kanade, 2016; Monteagudo and Ortiz, 2000).

1.4.3.3. Carbon Adsorption

Activated carbon (AC) is widely used for home-based water treatment systems (Sontheimer et al., 1988). It has been proven to be an effective adsorbent for a variety of organic and inorganic contaminants due to its high surface area, pore volume, effective regeneration, internal microporosity, and a wide spectrum of surface functional groups (Anisuzzaman et al., 2015; Rivera-Utrilla et al., 2011). However, it can produce carbon fines (Camper et al., 1986), and the activation (steam or chemical) process is expensive (Altenor et al., 2009; Rodriguez-Reinoso et al., 1995). Therefore, new and cheaper carbon-based adsorbents such as carbon nanotubes, fullerene, graphene, and biochar have gained a lot of attention in water treatment (Kookana, 2010; Macdonald, 2015; Yu et al., 2015). Biochar was found to be very effective in removing organic (agrochemicals, antibiotics, and hydrocarbons) and inorganic (heavy metals) contaminants from wastewater (Ahmad et al., 2014; Macdonald, 2015). However, very little research is present on their efficacy on microbial contaminant removal from wastewater (Abit et al., 2012; Mohanty and Boehm, 2014).

1.4.3.4. Granular Filtration

Granular filtration (GF) is a fluid-solid separation technique applied to remove

small colloidal contaminants from wastewater (Tien, 2013). The basic principle of GF is the filtration of water through various layers of granular filter bed composed of various materials such as sand with different porosity, diatomaceous earth, and coarse anthracite coal overlying finer sand (Betancourt and Rose, 2004; Tien, 2013). Various types of GF techniques such as slow sand filtration, rapid sand filtration, dual or multimedia filters, and pressure filters are widely used to produce clean water (Cleasby and Woods, 1975; Huisman et al., 1974). In recent years, efforts have been made to improve the efficiency of GF media by modifying the media surface with metal oxides and metal hydroxides (Foppen et al., 2006; Kim et al., 2008; Truesdail et al., 1998), in order to remove microbial contaminants. The disadvantages of GF are high backwash water requirements, short hydraulic retention time, and clogging of the pores of the filter media and, thereby, significantly reducing their filtration efficiency (Ngo and Vigneswaran, 1995; Tien, 2013).

Each of the above-mentioned water recycling and purification technology removes a specific type of contaminant (ions, microbes, colloids, organic or inorganics, and pyrogens), improves taste, or eliminate odour, but none can be relied upon to remove all contaminants to the levels recommended by various guidelines (NHMRC, 2011; NWQMS, 2000; WHO, 2003; WHO, 2008) for critical end use applications. A well-designed water recycling system uses a train of purification technologies to achieve final water quality. A significant amount of research is undergoing to develop a novel low-cost adsorbent or technology, which can remove a variety of contaminants. A few examples include zeolites (Jun-min et al., 2001), biochars or hydrochar (Macdonald, 2015), chitosan (Zeng et al., 2008), nanomaterials (Ali, 2012; Savage and Diallo, 2005; Xu et al., 2012), magnetic

separation (Ambashta and Sillanpää, 2010; De Latour, 1973), and polymer technology (Geise et al., 2010).

However, the above-explained techniques still demand a significant amount of capital cost, energy use, maintenance, infrastructure, engineering solutions, and labour. The location of the plant, transportation, long-term storage options, and post treatment before final potable use will have an impact on economic viability. Moreover, while water quality treatment techniques can ensure the quality of water supply, they do not provide storage, which is essential to provide long-term security of supply. Therefore, more energy efficient techniques, which can reduce the amount of expensive pre and post-treatment, and can, store water for a long-term period with minimal energy or capital expenditure are necessary to face the future global water crisis.

1.4.3.5. *Managed Aquifer Recharge*

Managed aquifer recharge (MAR) is a water resource management technique to facilitate water recycling and reuse by purposefully recharging water in aquifers for the subsequent recovery or environmental benefit (Dillon et al., 2010; Page, 2010). Aquifers can be recharged through numerous mechanisms, such as injection wells, infiltration basins, and rainwater infiltration galleries (Dillon, 2005; Pavelic et al., 2007; Sheng, 2005) using water from various sources such as rainwater, stormwater, treated wastewater, drinking water, water produced by mining sites, and the water recovered from other aquifers (Eslamian, 2015; Ward and Dillon, 2009). With suitable pre-treatment prior to recharge and sometimes post-treatment of recovered water, it may be used for drinking water supplies (Pyne et al., 1996; Wintgens et al., 2008), industrial water, irrigation (Parsons et al., 2012), and non-potable household use such as toilet flushing (Dillon et al., 2009; Sheng, 2005).

Other potential benefits include seasonal, long-term, and emergency storage (Dillon, 2015), sustaining groundwater dependent ecosystems, and replenishing groundwater resources (Dillon et al., 2009; Sheng, 2005).

Water quality improvements have been reported during MAR due to passive treatment in aquifers. MAR is considered as a storage option for recycled water which provides a natural buffer, increases public perception, and provides a residence time that can facilitate removal of biodegradable organic matter and pathogens (Dillon et al., 2008; Page et al., 2015b). Microorganisms such as viruses and bacteria are expected to decay (liquid phase inactivation) due to various factors such as temperature, dissolved oxygen, the activity of autochthonous microorganisms, and organic carbon concentration (Dillon et al., 2009; NRMMC-EPHC-NHMRC, 2009; Pavelic et al., 1998; Sidhu et al., 2015; Sidhu et al., 2010; Toze, 2003). However, due to an inadequate level of knowledge of passive treatment in aquifers, pathogen removal by adsorption to sediment surface is not considered as a sustainable pathogen removal mechanism in the national guidelines for MAR in Australia (NRMMC-EPHC-NHMRC, 2009; Page et al., 2015a). Therefore, understanding and validating the factors controlling the transport and retention of the pathogens through porous media will help to identify aquifer treatment as a potential tool in the treatment train. Thus, aquifer treatment combined with UV, and chlorine infection would help to meet the drinking water quality (Page et al., 2012) in a more energy and cost effective way, by bypassing other expensive pre and post water treatment technologies.

Chapter 1

1.5. Fate, Transport, and Retention of Colloidal Particles in Saturated Porous Media

Colloids refer to dispersions of small particles with dimensions ranging from 1 nm to 10 μm (Berg, 2010). Therefore, NPs (1–100 nm), viruses (20–100 nm) (Duan, 2006; La Scola et al., 2003), bacteria (0.3–2 μm) (Tully et al., 1981) and protozoa (1–10 μm) (Baron and Yaeger, 1996) are considered as colloids. The transport of colloids or solutes with the bulk flow of water is called advective transport or convection (Fetter and Fetter Jr, 1999). The one-dimensional flux of a solute through a porous medium is expressed as the product of average linear water velocity, the concentration of dissolved solids, and effective porosity of the geological medium (Silveira, 2009). Advective transport assumes that the mass of the colloid does not affect the pattern of flow, and the assumption is not true if the colloid or solute and solution have a significantly different density (Fetter and Fetter Jr, 1999). Solution of the Navier-Stokes equations at the pore scale indicates that the water flow path will be faster as it passes through a larger pore, a direct path or the centre of a pore as less friction is involved; the flow path will be slower closer to the grain boundaries due to the high friction; and pore velocity will be zero at regions of no pore connectivity (Narsilio et al., 2009). This local variation of the complex microscopic velocity through the pores and tortuosity of the convective paths results in the mechanical dispersion or mixing, of colloids or solutes (Acharya et al., 2007; Baumann and Werth, 2004; Logan, 2001). In addition, random molecular motion due to the thermal kinetic energy of molecules or colloids, and collision of particles to themselves can result in Brownian movements that can lead to diffusion of the colloids to the solid-water-interfaces (SWI) (Hida, 1980; Logan, 2001; Philibert, 2006).

23

Chapter 1

Thus, the one-dimensional microscopic mass balance equation or advection-dispersion-sorption (ADS) equation for colloids suspended in the aqueous phase can be expressed as (Marsily, 1986):

$$\frac{\partial C}{\partial t} = \lambda v \frac{\partial^2 C}{\partial z^2} - v \frac{\partial C}{\partial z} - \frac{\rho_b}{\theta} \frac{\partial S}{\partial t} \qquad (1)$$

where C [NL^{-3}, where N denotes number and L, denotes unit of length] is the mass concentration of suspended colloid in the aqueous phase, z [L] is the direction of mean water flow, λ [L] is the dispersivity, v [LT^{-1}, where T, denotes the unit of time] is the pore water flow velocity, ρ_b [ML^{-3}, where M, denotes the unit of mass] is the bulk density of the porous medium, θ is the water content, S is the total retained colloid concentration [NM^{-1}].

Colloid Filtration Theory (CFT) is commonly used for describing the attachment of colloids to a collector (solid grain) surface in saturated porous media (Yao et al., 1971). The attachment rate coefficient, (k_{att}), is defined as (Ryan and Elimelech, 1996)

$$k_{att} = \frac{3(1-n)}{2d_c} \alpha \eta v \qquad (2)$$

where n [-] is the porosity of porous media, d_c [L] is the collector diameter, η is the dimensionless single-collector contact efficiency (i.e., the frequency at which the colloids in aqueous phase come into contact with collector surface), and α is the dimensionless sticking efficiency of the colloid (i.e., the frequency at which particles coming into contact with the collector actually realize in attachment) (Nelson and Ginn, 2005).

The diffusion coefficient is inversely proportional to the mass of the molecule, particle, or solutes. Therefore, small colloids (size < 1 μm) like viruses and NPs

Chapter 1

have a much higher probability of transferring among streamlines via Brownian motion and to come in contact with the SWI (Yao et al., 1971). However, larger colloids such as bacteria, protozoa, or microspheres may come in contact with the SWI by either virtue of their own size (this transport process is called interception); or if the density of the colloid is higher than water, the colloid will flow in a different trajectory due to the combined effect of gravitational force, buoyant weight of the particle, and the fluid drag on the particle (this transport process is called sedimentation) (Yao et al., 1971). Therefore, aqueous phase mass transfer of colloids to the solid surface has been the subject of a significant amount of research (Bradford et al., 2011a). Not all the collisions of colloids to the collector surface result in an irreversible attachment. The colloids colliding on the unfavourable region on the collector surface may translate over the surface by tangential hydrodynamic forces to a favourable attachment site (Kuznar and Elimelech, 2007; Torkzaban et al., 2007). The rate of solid phase mass transfer of NPs and viruses to favourable attachment sites is likely affected by the blocking at the later stage of deposition and this has received much less research attention (this will be investigated in chapter 2).

Many factors that influence k_{att} have been extensively studied. Some of these factors include flow velocity (Hijnen et al., 2005; Torkzaban et al., 2007), type of virus or NP (Bradford and Kim, 2012; Chu et al., 2001; Fang et al., 2013), temperature (Chrysikopoulos and Aravantinou, 2014; Kim and Walker, 2009; McCaulou et al., 1995), solution chemistry (e.g., ionic strength, pH, ion type) (Gutierrez et al., 2010; Kim et al., 2009), solid surface roughness (Bradford and Torkzaban, 2013; Torkzaban and Bradford, 2016), and chemical heterogeneities (Johnson et al., 1996). However, a growing body of research suggests that the

experimental observations of colloids breakthrough curve concentration are inconsistent with the CFT prediction (Tufenkji and Elimelech, 2005a).

The CFT considers a clean-bed filtration model where the removal of suspended particles is represented by first-order kinetics, resulting in the concentration of suspended and retained colloids declining exponentially with distance (Tufenkji and Elimelech, 2005a). It has been shown that the rate of deposition changes with time, indicating that the previously deposited colloids can indeed affect the deposition rates (Adamczyk et al., 2013). However, many previous experiments (deposition or injection of colloids) were conducted for a very short time and employed the initial k_{att} for the transport prediction model (He et al., 2009; Lin et al., 2011; Torkzaban et al., 2010). Additionally, accurate detection of the effluent breakthrough concentration of colloids especially NPs at the initial stages of deposition may not be possible due to instrument detection limitations and this may lead to overestimation of α and therefore, k_{att}. Therefore, there is a need to conduct long-term deposition experiments, especially with NPs to determine their full deposition kinetics and to investigate their blocking behaviour at later stages of deposition (this will be discussed in chapter 2).

The Langmuirian (Adamczyk et al., 2013; Adamczyk et al., 1994) and random sequential adsorption models (Johnson and Elimelech, 1995; Talbot and Schaaf, 1989) assume that deposited colloids achieve a monolayer coverage on the fraction of the solid surface that is favourable for attachment (S_f). Many previous studies reported the effect of factors such as particle size (Wang et al., 2012), chemical and physical heterogeneities on collector surface (Tazehkand et al., 2008), solution chemistry (Torkzaban et al., 2010), and flow velocity (Bedrikovetsky et al., 2011; Torkzaban et al., 2007) on the value of S_f. However, the coupled effect of colloid

Chapter 1

size, hydrodynamics, solution chemistry, and temperature on S_f, especially for NPs and viruses is very limited in the literature (this will be discussed in chapter 2 and 3).

The sticking efficiency, α, is a strong function of net attractive and repulsive force between the colloid and the collector surface and depends on many physiochemical and biological factors (Schijven and Hassanizadeh, 2000). The interaction energy between collector and colloid is predicted by the extended Derjaguin-Landau-Verwey-Overbeek (XDLVO) theory, which consists of electrostatic double layer (EDL) and van der Waals (vdW) interactions (Derjaguin, 1941; Verwey, 1947), as well as poorly characterized short-range interactions such as Born, Lewis acid-base, and hydration (Van Oss, 1993; Yoon et al., 1997). The deposition of colloids on collector surface is determined by the energy barrier to attachment in the primary minimum ($\Delta\Phi_a$), the depth of the primary energy minimum ($\Delta\Phi_1^0{}_{min}$), and the depth of the secondary energy minimum ($\Delta\Phi_2^0{}_{min}$) (Grasso et al.; Schijven and Hassanizadeh, 2000; Shen et al., 2007). The classical DLVO theory considers the collector as a smooth homogeneous surface (Czarnecki and Warszyński, 1987) and predicts the presence of a significant $\Delta\Phi_a$ at unfavourable conditions and therefore, negligible deposition (Schijven and Hassanizadeh, 2000; Shen et al., 2007). However, many experimental studies showed a discrepancy between theoretical prediction and observed attachment under unfavourable conditions (Bendersky and Davis, 2011; Duffadar et al., 2009; Shen et al., 2012a) (Bradford and Torkzaban, 2013). Several explanations have been proposed to account for this discrepancy including deposition at $\Delta\Phi_2^0{}_{min}$ (Redman et al., 2004; Tufenkji and Elimelech, 2004b), hydrodynamic and adhesive torque balance (Bradford and Torkzaban, 2015; Bradford et al., 2007; Torkzaban et

al., 2007), and some recent studies extensively looked into developing theoretical simulations to incorporate the presence of chemical (Bradford and Torkzaban, 2012; Elimelech et al., 2003) and physical heterogeneity (Bhattacharjee et al., 1998; Bradford and Torkzaban, 2015; Hoek and Agarwal, 2006; Shen et al., 2012a; Torkzaban and Bradford, 2016) on the collector surface. However, the effect of physical and chemical heterogeneity on the XDLVO interaction energy profile and its influence on α and thereby, on the S_f value for viruses and NPs has not been well studied (this will be discussed in chapter 3).

1.6.   Scope and Objectives

This thesis aimed to gain a fundamental understanding of the mechanisms controlling the fate, transport, and retention of colloidal particles (viruses, bacteria, and nanoparticles) in saturated porous media. Specifically, this research focused on the interactions occurring between colloids and collector surfaces at the SWI under various physicochemical conditions. The overall objective was to relate the kinetics of colloid adsorption to the physical and chemical properties of the system.

1. Examine combined effects of hydrodynamics and solution chemistry on the long-term kinetics of NP deposition in saturated porous media. Investigate the coupled effects of solution ionic strength, cation type, colloidal particle size, and flow velocity on the k_{att} and S_f values of NPs. Identify an appropriate kinetic model to satisfactorily simulate and describe the long-term dynamics of the deposition process.

2. Experimentally and theoretically, investigate the influence of water temperature, coupled with solution chemistry and flow velocity, on the extent and kinetics of virus and NP attachment in porous media. Simulate

the experimental breakthrough concentrations using an appropriate kinetic model, and calculate α and S_f values using the fitted parameter values. Conduct XDLVO calculations between a chemically and physically heterogeneous collector, and a homogeneous colloid to explain the observed enhanced attachment of the viruses and nanoparticles at a higher temperature.

3. Understand the efficacy of biochar amendment of sand porous media on virus and bacteria removal. Conduct batch experiments to specifically examine the extent of microbial attachment to non-treated and chemically treated biochar, and sand surfaces. Conduct systematic column experiments to understand the combined effect of attachment and straining on the microbe retention. Compare between batch and column experiments using viruses and bacteria to identify the underlying mechanism controlling the colloid retention in the biochar-amended sand.

1.7. Outline of Thesis

This thesis consists of five chapters, beginning with this introduction (Chapter 1). The following three chapters (Chapter 2, 3, and 4) are written as manuscripts for publication in peer-reviewed international journals. Each of these chapters is published or under review, and can be read independently.

Chapter 2:

Sasidharan, S., S. Torkzaban, S. A. Bradford, P. J. Dillon and P. G. Cook (2014). Coupled effects of hydrodynamic and solution chemistry on long-term nanoparticle transport and deposition in saturated porous media. *Colloids and Surfaces A: Physicochemical and Engineering Aspects* **457**(1): 169-179.

Chapter 3:

Sasidharan, S., S. Torkzaban, S. A. Bradford, P. G. Cook and V.V.S.R Gupta (2016). Temperature Dependency of Virus and Nanoparticle Transport and Retention in Saturated Porous Media. *Water Research*, WR35849. (under review).

Chapter 4:

Sasidharan, S., S. Torkzaban, S. A. Bradford, R. Kookana, D. Page and P. G. Cook (2016). Transport and retention of bacteria and viruses in biochar-amended sand. *Science of the Total Environment* 548–549: 100-109.

These chapters are followed by the conclusion (Chapter 5), which summarises the broader implications of the research presented in this thesis and make recommendations for future work.

The characteristics of the bacteriophages used in this research and their host information, a brief methodology for bacteria and bacteriophage preparation, and double layer agar method (DLA) is presented in Appendix A, which is adapted from the supporting information of the manuscript presented in Chapter 4. Detailed systematic methodology for growth media, bacteria, and bacteriophage preparation, analysis of bacteriophage using double layer agar method, and the long-term storage and maintenance of microbial cultures, in order to establish these techniques in a new institution facility, is presented in Appendix B. Conference papers resulted directly from this research are presented in Appendix C.

CHAPTER 2

Coupled Effects of Hydrodynamic and Solution Chemistry on Long-Term

Nanoparticle Transport and Deposition in Saturated Porous Media
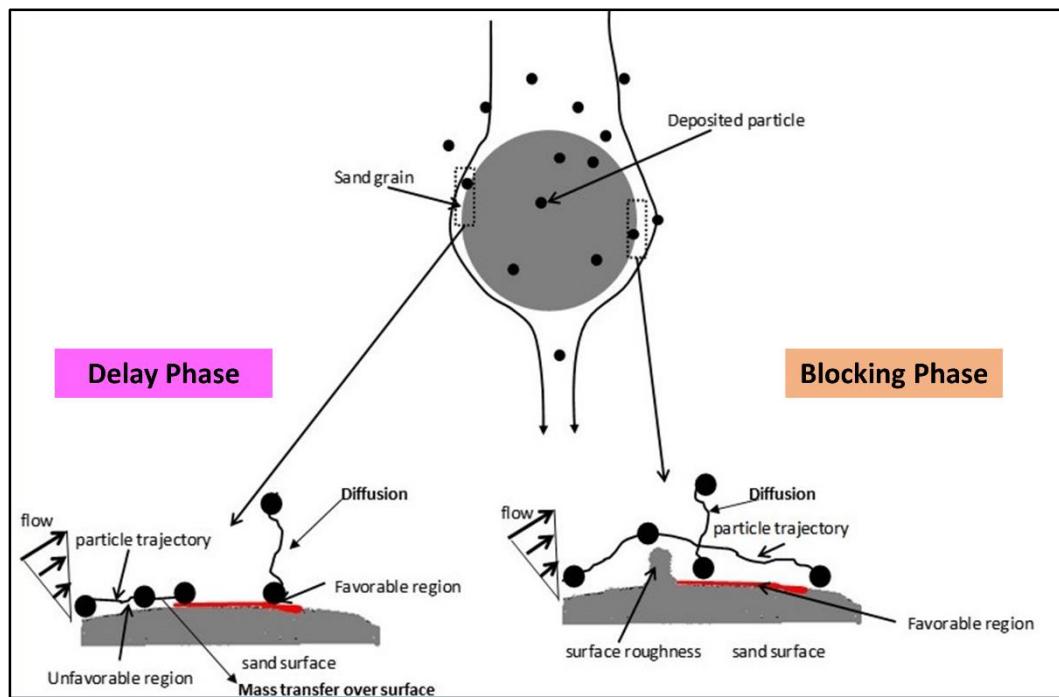
HIGHLIGHTS

- The breakthrough curves of the NPs exhibited a bimodal shape with increasing solution ionic strength.
- Deposition dynamics of the NPs was simulated using a two-site kinetic model.
- NP deposition is controlled by the coupled effects of flow velocity, solution chemistry, and particle size.
- NP interactions with the collector tend to strengthen with increasing contact time.

Chapter 2

Abstract

This study aims to systematically explore the coupled effects of hydrodynamic and solution chemistry conditions on the long-term transport and deposition kinetics of nanoparticles (NPs) in saturated porous media. Column transport experiments were carried out at various solution ionic strengths (IS), ionic composition, and flow velocities utilising negatively charged carboxyl-modified latex NPs of two different sizes (50 and 100 nm). These experiments were designed to obtain the long-term breakthrough curves (BTCs) in order to unambiguously determine the full deposition kinetics and the fraction of the solid surface area (S_f) that was available for NP deposition. The BTCs exhibited a bimodal shape with increasing solution IS; i.e., BTCs were initially delayed, next they rapidly increased, and then they slowly approached the influent particle concentration. NP deposition was much more pronounced in the presence of Ca^{2+} than Na^+ at any given solution IS. Deposition kinetic of NPs was successfully simulated using a two-site kinetic model that accounted for irreversible deposition and blocking on each site, i.e., a decreasing deposition rate as the site filled. Results showed that S_f values were controlled by the coupled effects of flow velocity, solution chemistry, and particle size. Data analyses further demonstrated that only a small fraction of the sand surface area contributed in NP deposition even at the highest IS (60 mM) and lowest flow velocity (1 m day^{-1}) tested. Consistent with previous studies, our results imply that NP deposition is controlled by physicochemical interactions between the NPs and nanoscale physical and/or chemical heterogeneities on the sand surfaces that produce localised nanoscale favourable sites for deposition. Furthermore, our results suggest that the NP interactions with the collector surfaces tended to strengthen with increasing contact time.

Chapter 2

Keywords

Breakthrough curves, Nanoparticle, Column studies, Hydrodynamic, Solution chemistry, Two-site kinetic model

2.1. Introduction

An understanding of nanoparticle (NP) transport and deposition in porous media is important in a range of processes in natural and engineered systems. These processes may include the transport and fate of pathogenic viruses and engineered NPs in soils and aquifers (Bradford et al., 2012; Jin and Flury, 2002; Petosa et al., 2010; Torkzaban et al., 2012), and deep bed filtration in water and wastewater treatment systems (Anders and Chrysikopoulos, 2005; Schijven and Hassanizadeh, 2000). Most experimental studies of NP deposition in porous media have focused on the initial, clean-bed, deposition behaviour when the collector surfaces are devoid or only contain small amounts of deposited particles (Jaisi and Elimelech, 2009; Petosa et al., 2010; Solovitch et al., 2010). In this case, the deposition rate is constant and a first-order kinetic model is commonly employed to describe the deposition behaviour (Bradford et al., 2014; Pelley and Tufenkji, 2008). However, as NP deposition on collector surfaces proceeds, a decrease in the deposition rate occurs due to blocking (filling) of the available sites (Adamczyk et al., 2009; Li et al., 2008b; Torkzaban et al., 2010; Torkzaban et al., 2012; Virkutyte et al., 2014). This blocking phenomenon usually occurs when a considerable net-repulsive energy barrier exists between the NPs and collector surfaces. Therefore, in most natural systems only a small fraction of the solid surface contributes to NP deposition because of the prevalence of net-repulsive electrostatic conditions (Bradford and Torkzaban, 2013; Jin et al., 2000; Shang et al., 2013; Torkzaban et al., 2012; Wang et al., 2008). Consequently, it is imperative that theoretical models

are able to describe the entire dynamics of deposition from the initial to later stages when a decline in deposition rates occurs. An understanding of the dynamics of NP deposition is especially important because NP deposition is essentially irreversible (insignificant detachment) during steady-state chemical and hydrodynamic conditions (Liang et al., 2013; Shen et al., 2007; Shen et al., 2012b; Torkzaban et al., 2013; Torkzaban et al., 2012).

Two different blocking models have been developed to describe the declining rate of deposition during the filling process, namely: the Langmuirian model (Adamczyk et al., 2013; Adamczyk et al., 1994) and the random sequential adsorption (RSA) model (Johnson and Elimelech, 1995; Talbot and Schaaf, 1989). The Langmuirian and RSA models assume a linear and a nonlinear decrease in the deposition rate during filling of deposition sites, respectively. The Langmuirian approach is commonly employed in short-term colloid deposition modelling studies (Bradford et al., 2012; Liang et al., 2013). However, the RSA model provides a superior description of deposition dynamics when the coverage of collector surfaces approaches the maximum attainable coverage (~54%), often referred to as the hard sphere jamming limit (Adamczyk et al., 2003; Adamczyk et al., 1994; Massoudieh et al., 2013; van Loenhout et al., 2009). Both Langmuirian and RSA models assume that deposited NPs eventually achieve monolayer coverage on the fraction of the solid surface area that is favourable for deposition (S_f).

Previous studies have reported that S_f is influenced by a range of physicochemical factors such as particle size, the amount and size of physical and/or chemical heterogeneities, solution chemistry, and flow rate (Bradford et al., 2011a; Quevedo and Tufenkji, 2009; Tazehkand et al., 2008; Torkzaban et al., 2010). In particular, S_f has been reported to increase with increasing ionic strength

(IS) under net-repulsive electrostatic conditions, suggesting that deposition locations on the collector surfaces are largely determined by nanoscale heterogeneities and/or increasing the depth of the secondary energy minimum (Kalasin et al., 2010; Rizwan and Bhattacharjee, 2009; Shani et al., 2008; Torkzaban et al., 2008). Furthermore, increasing the flow velocity and/or particle size has been shown to decrease S_f, suggesting that hydrodynamic conditions are also important in determining deposition kinetics and blocking (Bradford et al., 2012; Ko and Elimelech, 2000; Song and Elimelech, 1993). Several explanations have been proposed in the literature to explain the role of flow velocity or particle size on the deposition behaviour. Some researchers have attributed the decrease in S_f at higher velocities to the "shadow effect" (Ko and Elimelech, 2000) e.g., the excluded region created down gradient of micro-scale surface roughness or deposited particles. More recently, the influence of hydrodynamic conditions on S_f has been explained by the balance of applied hydrodynamic and resisting adhesive torques (Bedrikovetsky et al., 2011; Bradford et al., 2009; Bradford et al., 2013; Kalantariasl and Bedrikovetsky, 2013; Torkzaban et al., 2007). Only limited experimental information is available in the literature on the dependence of S_f on physicochemical and hydrodynamic factors, especially for NPs. In this paper, we will systematically explore the coupled effects of these factors on the value of S_f. This information is required to better deduce the underlying mechanisms and theoretical description of NP deposition kinetics under net-unfavourable conditions.

The overall deposition rate of NPs in porous media depends not only on S_f but also on the mass transfer of NPs to favourable sites on the solid surfaces where deposition can occur. Mass transfer of NPs to favourable sites occurs by two

means: (1) aqueous phase mass transfer from the bulk aqueous phase to the solid surface (Nelson and Ginn, 2011; Tufenkji and Elimelech, 2005b) and (2) solid phase mass transfer on unfavourable regions of the solid surface to favourable sites (Bradford et al., 2011a; Shani et al., 2008; Yuan and Shapiro, 2011). Aqueous phase mass transfer of NPs to the solid surface has been the subject of much research (Bradford et al., 2014) and colloid filtration theory (Yao et al., 1971) is commonly used to quantify this process. Conversely, the role of solid phase mass transfer has received less research attention (Bradford et al., 2011a). It has been shown that particles colliding with unfavourable regions of the solid surface may become weakly associated with the solid surface via a shallow secondary energy minimum. These particles can be translated along the collector surface by tangential hydrodynamic forces to the favourable deposition sites (Kuznar and Elimelech, 2007). It is expected that nano- and micro-scale surface roughness and the pore-space topography should influence the solid phase mass transfer of the NPs. Furthermore, the amount of colloid transfer on the solid surface is expected to increase with increasing IS and decreasing flow velocity (Kalasin et al., 2010; Shani et al., 2008). The solid phase mass transfer rate of NPs is likely to decrease during the filling processes, but little research has been conducted to address this issue.

The objective of this study is to develop a more thorough understanding of the combined effects of hydrodynamics and solution chemistry on the long-term kinetic of NP deposition in saturated porous media. Specifically, a series of laboratory experiments was carried out in saturated sand columns to investigate the coupled effects of solution IS, cation type, particle size, and flow velocity on the deposition rate constants and the fraction of the solid surface area available for NP deposition. A two-site kinetic model was found to satisfactorily simulate and describe the long-

term dynamics of the deposition process. Fitted values of S_f and deposition rate constants over a wide range of physicochemical conditions increased our understanding of the dynamics of long-term NP deposition in porous media. This information is needed to improve our theoretical description of these processes and to improve continuum scale models for predicting the long-term fate and mobility of NPs in the subsurface environment.

2.2. Materials and Method

2.2.1. NPs

Carboxylate-modified latex (CML) microspheres have often been used as model NPs in transport studies due to their spherical shape, well-defined size and surface charge, and ease in detection at low concentration (Bradford et al., 2012). Two sizes (50 and 100 nm) of Fluoresbrite®Yellow-Green CML microspheres *(Polysciences, Inc),* that have an excitation wavelength at 441 nm and an emission wavelength at 486 nm, were used in this research. Stock solutions of CML NPs were diluted in selected electrolyte solutions to achieve a desired initial concentration (C_0). All solutions were prepared using analytical grade reagents and Milli-Q water with its unadjusted pH = 5.8. A near neutral pH and negatively charged NPs were chosen in order to understand the NP transport mechanism under most unfavourable condition. The initial concentration for 50 and 100 nm CML NPs was typically 4.55×10^{10} mL^{-1}. NP aqueous phase concentrations were determined using a fluorescence spectrophotometer (Synergy HT, BioTek Instruments, Inc., Winooski, VT, USA) and a calibration curve. The CML NPs have carboxylate groups on their surfaces that are highly negatively charged. The zeta potential and size uniformity of the CML microspheres in various electrolyte and pH solutions were determined using a Malvern, Zetasizer Nano Series, Nano-

ZS. It was confirmed that the CML suspension at the highest tested concentrations of 60 mM NaCl and 3 mM $CaCl_2$ was stable and did not show any aggregation. The manufacturer reported that the CML NPs had a density of 1.05 g cm^{-3}.

2.2.2. Porous Media

Natural graded river sand (River sand Pty Ltd) was used as the granular porous media for the transport experiments. The average grain diameter of the sand was 255 µm, and the grain size ranged between 106 and 300 µm. The sand was cleaned prior to use to remove the impurities from the sand surface and to reduce the surface heterogeneity. Sieved sand was soaked in 37% HCl for three days to remove dissolved organic matter and metal oxides. After discarding the excess acid, the sand was alternatively rinsed with 0.1 M NaOH and deionized (DI) water until the pH reached 7. The sand was subsequently soaked in boiling 1 M NaCl for 3 h and then washed with boiling DI water for 3 h. These processes (boiling alternatively in 1 M NaCl and DI water) were repeated eight times to remove the clay particles on the sand surface by the combined influence of cation exchange and expansion of the double layer. Finally, the sand was rinsed with DI water several times until the effluent turbidity and UV-visible absorbance was virtually zero. Scanning electron microscopy (SEM) (Quanta 450, Adelaide microscopy, The University of Adelaide, Australia) of the sand before and after cleaning demonstrated that this procedure removed most of the surface impurities and clays from the sand.

2.2.3. Electrokinetic Characterization and DLVO Calculations

The electrophoretic mobility of the colloids and crushed sand grains was measured in various NaCl electrolyte solutions using a Zetasizer at pH 5.8. The Smoluchowski equation (Elimelech, 1994) was used to convert the measured electrophoretic mobility values to zeta potentials. The measurements were repeated five times for each colloid suspension and the average values are reported in Table

Chapter 2

2. Classical DLVO theory (Derjaguin and Landau, 1993; Verwey, 1947) was used to calculate the total interaction energy, that is, the sum of the London-van der Waals attraction and the electrostatic double-layer repulsion, for the colloids upon close approach to quartz surfaces (assuming sphere-plate interactions) for the various solution IS used in our experiments. The retarded London-van der Waals interaction force was determined from the expression of Gregory (Gregory and Wishart, 1980) utilising a value of 4.04×10^{-21} J for the Hamaker constant (Bergendahl and Grasso, 1999) to represent the latex-water-quartz system. In these calculations, constant-potential electrostatic double layer interactions were quantified using the linear superposition approximation model given in (Gregory, 1975), with zeta potentials in place of surface potentials.

2.2.4. Column Studies

Column experiments were conducted using 11 cm long polycarbonate chromatography columns with a 1.9 cm internal diameter and a total inner volume of 31.19 cm^2. Tubing to and from the columns, fittings, and column O-rings were composed of chemically inert material such as Teflon and viton. The columns were set-up vertically and wet packed with the cleaned river sand, using vibration to minimise air entrapment and to ensure the uniformity of packing. A sodium nitrate (NaNO$_3$) tracer test was conducted to obtain the parameter values for the transport modelling. Each column was packed with ~50 g of sand and the porosity was calculated gravimetrically to be 0.40. One pore volume (PV), which is the amount of solution required to fill in the void space of the sand in the column was determined to be 14 mL. The packed columns were flushed with several pore volumes of a selected electrolyte solution to equilibrate the system before injecting a NP suspension at a constant velocity with a syringe pump (Harvard apparatus 22). Effluent samples (every 3 mL) were continuously collected using a

Spectra/Chrom® CF-1 Fraction Collector. In order to calculate the amount of surface area that contributed in NP deposition, the injection of the NPs was continued until the effluent concentration (C) approached C_0 or a stable concentration level. The columns were then flushed with several PV of the same electrolyte solution, but without NPs. Table 2 summarises the experimental conditions. Table 3 contains the number of injected PV at which the influent was switched to the NP-free electrolyte solution.

A few sand grains were collected carefully from the column after the deposition phase. The samples were analysed using SEM to observe the distribution of NPs on the sand surfaces. Sand grains were placed on the top of a carbon tape mounted on a stub, with a 3 nm thickness platinum coating and imaged at 10 kV using Quanta 450 SEM. It was confirmed that the platinum coating force and the vacuum in the SEM chamber were not enough to detach the deposited NPs.

2.2.5. Modelling

Major processes controlling the transport and deposition of NPs in porous media are advection, dispersion, and attachment caused by particle interactions with the collector surfaces. The detachment process is often negligible under steady-state chemical and hydrodynamic conditions (Bradford et al., 2012) and will be neglected in this work. The advection-dispersion equation (ADE) with irreversible attachment is given for uniform and one-dimensional flow as:

$$\frac{\partial C}{\partial t} = \lambda v \frac{\partial^2 C}{\partial z^2} - v \frac{\partial C}{\partial z} - r_{att} \tag{1}$$

where t [T] is time, z [L] is the direction of mean water flow, C [NL^{-3}] is the number of NPs per unit volume of the aqueous phase, λ is the dispersivity [L], v is the average pore water velocity [LT^{-1}], and r_{att} is the NP attachment rate to the solid

Chapter 2

surfaces [NL^{-3}T^{-1}]. The mean pore-water velocity and dispersivity used in NP simulations were obtained by fitting to the tracer (NaNO$_3$) BTCs.

Typically, the BTCs could be simulated reasonably well during the first few PV using Eq. [1] in conjunction with a one-site, irreversible attachment model that included a Langmuirian blocking function. However, as it will be discussed later, this model does not provide an adequate description of the deposition dynamics at later times. To investigate whether multiple kinetic deposition sites could account for this discrepancy, a two-site kinetic model was used for analysing the BTCs. In this case, the value of r_{att} is given as:

$$r_{att} = \rho_b \frac{\partial(S_1 + S_2)}{\partial t} = \theta k_1 \psi_1 C + \theta k_2 \psi_2 C \qquad (2)$$

where ρ_b is the soil bulk density [ML^{-3}], θ is the water content [-], S_1 is the solid phase NP concentration on site 1 [NM^{-1}], k_1 is the attachment rate coefficient for site 1 [T^{-1}], and Ψ_1 is a dimensionless Langmuirian blocking function for site 1 that is given as (Adamczyk et al., 2013):

$$\Psi_1 = \left(1 - \frac{S_1}{S_{max1}}\right) \qquad (3)$$

Here S_{max1} [NM^{-1}] is the maximum solid phase concentration of attached NPs on site 1. Corresponding values of S_2, S_{max2}, k_2 and Ψ_2 are defined for site 2. When the value of S_{max1} and S_{max2} are large, the blocking function approaches a value of 1 and time-dependent deposition behaviour becomes irrelevant. A modified version of HYDRUS-1D (Simunek et al., 2005) was used to solve Eqs. [1]–[3].

The fraction of the solid surface area that is available for deposition (S_f) may be determined from the sum of fitted values of S_{max1} and S_{max2} using the following equation (Kim et al., 2009):

41

Chapter 2

$$S_f = \frac{A_c \rho_b S_{max}}{(1-\gamma)A_s} \tag{4}$$

where A_c [$L^2 N^{-1}$] is the cross-section area per colloid, A_s [L^{-1}] is the solid surface area per unit volume, S_{max} [NM^{-1}] is the maximum solid phase concentration of attached NPs on both sites, and γ [-] is the porosity of a monolayer packing of colloids on the solid surface. In this work, we assume a value of $\gamma = 0.5$ in all simulations based on information presented by (Johnson and Elimelech, 1995). For those experiments where C/C_0 reached unity during the deposition phase, the value of S_f can also be estimated from the effluent BTCs based on the following mass balance equation (Ko and Elimelech, 2000):

$$S_f = \frac{\pi r_p^2 r_c q_w \left(C_o T_{pulse} - \int_0^{T_{total}} C dt \right)}{3L(1-n)} \tag{5}$$

where r_p [L] is the radius of the NP, r_c [L] is the radius of the sand grain, q_w [L T^{-1}] is the Darcy velocity, T_{pulse} [T] is the injection time, and T_{total} [T] is the entire time of the experiment, L [L] is the length of the packed column and n is the porosity of the porous media. As it will be shown later in the paper, Eqs. [4] and [5] were found to yield comparable values of S_f.

2.3.   Results and Discussion

2.3.1. Surface Charge of NPs and Sand Grains

Zeta potentials of the NPs and colloidal particles collected from crushed sand grains over the range of solution chemistries used in the column experiments are presented in Table 2. As expected, the absolute value of the zeta potential of the NPs and sand grains decreased with increasing the concentration of Na$^+$ and Ca^{2+} due to compression of the electrostatic double layer (Elimelech, 1994). Increasing

the Ca^{2+} concentration was more effective in decreasing the magnitude of the zeta potential than similar changes in Na^+ due to the combined effects of charge screening of the divalent cations and the adsorption (binding) of cationic Ca^{2+} to anionic COO^- groups on the NPs and SiO_2 sites on the collectors (Israelachvili, 2011).

Calculated DLVO interaction energies presented in Table 2 indicate a negligible secondary energy minimum in all solutions for both of the particle sizes. Therefore, the NPs are expected to experience negligible deposition or aggregation due to the secondary energy minimum. DLVO calculations show high energy barriers (16–52 kT) between the NPs and sand surfaces at all of the considered solution chemistries. The height of energy barriers decreased with IS and decreasing NP size. The Maxwellian kinetic energy model (Bradford et al., 2011b; Shen et al., 2007) predicts that it is unlikely for the NPs to diffuse over these energy barriers into the primary energy minimum. Higher energy barriers and negligible secondary minima suggest that net repulsive interactions should have existed between the NPs and sand grains. However, it should be noted that these interaction energies only reflect mean values of interaction energies between the NPs and sand surfaces and do not account for the potential influence of nanoscale chemical and physical heterogeneities which always exist on natural mineral surfaces (Bradford and Torkzaban, 2013; Hoek and Agarwal, 2006). It has been demonstrated that nanoscale roughness on the collector and colloid surfaces tend to reduce the magnitude of the interaction energies (Bradford and Torkzaban, 2013; Shen et al., 2012b).

2.3.2. Deposition Kinetics of NPs

In contrast with most previous studies on NP deposition, reviews of which may

be found in (Petosa et al., 2010), long-term injections of the NPs were carried out in order to determine the full dynamics of deposition and the associated blocking model parameters. Figure 1 presents measured and simulated BTCs for 100 (Figure 1a) and 50 nm (Figure 1b) NPs in various concentrations of NaCl solutions when the pore-water velocity was 1 m day^{-1}. Figure 2 presents similar BTC information for different concentrations of $CaCl_2$ solutions and the two NP sizes at 1 m day^{-1} pore water velocity. Figure 3 shows measured and simulated BTCs for the two NP sizes at various flow velocities ranging from 1 to 20 m day^{-1} when the IS was 50 mM NaCl. Figure 4 presents similar BTC information for the two NP sizes at different velocities, but for 2 mM $CaCl_2$. The BTCs are plotted herein as normalised effluent concentrations (C/C_0) versus the number of pore volumes that passed through the column. Table 3 summarises the fitted model parameters, along with their 95% confidence intervals. The fitted deposition parameters were found to be unique, as the final fitted values were not affected by the initial guess.

In general, the BTCs were initially delayed (arriving after 1 pore volume), next they rapidly increased, and then they slowly approached the influent particle concentration. These trends can be explained by considering the simulated kinetics of the deposition process using Eqs. [1]–[3]. The one-site kinetic model incorporating the Langmuirian or RSA blocking function failed to fit the entire BTC obtained at various chemical and physical conditions (data not shown). Conversely, the two-site kinetic model with a Langmuirian blocking function for each site provided an excellent description for all the BTCs shown in Figures 1–4 ($R^2 > 94\%$). In general, the value of k_1 was around one order of magnitude greater than k_2, and S_{max1} was much smaller than S_{max2}. The time delay of the breakthrough curve was mainly determined by the values of k_1 and S_{max1}. A high value of k_1 results in

complete deposition until the solid phase concentration of NPs in site 1 approaches S_{max1}. Consequently, more delay is expected for higher values of k_1 and S_{max1}. Other studies on NP transport in porous media have observed a similar delay in their BTCs e.g., (Liang et al., 2013; Quevedo and Tufenkji, 2009; Torkzaban et al., 2012). After the BTCs begin their sharp rise due to filling of site 1, the shape of the BTCs is mainly controlled by site 2. In particular, the skewness of the rising portions of the BTCs is strongly affected by the values of k_2 and S_{max2}. Neglecting detachment in the model is justified by the negligible tailing in the BTCs.

Table 2. The average of zeta potentials of NPs and sand as well as calculated DLVO interaction parameters in the indicated solution chemistries.

NP size	Solution chemistry	IS	Zeta potential (NP)	Zeta potential (sand)	Energy barrier height	Secondary minimum depth
[nm]		[mM]	[mV]	[mV]	[kT]	[kT]
50	10 mM NaCl	10	-51	-29	57	~0
	20 mM NaCl	20	-48	-30	52	~0
	50 mM NaCl	50	-31	-26	24	-0.08
	0.5 mM CaCl$_2$	1.5	-43	-21	28	~0
	2 mM CaCl$_2$	6	-32	-19	16	~0
100	40 mM NaCl	40	-41	-15	47	-0.2
	60 mM NaCl	60	-30	-15	19	-0.3
	2 mM CaCl$_2$	6	-35	-19	34	~0
	3 mM CaCl$_2$	9	-27	-17	20	-0.22

Two-site kinetic models have previously been employed in colloid and NP transport studies (Bales et al., 1991b; Harmand et al., 1996; Schijven et al., 2002). There are a variety of potential explanations for the need to a multiple deposition site model. Macro-scale patch-wise charge heterogeneities have been demonstrated to cause two types of kinetic rates (Tufenkji and Elimelech, 2005a). Primary and secondary minimum interactions may also produce irreversible and reversible deposition sites, respectively (Tufenkji and Elimelech, 2005a). Nanoscale physical
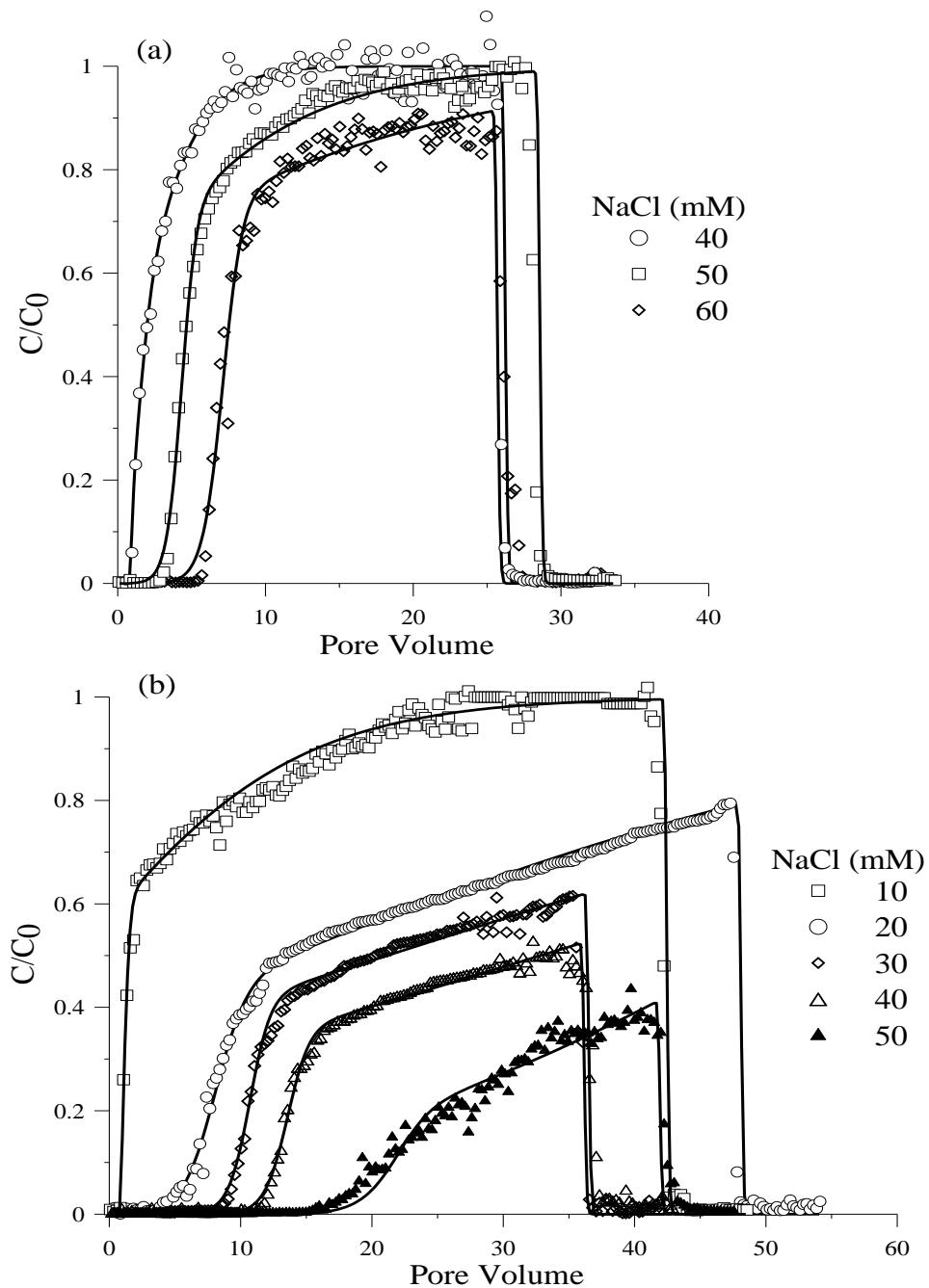
Figure 1. Representative measured and fitted breakthrough curves for 100 nm (a) and 50 nm (b) modified latex nanoparticles obtained from column experiments at pore water velocity of 1 m day^{-1} at various NaCl concentrations. Table 3 provides summary information on the model parameters.
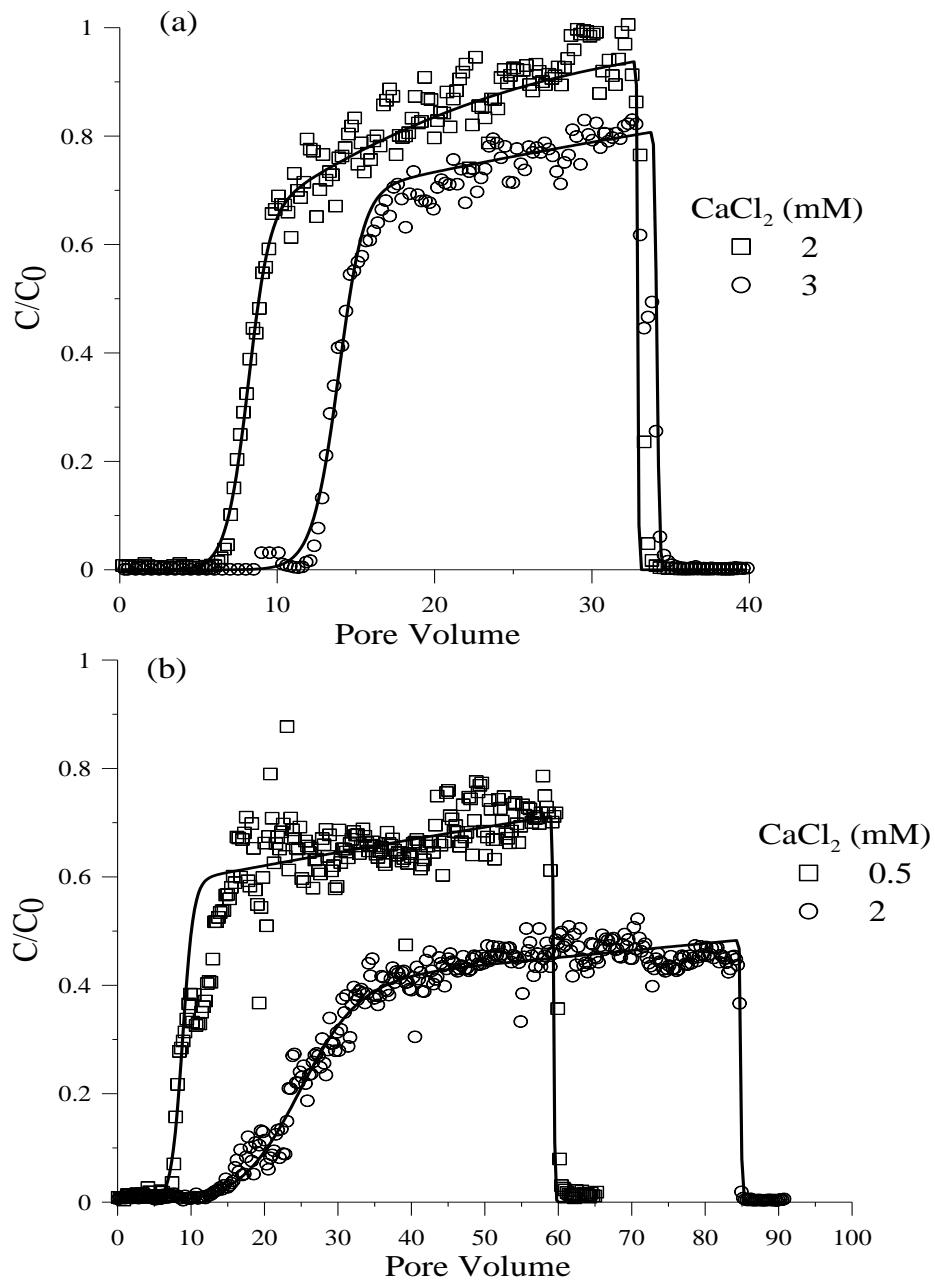
Figure 2. Representative measured and fitted breakthrough curves for 100 nm (a) and 50 nm (b) modified latex nanoparticles obtained from column experiments at pore water velocity of 1 m day^{-1} at various CaCl$_2$ concentrations. Table 3 provides summary information on the model parameters.

and chemical heterogeneity may affect the amount and strength of these primary

and secondary minimum interactions (Bradford and Torkzaban, 2012; Duffadar and

Davis, 2007; Santore and Kozlova, 2007; Torkzaban et al., 2008). Differences in

Table 3. Experimental conditions and fitted model parameters for column experiments shown in Figures 1–4.

NP size	Flow velocity	NaCl or CaCl$_2$	Pulse duration	k_1	k_2	S_{max1}/C_0	S_{max2}/C_0	S_f (fitted) [a]	S_f (BTC) [b]
[nm]	[m day^{-1}]	[mM]	[PV]	[min^{-1}]	[min^{-1}]	[m^3 kg^{-1}]	[m^3 kg^{-1}]	[%]	[%]
50	1	10 Na$^+$	41.5	$(7.3\pm0.4)\times10^{-3}$	$(3.2\pm0.6)\times10^{-3}$	$(4.2\pm0.3)\times10^{-5}$	$(9.8\pm0.6)\times10^{-4}$	0.04	0.03
50	1	20 Na$^+$	41.2	$(4.8\pm0.1)\times10^{-2}$	$(5.8\pm0.3)\times10^{-3}$	$(1.1\pm0.4)\times10^{-3}$	$(5.4\pm0.8)\times10^{-3}$	0.95	ND [c]
50	1	30 Na$^+$	35.5	$(1.1\pm0.5)\times10^{-1}$	$(6.4\pm0.6)\times10^{-3}$	$(1.4\pm0.2)\times10^{-3}$	$(7.2\pm0.5)\times10^{-3}$	1.24	ND
50	1	40 Na$^+$	35.1	$(1.5\pm0.4)\times10^{-1}$	$(7.7\pm0.3)\times10^{-3}$	$(1.6\pm0.6)\times10^{-3}$	$(9.1\pm0.7)\times10^{-3}$	1.46	ND
50	1	50 Na$^+$	41.0	$(1.7\pm0.5)\times10^{-1}$	$(1.5\pm0.6)\times10^{-2}$	$(1.7\pm0.2)\times10^{-3}$	$(1.0\pm0.5)\times10^{-2}$	1.78	ND
50	5	50 Na$^+$	29.7	$(3.7\pm0.2)\times10^{-1}$	$(2.3\pm0.3)\times10^{-2}$	$(1.8\pm0.3)\times10^{-3}$	$(3.6\pm0.6)\times10^{-3}$	1.54	ND
50	20	50 Na$^+$	38.9	(1.1 ± 0.6)	$(6.9\pm0.5)\times10^{-2}$	$(1.6\pm0.4)\times10^{-3}$	$(2.3\pm0.7)\times10^{-3}$	1.33	ND
100	1	40 Na$^+$	25.2	$(6.3\pm0.3)\times10^{-3}$	$(4.3\pm0.4)\times10^{-3}$	$(7.8\pm0.6)\times10^{-5}$	$(3.5\pm0.2)\times10^{-4}$	1.45	1.7
100	1	50 Na$^+$	27.6	$(4.7\pm0.2)\times10^{-2}$	$(2.6\pm0.3)\times10^{-3}$	$(6.5\pm0.3)\times10^{-4}$	$(6.3\pm0.7)\times10^{-4}$	4.32	4.9
100	1	60 Na$^+$	24.7	$(6.6\pm0.5)\times10^{-2}$	$(2.3\pm0.1)\times10^{-3}$	$(1.2\pm0.1)\times10^{-3}$	$(1.2\pm0.3)\times10^{-3}$	8.16	ND
100	5	50 Na$^+$	26.8	$(1.1\pm0.2)\times10^{-1}$	$(2.0\pm0.2)\times10^{-2}$	$(2.7\pm0.5)\times10^{-4}$	$(7.9\pm0.8)\times10^{-4}$	2.57	2.3
100	20	50 Na$^+$	21.0	$(6.0\pm0.4)\times10^{-2}$	$(4.7\pm0.3)\times10^{-2}$	$(9.7\pm0.6)\times10^{-5}$	$(2.9\pm0.3)\times10^{-4}$	1.30	1.2
50	1	0.5 Ca^{2+}	58.4	$(3.6\pm0.2)\times10^{-2}$	$(3.7\pm0.3)\times10^{-3}$	$(1.4\pm0.1)\times10^{-3}$	$(1.2\pm0.2)\times10^{-2}$	1.29	0.03
50	1	2 Ca^{2+}	83.8	$(5.2\pm0.6)\times10^{-2}$	$(6.0\pm0.5)\times10^{-3}$	$(3.5\pm0.4)\times10^{-3}$	$(4.1\pm0.5)\times10^{-2}$	3.28	ND
50	5	2 Ca^{2+}	57.1	$(1.1\pm0.2)\times10^{-1}$	$(1.7\pm0.4)\times10^{-2}$	$(3.9\pm0.2)\times10^{-3}$	$(1.8\pm0.3)\times10^{-3}$	3.34	ND
50	25	2 Ca^{2+}	14.4	$(1.9\pm0.3)\times10^{-1}$	$(1.7\pm0.5)\times10^{-1}$	$(7.8\pm0.6)\times10^{-5}$	$(6.8\pm0.5)\times10^{-4}$	0.07	0.05
100	1	2 Ca^{2+}	32.5	$(8.2\pm0.6)\times10^{-2}$	$(3.4\pm0.2)\times10^{-3}$	$(1.3\pm0.2)\times10^{-3}$	$(1.6\pm0.1)\times10^{-3}$	4.57	5.3
100	5	2 Ca^{2+}	22.7	$(7.6\pm0.5)\times10^{-2}$	$(6.8\pm0.7)\times10^{-3}$	$(2.3\pm0.3)\times10^{-4}$	$(4.7\pm0.6)\times10^{-4}$	0.79	0.62
100	1	3 Ca^{2+}	33.1	$(1.2\pm0.1)\times10^{-1}$	$(2.7\pm0.2)\times10^{-3}$	$(2.5\pm0.2)\times10^{-3}$	$(3.3\pm0.5)\times10^{-3}$	8.51	ND

[a] Determined by the sum of fitted values of S_{max1} and S_{max2} and using Eq. (4).
[b] Determined from a mass balance calculation of the BTCs and using Eq. (5).
[c] Not determined.

the rate and extent of deposition can also occur on flat surfaces, at surface roughness locations, and grain-grain contacts due to changes in the adhesive and hydrodynamics torques (Kalasin et al., 2010). Figure 5 presents typical SEM images of the NP deposition on the sand surfaces. SEM images reveal significant surface roughness and irregularities, with depressions and grooves having dimensions much larger in scale than the NPs used in the experiments. Greater
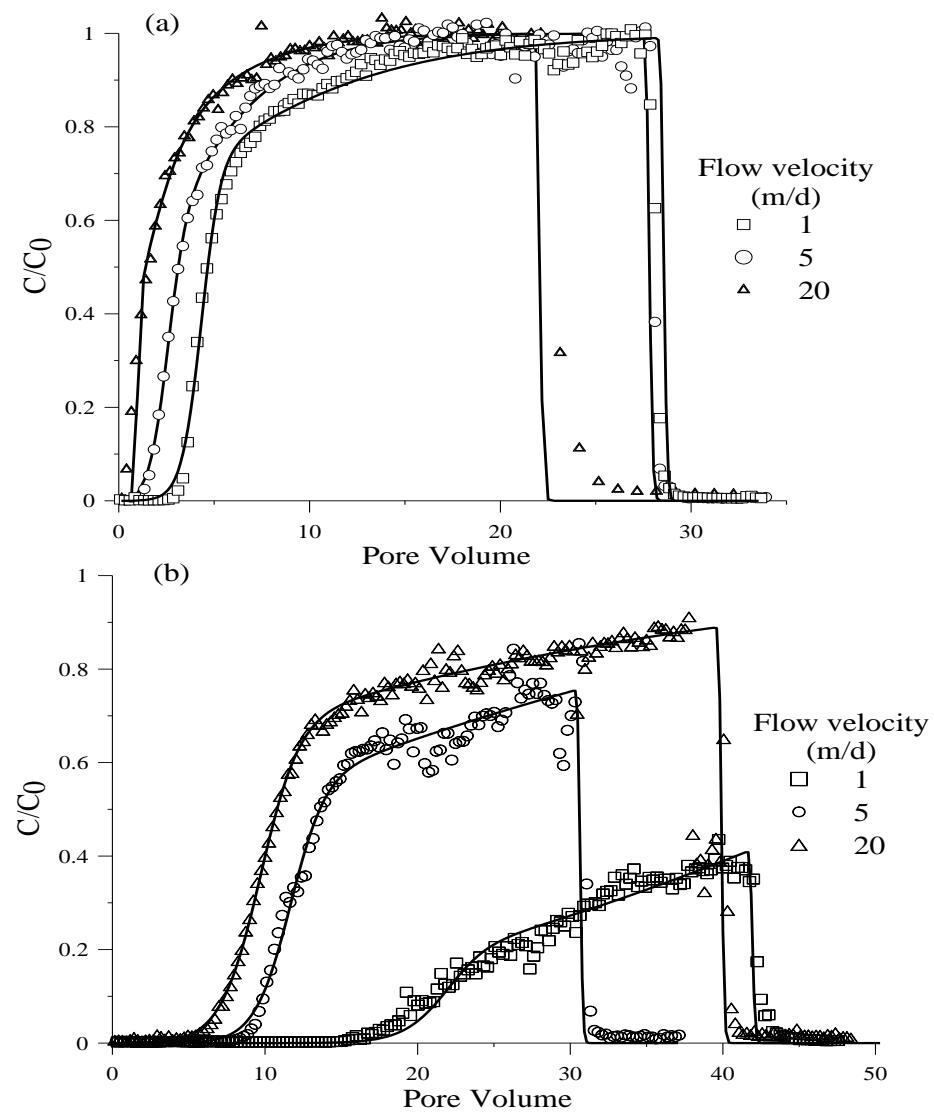
Figure 3. Representative measured and fitted breakthrough curves for 100 nm (a) and 50 nm (b) modified latex nanoparticles obtained from column experiments at 50 mM NaCl and various flow velocities. Table 3 provides summary information on the model parameters.
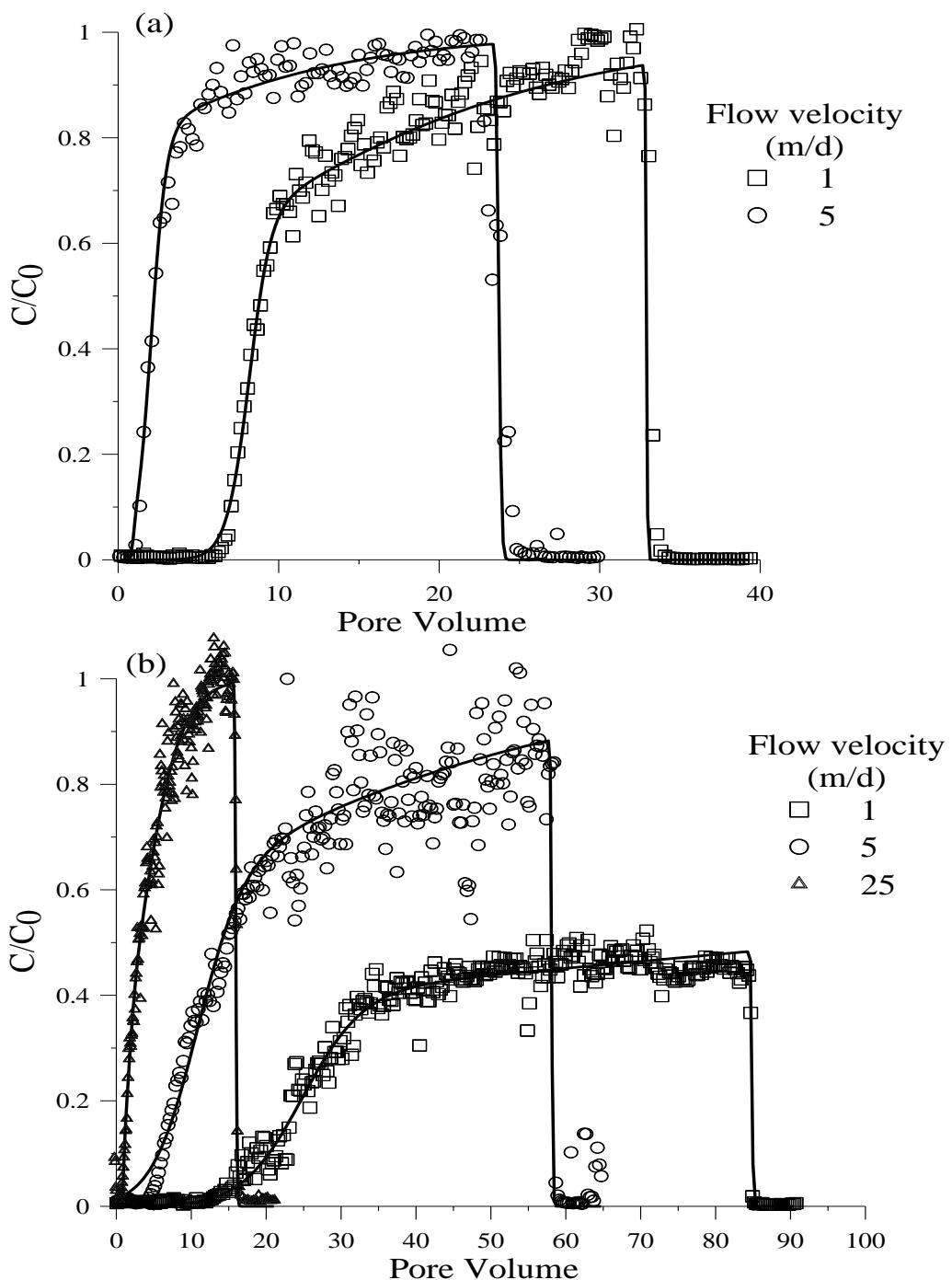
Figure 4. Representative measured and fitted breakthrough curves for 100 nm (a) and 50 nm (b) modified latex nanoparticles obtained from column experiments at 2 mM $CaCl_2$ and various flow velocities. Table 3 provides summary information on the model parameters.

amount of NP deposition occurred on microscopically rough than smooth regions on the sand grains in further support of our two-site modelling approach.

Variations of mass transfer rates of NPs to deposition sites on sand grains may

also contribute to the need for a model with multiple deposition sites. Colloid filtration theory (CFT) predicts that aqueous phase mass transfer of colloidal particles to the collector surface occurs by Brownian diffusion, interception, and sedimentation (Yao et al., 1971). In general, the mass transfer rate varies with distance over the collector surface (Chatterjee et al., 2011). Brownian diffusion is predicted by CFT to be the dominant process of the aqueous phase mass transfer for the NPs, and it is more uniformly distributed over the collector surface than sedimentation or interception. In addition, variations in the sand surface topography affect the rates of mass transfer to specific locations on a sand grain (Chatterjee et al., 2011; Kalasin et al., 2010). These spatial variations in mass transfer have less of an influence on the overall deposition rate under clean-bed conditions than when the selected sites are filled.

In addition, CFT does not account for the potential contribution of solid phase mass transfer and the shadow effect on NP deposition kinetics. Experimental and theoretical results indicate that colloids that are weakly associated with the solid surface via a shallow secondary minimum may translate over the solid surface by hydrodynamic forces to regions where deposition is favourable (Kuznar and Elimelech, 2007; Torkzaban et al., 2010); e.g., regions with greater adhesive forces (chemical heterogeneity) or lower hydrodynamic forces (large scale surface roughness or grain-grain contact). (Malysa et al., 1986) and (Ko and Elimelech, 2000) reported that micro-scale surface roughness or deposited particles can create excluded zones for colloid deposition immediately behind physical barriers. Indeed, (Meinders et al., 1992) and (van de Ven et al., 1994) microscopically studied colloid attachment on glass surfaces in a parallel flow chamber and observed that particle deposition was less probable on areas downgradient of

already deposited particles. It is important to recognise that shadow regions can only be filled up by diffusive transport of NPs from the bulk solution, and not by rolling or translating colloids on unfavourable regions of the collector surface. Figure 6 schematically illustrates a shadow region created down gradient of a surface protrusion due to the combined effects of weak interaction energies on the up-gradient unfavourable regions and hydrodynamic shear forces. It is, therefore, logical to anticipate that solid phase NP transport will contribute to higher values of k_1 than k_2, and that k_2 will be impacted by the shadow effect.
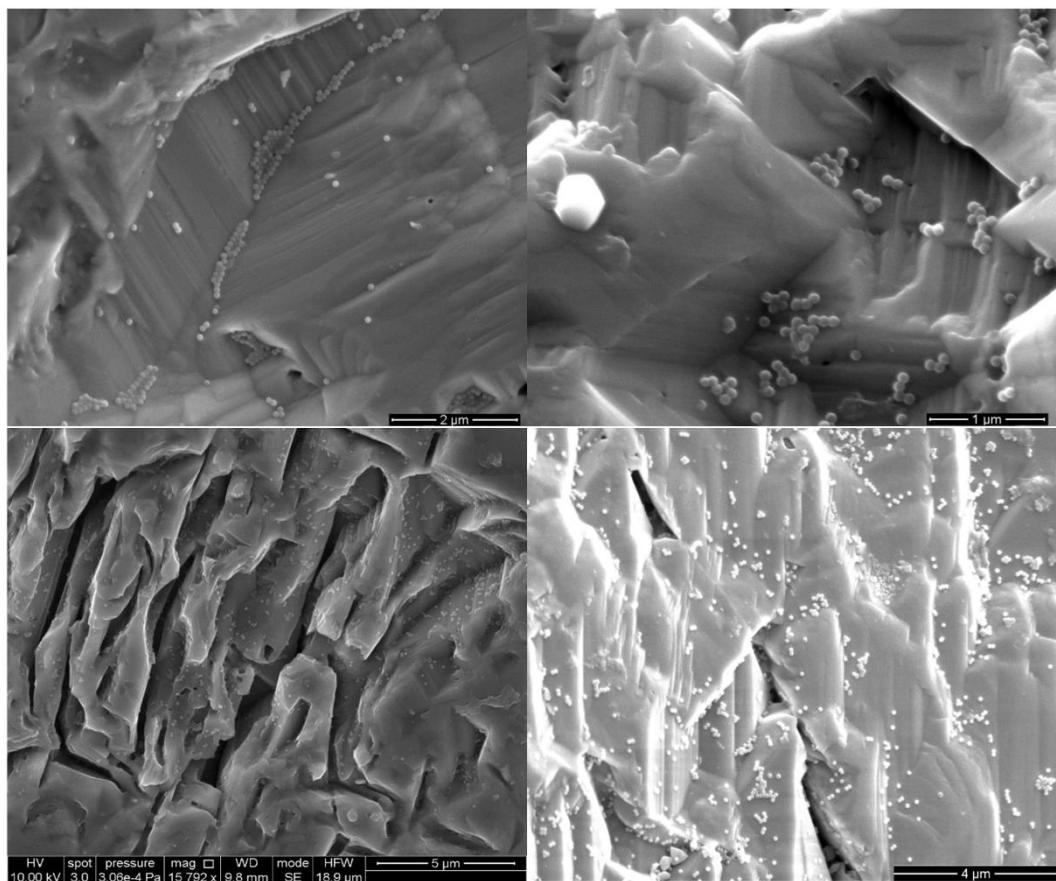
Figure 5. SEM images showing significant surface roughness and irregularities, with depressions and grooves having dimensions much larger in scale than the NPs. Greater amount of NP (100 nm) deposition occurred on depression and groove regions. SEM images were performed for a few sand grains randomly taken from the column at 50 mM NaCl and flow velocity of 1 m day^{-1} following the completion of the deposition experiment in which the effluent NP concentration reached the influent concentration implying that all the deposition sites were filled up.

2.3.3. The effect of solution chemistry

Inspection of Figure 1 reveals that the deposition behaviour is highly dependent on the NP size and IS. In particular, greater amounts of deposition occurred at a higher IS and for the smaller NP (at a given IS). The BTCs were delayed longer and the rising limb approached unity much slower at a higher IS and for the smaller NP size (50 nm). Consistent with this blocking behaviour, Table 3 indicates that S_f increased in a linear manner with IS, and that larger values of S_f were associated with the smaller NP. It is interesting to note that only a small fraction of the solid surface contributed to NP deposition even at the highest IS (60 mM).
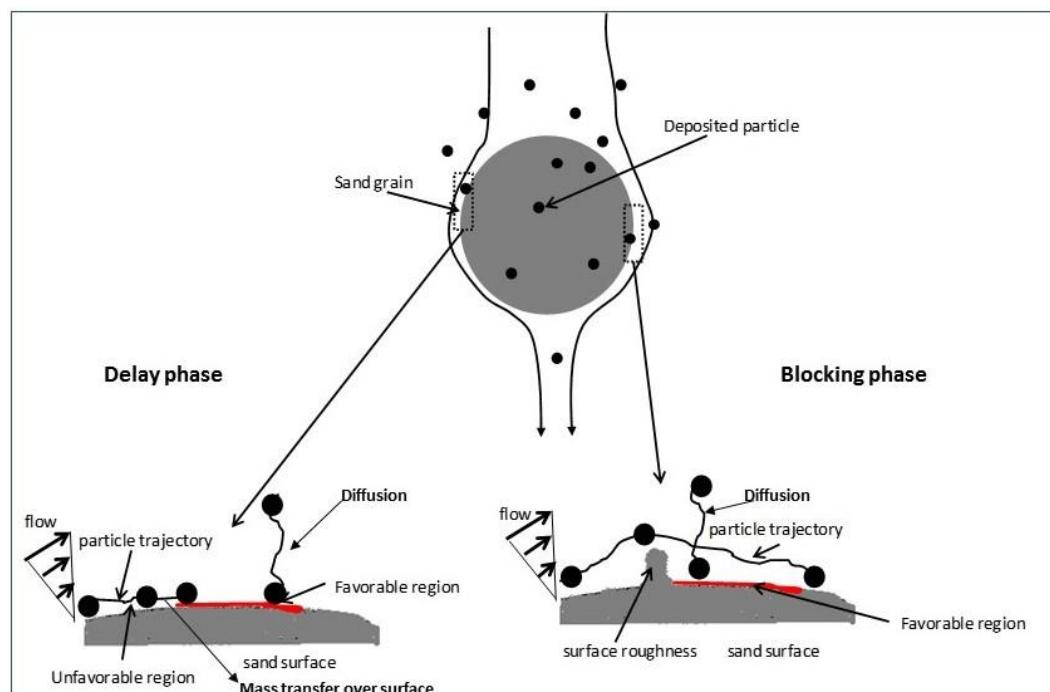
Figure 6. Schematic of the NP attachment process on a sand grain illustrating the process of mass transfer of NPs over the unfavourable regions and NP attachment on the favourable regions (red area); and a favourable site for attachment located in the "shadow region" down gradient of a surface protrusion. Note that the NPs transferred from the up-gradient unfavourable regions cannot land on the favourable region and NP attachment may only occur due to direct diffusion from the bulk solution.

These results are in agreement with experimental and theoretical findings that

indicate that colloid deposition is highly dependent on the size and amount of nanoscale heterogeneity (Duffadar et al., 2009; Duffadar and Davis, 2008; Santore and Kozlova, 2007). (Santore and Kozlova, 2007) experimentally demonstrated that 0.5 μm silica particles attached to net-negative and net-repulsive substrates on which nano-textured positive patches (11 nm) were randomly distributed. Transport experiments and simulations revealed that negative colloids (500–2000 nm) attached to positive patches on negative surfaces at high IS, but not at low IS (Duffadar et al., 2009). Theoretical calculations further demonstrated that the nanoscale physical and/or chemical heterogeneities exerted a greater effect on interaction energies at higher IS and for smaller colloid sizes, and that the energy barrier can be completely eliminated to produce finite primary minimum interactions depending on the relative size of heterogeneity to the NP, density of heterogeneity, and solution IS (Bendersky and Davis, 2011; Bradford and Torkzaban, 2012; Bradford and Torkzaban, 2013; Duffadar and Davis, 2008). The aforementioned results indicate that the size and density of nanoscale heterogeneity plays a critical role on the amount and rate of NP deposition. It should be noted that negligible deposition of NPs was observed when the solution IS was 1 mM NaCl (data not shown), ruling out the importance of micro- and macro-scale positively charged heterogeneities (e.g., patches of metal oxides on the sand surfaces) on the NP deposition at higher IS.

Figure 2 exhibit similar trends to Figure 1 with regard to the effects of IS and NP size. In contrast, greater amounts of deposition occurred in the presence of Ca^{2+} (Figure 2) than Na^+ (Figure 1) at a smaller solution IS. This also produced correspondingly higher values of S_f presented in Table 3. The higher deposition in the presence of Ca^{2+} can be explained by the formation of divalent cation (Ca^{2+})

bridging as described by previous studies (Janjaroen et al., 2010; Roy and Dzombak, 1996; Torkzaban et al., 2012). These studies have reported that complexation of Ca^{2+} ions to the silanol groups on the mineral surfaces and carboxylic acid groups on the surface of the NPs produces localised nanoscale chemical heterogeneities that are favourable for deposition.

2.3.4. The Effect of Flow Velocity

Figures 3 and 4 demonstrate that the delay in the BTCs becomes shorter and NP deposition decreased with increasing flow velocity. Consistent with our observations, CFT predicts that NP deposition decreases with increasing velocity (Schijven and Hassanizadeh, 2000). Table 3 indicates that values of S_f are sensitive to the flow velocity. In particular, higher values of S_f occurred at a lower velocity and for a smaller NP size. These trends may partially be explained by torque balance considerations. In particular, a smaller hydrodynamic torque/force acts on NPs adjacent to the solid surface as the flow velocity decreases and for smaller NP size (Bradford et al., 2013). To further explore the underlying mechanisms, the flow rate was increased to yield a flow velocity of 100 m day^{-1} following the completion of transport experiments at 1 m day^{-1}. If the torque balance was the only factor determining S_f, there should be some NP release when the flow velocity was increased to 100 m day^{-1} because the higher drag force should be sufficient to overcome the resisting adhesive torque leading to NP release. However, the effluent breakthrough concentrations did not show any NP release when the velocity was increased to 100 m day^{-1}. This result indicates the presence of a sizable adhesive torque and/or negligible hydrodynamic torque acting on the deposited NP. Several other explanations have been proposed in the literature for the effect of velocity on NP deposition. These explanations are briefly examined below.

(Ko and Elimelech, 2000) observed that increasing flow velocity decreased S_f at a given IS in packed column experiments. They attributed this observation to larger shadow areas downgradient of deposited particles and protrusions on sand grains. It was postulated that these shadow regions were not accessible for particle deposition at higher velocities. However, diffusive transport is very high for our NPs and particle deposition on regions down gradient of protrusions (shadow areas) should be accessible as quantified by k_2. Therefore, we postulate that the shadow effect or depletion zone only influenced the deposition rates of the NPs and does not affect the values of S_f. Alternatively, assuming that the adhesion strength increases with the residence time can provide a viable explanation for higher S_f values at lower velocities (higher residence time). The adhesion strength of latex particles and bacteria to glass surfaces has been observed to increase with the residence time of the particle on the substrate (Dabroś and van de Ven, 1983; Meinders et al., 1992; Xu and Logan, 2006; Xu et al., 2005). For example, (Xu et al., 2005), using colloid probe atomic force microscopy (AFM) observed that the adhesion force between a latex microsphere and glass surfaces increased with residence time over a range of 0.001–50 s. This observation has been ascribed to progressive removal of interfacial water and/or rearrangement of the functional groups on the surface of latex particles to bridge and then bind to the opposing surface until all bonds reach the lowest energy state. Ageing of the bond between adhering microorganisms and solid surfaces has been documented (Meinders et al., 1995; Wiencek and Fletcher, 1995), and attributed to possible collapse of surface appendages, biosurfactant release, and the metabolic activity of the organisms.

2.4. Conclusions

Spatial and temporal variations in the rate of NP deposition may occur in porous

media for a variety of reasons, including different strengths of interaction energy; enhanced retention in specific locations; spatial variations in NP mass transfer rates to retention locations; and the shadow effect. The influence of multiple rates of deposition may not be apparent on NP BTCs under clean-bed conditions because the retention locations are far from being filled. Conversely, as retention locations are filled, the influence of multiple deposition rates becomes more apparent. Long-term BTCs (25–85 pore volumes) were therefore obtained for (50 and 100 nm) NPs in order to determine their full deposition kinetics under various physicochemical conditions.

The long-term BTCs exhibited a bimodal shape that was successfully simulated using a two-site kinetic model that accounted for irreversible deposition and blocking on each site. Results showed that S_f values (related to the maximum solid concentration of the NPs) were small ($< 9\%$) in an acid-washed sand and controlled by the coupled effects of flow velocity, solution chemistry, and particle size; e.g., increasing with decreasing particle size and flow velocity, and increasing IS. NP deposition was much more pronounced in the presence of Ca^{2+} than Na^+, implying that NP deposition occurred because of physicochemical interactions between the negatively charged COOH groups on the NPs and nanoscale heterogeneities on the sand surface. Our results suggest these NP interactions tended to strengthen with increasing contact time.

Acknowledgment

in the CSIRO Land and Water Laboratory on the Waite Campus, Adelaide, South

Australia.

CHAPTER 3

Temperature Dependency of Virus and Nanoparticle Transport and

Retention in Saturated Porous Media
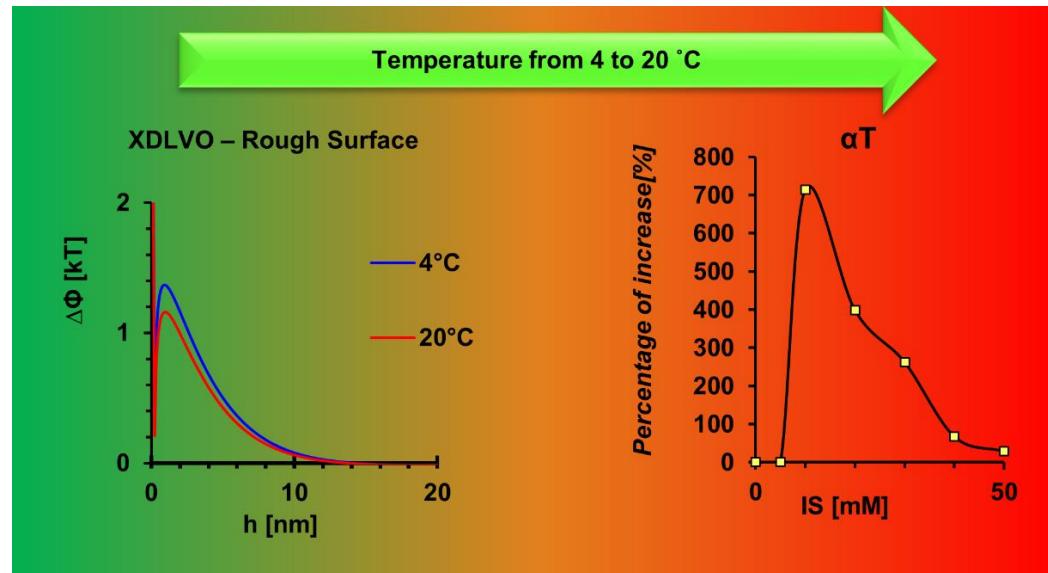
HIGHLIGHTS

- Viruses and latex NP retention dramatically increased with temperature at intermediate IS.
- Temperature had negligible influence on NP retention when the IS was 1 mM or 50 mM.
- XDLVO calculations that included nanoscale heterogeneity explained these observations.
- Simulations accurately described the temperature dependency of retention parameters.

Chapter 3

Abstract

The influence of temperature on virus and nanoparticle attachment was examined in sand-packed columns under various physiochemical conditions. When the solution ionic strength (IS) equalled 10 and 30 mM, the attachment rate coefficient (k_{att}) increased up to 109% and the percentage of the sand surface area that contributed to attachment (S_f) increased up to 160% when the temperature was increased from 4 to 20 °C. Temperature effects at IS = 10 and 30 mM were also dependent on the system hydrodynamics. Conversely, this same temperature increase had a negligible influence on k_{att} and S_f values when IS was 1 mM or greater than 50 mM. An explanation for these observations was obtained from extended interaction energy calculations that considered nanoscale roughness and chemical heterogeneity on the sand surface. Interaction energy calculations demonstrated that the energy barrier to attachment in the primary minimum ($\Delta\Phi_a$) decreased with increasing IS, chemical heterogeneity, and temperature, especially in the presence of small amounts of nanoscale roughness. Temperature had a negligible effect on k_{att} and S_f when the IS = 1 mM because of the large energy barrier, and at IS = 50 mM because of the absence of an energy barrier. Conversely, temperature had a large influence on k_{att} and S_f when the IS was 10 and 30 mM because of the presence of a small $\Delta\Phi_a$ on sand with nanoscale roughness and a chemical (positive zeta potential) heterogeneity. This has large implications for setting parameters for the accurate modelling and transport prediction of contaminants in ground water systems.

Chapter 3

Keywords

Temperature, virus, nanoparticle, retention, surface roughness, XDLVO theory

Nomenclature

k_{att} attachment rate coefficient (day^{-1})

S_f percentage of the sand surface area that contributed to attachment (%)

S_{fT} theoretical values of S_f

$S_{\max 1}$ maximum solid phase concentrations of attached latex NPs on site 1 ($N\,Kg^{-1}$)

$S_{\max 2}$ maximum solid phase concentrations of attached latex NPs on site 2 ($N\,Kg^{-1}$)

C_0 input concentration ($N\,mL^{-1}$)

C effluent concentration ($N\,mL^{-1}$)

C/C_0 relative effluent concentrations

v flow velocity ($m\,day^{-1}$)

A_z zone of influence on the solid-water-interface (nm^2)

f_r nanoscale roughness density (%)

h_r roughness height (nm)

f_+ positive zeta potential fraction (%)

ζ_+ positive zeta potential (mV)

Chapter 3

Greek symbols

η single-collector efficiency

α attachment efficiency

α_T theoretical values of α

$\Phi_1{}^0{}_{min}$ depth of the primary energy minimum (kT)

Φ_{max} height of the energy barrier (kT)

$\Delta\Phi_a$ energy barrier to attachment in the primary minimum (kT)

$\Phi_2{}^0{}_{min}$ depth of secondary energy minimum (kT)

Abbreviation

IS Ionic Strength

XDLVO Extended Derjaguin-Landau-Verwey-Overbeek

NPs Nanoparticles

CFT Colloid Filtration Theory

EDL Electrostatic Double Layer Interaction

vdW van der Waals Interaction

PFU Plaque Forming Unit

BTC Breakthrough Concentrations

EM Electrophoretic Mobility

PV Pore Volumes

Chapter 3

3.1. Introduction

Groundwater may become contaminated with enteric pathogenic viruses from contaminated recharge water sources, such as infiltration beneath septic tanks, leaking sewer pipes, and managed aquifer recharge with treated wastewater and urban stormwater (Da Silva et al., 2011; Torkzaban et al., 2006; You et al., 2005). Additionally, the increasing use of nanotechnology in a wide range of applications and products will inevitably result in the release of engineered nanoparticles into the subsurface environment (Torkzaban et al., 2013; Wiesner et al., 2006). An understanding and ability to predict the fate and transport of viruses and nanoparticles (NPs) in soils and aquifers are therefore very important for protection of human and environmental health. During passage through porous media, various physicochemical and biological factors influence the attachment of viruses and NPs to solid surfaces, which in turn affects their transport in the subsurface environment. Some of these factors include flow velocity (Hijnen et al., 2005), type of virus or NP (Chu et al., 2001; Fang et al., 2013), temperature (Bradford et al., 2006; Castro and Tufenkji, 2007; Chrysikopoulos and Aravantinou, 2014; Gallardo-Moreno et al., 2003; García-García et al., 2006; Kim and Walker, 2009; McCaulou et al., 1995), solution chemistry (e.g., ionic strength, pH, ion type) (Gutierrez et al., 2010; Kim et al., 2009), solid surface roughness (Bradford and Torkzaban, 2013; Torkzaban and Bradford, 2016) and chemical heterogeneities (Johnson et al., 1996). While temperature has been noted to affect transport, little research attention has been given to understanding how the temperature influences the attachment process of viruses and NPs (Chrysikopoulos and Aravantinou, 2014).

Attachment of viruses and NPs to solid surfaces of porous media under saturated conditions is commonly described using colloid filtration theory (CFT). According

to this theory, the attachment rate is dependent on the mass transfer rate of particles from the bulk solution to the collector surface (quantified by the single-collector efficiency, η) and subsequent particle-surface interaction (quantified by the attachment sticking efficiency, α) (Schijven and Hassanizadeh, 2000; Tufenkji and Elimelech, 2004a). Correlation equations have been developed for calculating η as a function of parameters such as flow velocity, viscosity, temperature, diffusion, and particle size. It is predicted that the value of η, and consequently the attachment rate coefficient (k_{att}), increases with temperature due to an increase in the diffusion coefficient (Schijven and Hassanizadeh, 2000; Tufenkji and Elimelech, 2004a; Yao et al., 1971). For example, the value of η increases by about 37 % with an increase in temperature from 4 to 20 °C. However, several studies have reported that the value of k_{att} increased with temperature to a much greater extent than η (Kim and Walker, 2009; McCaulou et al., 1995). For example, (Kim and Walker, 2009) observed that k_{att} for latex microspheres at 25 °C was 173% greater than that at 10 °C. It is, therefore, reasonable to expect that the value of α should also increase with temperature.

The value of α strongly depends on the interaction energy between a particle (e.g., virus and NP) and collector (e.g., sand grain) surface (Shen et al., 2010; Tufenkji and Elimelech, 2004a). Extended Derjaguin-Landau-Verwey-Overbeek (XDLVO) theory predicts that the total interaction energy consists of electrostatic double layer (EDL) and van der Waals (vdW) interactions (Derjaguin, 1941; Verwey, 1947), as well as poorly characterized short-range interactions such as Born, Lewis acid-base, and hydration interactions (Van Oss, 1993; Yoon et al., 1997). The depth of secondary energy minimum ($\Phi_{2\ min}^{0}$) is very small for NPs (Bhattacharjee et al., 1998). Consequently, the value of α for NPs is mainly

controlled by the energy barrier to attachment in the primary minimum ($\Delta\Phi_a$) and the depth of the primary energy minimum ($\Phi_1{}^0{}_{min}$); the value of $\Delta\Phi_a = \Phi_{max} - \Phi_2{}^0{}_{min}$ where Φ_{max} is the height of the energy barrier. The attractive vdW energy is expected to increase with temperature, due to an increase in the Hamaker constant with temperature (Yan et al., 2015). The magnitude of the repulsive EDL energy is predicted to slightly decrease with increasing temperature due to the decrease in the dielectric constant of the solution, surface potentials of the particle and solid surfaces, and the inverse Debye length (Adamczyk, 2006; Galisteo et al., 1990; Yan et al., 2015). Consequently, an increase in temperature may enhance particle attachment in the primary minimum by lowering $\Delta\Phi_a$ to levels that allow a nanoparticle to diffuse over the energy barrier. However, XDLVO theory for homogeneous interacting surfaces commonly predicts the existence of a sizable energy barrier against attachment in the primary minimum (e.g., > 7 kT, where k is the Boltzmann constant and T is the absolute temperature) under unfavorable chemical conditions typical of fresh groundwater (e.g., ionic strength < 10 mM) (Bradford and Kim, 2012; Bradford and Torkzaban, 2013; USGS, 2013). Note that the thermal energy of diffusing particles is considerably less than a few kT with an average of 1.5 kT (Shen et al., 2007). Hence, the energy barrier approach (Bhattacharjee et al., 2000) predicts that a small reduction of $\Delta\Phi_a$ with temperature is unlikely to produce enhanced attachment in the primary minimum when $\Delta\Phi_a$ is large (Bradford et al., 2004). In contrast, a substantial increase in the rate and extent of particle attachment has been experimentally observed when the temperature of the solution was increased by 10 or 20 degrees (Kim and Walker, 2009).

Nanoscale roughness and chemical heterogeneities on grain surfaces have been shown to substantially reduce or eliminate $\Delta\Phi_a$ at some localised locations

under a net-unfavourable condition (Bhattacharjee et al., 1998; Shen et al., 2012a; Suresh and Walz, 1997; Torkzaban and Bradford, 2016). For example, under low ionic strength (< 10 mM) conditions, particle attachment may occur on some localised "favourable" sites that exhibit no repulsion or a shallow energy barrier (a few kT) to attachment in the primary energy minimum (Huang et al., 2009). Therefore, the value of α is proportional to the fraction of the solid surface that is "favourable" for attachment. Indeed, numerous studies have shown that only a small percentage of the surface area of a porous medium is favourable for particle attachment (S_f) under a given chemical condition (Argent et al., 2015; Magal et al., 2011; Sasidharan et al., 2014; Treumann et al., 2014). Therefore, we hypothesise that nanoscale surface roughness and chemical heterogeneity play the main role in enhancing the influence of temperature on NP attachment. Moreover, it is reasonable to expect that the value of S_f would increase with temperature. However, no systematic theoretical and experimental studies have been conducted to investigate the effect of temperature on the value of S_f.

The objective of this study was to experimentally and theoretically investigate the influence of water temperature, coupled with solution chemistry and flow velocity, on the extent and kinetics of virus and NP attachment in a porous medium. For this purpose, two different biotic (PRD1 and ΦX174 viruses) and abiotic (50 and 100 nm carboxyl-modified latex NPs) nanoparticles were employed in this study. The transport experiments were performed at 4 and 20 °C at various solution ionic strength (IS) and flow velocities. Values of k_{att} and S_f were determined by parameter fitting to the observed breakthrough concentrations of the NPs. XDLVO calculations between a chemically and physically heterogeneous collector and homogeneous particle were conducted to explain the observed

enhanced attachment of the viruses and latex NPs at the higher temperature. Specific solution chemistry conditions were identified when temperature-dependent particle transport is expected. Results from this work provide insight into the underlying mechanisms that control the influence of temperature on particle attachment in porous media and have important implications for determining the potential importance of transients in water temperature on virus and nanoparticle fate and transport in the subsurface environment.

3.2. Materials and Method

3.2.1. Electrolyte Solutions and Porous Medium

Electrolyte solutions of 1, 10, 30, and 50 mM NaCl were prepared using analytical grade NaCl and Milli-Q water at pH = 5.5–5.8. Ultra-pure quartz sand (Charles B. Chrystal CO., Inc., NY, USA) with size ranging from 125–300 μm was employed in transport experiments. This sand was cleaned by acid wash and boiling procedure described by (Sasidharan et al., 2014). This idealised quartz sand was selected in order to minimise many of the complexities associated with natural soil and aquifer materials such as organic matter, clay, and metal oxides (Castro and Tufenkji, 2007; Chrysikopoulos and Aravantinou, 2012; Kim and Walker, 2009).

3.2.2. Viruses

Bacteriophage PRD1 and ΦX174 were used in this study. The characteristics of these phages and their production and quantification using the double layer agar (DLA) method are described in our previous study (Sasidharan et al., 2016). The DLA method has a detection limit of around 30 plaque forming unit (PFU) mL^{-1} (10705-2-2000, 2000). Stock solutions of phages were diluted in each electrolyte solution and equilibrated at the experimental temperature (4 and 20 °C)

to obtain an input concentration (C_0) of about 5×10^6 PFU mL^{-1}. The inactivation rate of viruses over a period of 140 h was determined in representative electrolyte solutions at both temperatures and a representative result is given in Figure 8.

3.2.3. Latex Nanoparticles

Carboxyl-modified latex NPs (Polysciences, Inc.) of two different sizes (50 and 100 nm) were used in this study. Stock solutions of 50 and 100 nm NPs were diluted to obtain a C_0 of 1.1×10^{11} and 2.4×1.0^{10} particles mL^{-1}, respectively. The aqueous phase concentrations of NPs were determined using a fluorescence spectrophotometer (Synergy HT, BioTek Instruments, Inc., Winooski, VT, USA) and a calibration curve at an excitation and emission wavelength of 441 nm and 486 nm, respectively. The manufacturer reported that the NPs had a density of 1.05 g cm^{-3}. The detection limit for the 50 and 100 nm latex NPs is $\sim 6.5 \times 10^8$ and $\sim 4.5 \times 10^8$ NPs mL^{-1}, respectively.

3.2.4. Zeta Potential and Size Measurements

The electrophoretic mobility (EM) of latex NPs, viruses, and crushed quartz (< 2 µm) was measured in the electrolyte solutions using a Zetasizer (Malvern, Zetasizer Nano Series, Nano-ZS). The temperature setup option available in the instrument was used to measure the EM at different temperatures. The samples were first equilibrated to the selected temperature (4 and 20 °C) for 10 min and then EM measurements were repeated five times with more than twenty runs per measurement. The Smoluchowski equation (Elimelech et al., 1994) was used to convert the measured EM values to zeta potentials. The changes in fluid properties (viscosity and dielectric constant) at different temperatures were taken into account in these calculations.

The size distribution of the viruses and latex NPs in different electrolyte

solutions and temperatures was measured using a dynamic light scattering (DLS) process (Malvern, Zetasizer Nano Series, Nano-ZS).

3.2.5. Column Transport Experiments

The column experiments were conducted in temperature-controlled laboratories (4 ± 1 and 20 ± 1 °C). Sterilised polycarbonate columns (1.9 cm inside diameter and 5 cm height) were wet-packed using clean quartz sand while the column was being vibrated. After packing, the column was preconditioned with > 10 pore volumes (PV) of a selected electrolyte solution using a syringe pump (Model 22, Harvard Apparatus) at a flow rate of 0.394 mL min^{-1}. The columns were equilibrated to the selected temperature (4 and 20 °C) for 12 h before starting the experiment.

A virus (PRD1 and ΦX174) or latex NP (50 and 100 nm) suspension at selected IS (1, 10, 30, and 50 mM Na$^+$) and temperature (4 or 20 °C) was introduced into the column using a syringe pump at an average pore water velocity of 0.1 or 1 m day^{-1} (velocity more relevant to subsurface environment) for 20 PV (Phase 1). This phase was followed by injection of ~10 PV of particle-free solution at the same IS and temperature (Phase 2). The column effluent samples were collected using a Spectra/Chrom® CF-1 Fraction Collector and the concentration of viruses or latex NPs was quantified using methods explained above. The total mass of retained particles during Phases 1 and 2 (N_{1+2}) was determined by calculating the difference between the mass of injected particles into the column in Phase 1 (N_{in}) and the mass of particles that was recovered in the effluent during Phases 1 and 2 (N_{out}). This information was used to calculate the mass percentage of retained particles (PR) in the column in each experiment.

All experiments were duplicated and the statistical differences of mean

removal efficiencies were identified by one-way ANOVA. The mean removal efficiencies were separated by Tukey's honestly significant difference (HSD) test ($p < 0.05$). All statistical analyses were performed using IBM SPSS Statistics for Windows Version 22.0 (SPSS, 2013).

It should mention that retention profiles for viruses and latex NPs were not determined in this study because of significant amounts of irreversible primary minimum attachment, as well as solid phase inactivation for viruses (Bradford et al., 2006; Bradford et al., 2012). The relative importance of surface straining processes on retention and release decreases for smaller particle size and higher solution ionic strengths (Bradford and Torkzaban, 2015).

3.3. Theoretical Consideration

3.3.1. Breakthrough Curve (BTC) Simulations

The experimental BTCs for viruses and latex NPs were simulated using the Hydrus-1D model (Simunek, 2005). This model allows for advective and dispersive transport, irreversible attachment on site 1, and reversible attachment on site 2. The following aqueous and solid phase mass balance equations were considered in this model:

$$\frac{\partial C}{\partial t} = \lambda v \frac{\partial^2 C}{\partial z^2} - v \frac{\partial C}{\partial z} - r_{att} \tag{1}$$

$$r_{att} = \frac{\rho_b}{\theta} \frac{\partial (S_1 + S_2)}{\partial t} = k_{att1} \psi_1 C + k_{att2} \psi_2 C - \frac{\rho_b}{\theta} k_{det2} S_2 \tag{2}$$

where t (T; T denotes units of time) is time, z (L; L denotes units of length) is the direction of mean water flow, C (NL^{-3}; N denotes number) is the number of viruses or latex NPs per unit volume of the aqueous phase, λ (L) is the dispersivity,

Chapter 3

v (LT^{-1}) is the average pore water velocity, r_{att} (NL^{-3}T^{-1}) is the particle attachment rate to the solid surfaces, ρ_b (ML^{-3}; M denotes units of mass) is the bulk density, θ is the water content, S_1 and S_2 (NM^{-1}) are the solid phase concentrations of particles (viruses or latex NPs) on site 1 and site 2, respectively, k_{att1} and k_{att2} (T^{-1}) are the attachment rate coefficients for site 1 and site 2, respectively, and k_{det2} (T^{-1}) is the detachment rate coefficient for site 2. The parameters ψ_1 and ψ_2 are dimensionless Langmuirian blocking functions that are given as (Adamczyk et al., 2013):

$$\psi_1 = \left(1 - \frac{S_1}{S_{\max 1}}\right) \qquad and \qquad \psi_2 = \left(1 - \frac{S_2}{S_{\max 2}}\right) \tag{3}$$

where $S_{\max 1}$ and $S_{\max 2}$ (NM^{-1}) are the maximum solid phase concentrations of attached latex NPs on site 1 and site 2, respectively. As it will be shown, negligible detachment was observed for the latex NPs, and therefore the value of k_{det2} was set to zero for the latex NP simulations. Blocking was not observed in the BTCs of viruses. The C_0 of viruses is ~10^5 times smaller than that for the latex NPs. Considering the smaller size and attachment rate for viruses, the time that it takes for viruses to fill S_f will be ~10^5 times longer. Therefore, blocking was neglected for viruses by setting ψ_1 and ψ_2 to 1. Solid and liquid inactivation of viruses was found to be negligible over the relatively short duration of these transport experiments (Figure 8) and therefore, all the removal was attributed to attachment.

The total value of k_{att} and S_{max} for the viruses and latex NPs were defined as $k_{att1}+k_{att2}$ and $S_{max1}+S_{max2}$, respectively. The value of α was calculated from k_{att} using filtration theory as (Schijven and Hassanizadeh, 2000; Yao et al., 1971):

$$\alpha = \frac{2d_c k_{att}}{3(1-n)v\eta} \tag{4}$$

71

where n is the porosity (0.4), d_c (L) is the collector diameter and v (LT^{-1}) is the flow velocity. Many correlations have been developed to predict η (Ma et al., 2013; Schijven and Hassanizadeh, 2000; Tufenkji and Elimelech, 2004a; Yao et al., 1971). However, when the flow velocity is very low (e.g. ~0.1 md^{-1} that is more typical to groundwater flow), some of these correlations predict a η value that is greater than one, which is physically questionable (Ma et al., 2013). (Messina et al., 2015) have recently developed a correlation equation for predicting η to overcome this shortcoming. This correlation equation was therefore employed to determine the value of η in this study.

The value of S_f was calculated from S_{max} as (Kim et al., 2009):

$$S_f = \frac{A_c \rho_b S_{max}}{(1-\gamma)A_s} 100 \tag{5}$$

where A_c (L^{2}N^{-1}) is the cross sectional area of a particle, A_s (L^{-1}) is the solid surface area per unit volume, and γ is the porosity of a monolayer packing of particles on the solid surface (0.5) (Johnson and Elimelech, 1995; Sasidharan et al., 2014).

3.3.2. XDLVO Interaction Energy Calculations

The surface element integration (SEI) technique (Bhattacharjee and Elimelech, 1997) was utilised to calculate the total interaction energy between a particle and collector of homogeneous surfaces with the following components:

$$\Phi_{Total} = \Phi_{vdW} + \Phi_{EDL} + \Phi_{BR} \tag{6}$$

where Φ_{Total} (ML^{2}T^{-2}) is the total interaction energy, Φ_{vdW} (ML^{2}T^{-2}) is the van der Waals interaction, Φ_{EDL} (ML^{2}T^{-2}) is the electrostatic double layer interaction, and Φ_{BR} (ML^{2}T^{-2}) is the interaction due to Born repulsion. The value of Φ_{vdW} was

determined from the expression of (Gregory, 1981). The Hamaker constant for each particle-water-quartz system was determined by including the temperature dependency of the refractive index and the dielectric constant as explained in detail by (Yan et al., 2015). A combined Hamaker constant value of 6.5×10^{-21} (4 °C) and 6.8×10^{-21} (20 °C) J for the latex NP-water-quartz system, and 4.04×10^{-21} (4 °C) and 4.24×10^{-21} (20 °C) J for the virus-water-quartz system was calculated in this study. The value of Φ_{EDL} was calculated using the Hogg-Healy-Fuerstenau expression (Hogg et al., 1966) with zeta potentials in place of surface potentials. The value of Φ_{BR} was calculated using the approach of (Ruckenstein and Prieve, 1976) by setting the collision diameter at 0.21 nm to achieve a primary minimum depth at 0.157 nm (Van Oss et al., 1988).

Natural solid surfaces like sand grains always contain a wide distribution of physical (roughness) or chemical (e.g. metal oxides) heterogeneities. The interaction energy between a homogenous particle and a heterogeneous collector was calculated by assuming that the zone of influence (A_z) on the solid-water-interface contained nanoscale chemical and physical heterogeneities. Each A_z was assumed to contain a nanoscale roughness density (f_r) of 1–10% with a height (h_r) = 1–20 nm and a positive zeta potential fraction (f_+) of 1–10% with a positive zeta potential (ζ_+) of 1–10 mV. The value of interaction energy (Φ) within A_z was subsequently quantified using a linear combination of interaction energies associated with nanoscale heterogeneities and the homogenous surface as explained by (Bradford and Torkzaban, 2015). Theoretical values of α and S_f (α_T and S_{fT}) were calculated as the average of 10,000 A_z realisations using the approach described by (Bradford and Torkzaban, 2015).

3.4. Results and Discussion

3.4.1. Interaction Energy for Homogenous Surfaces

Table 4 presents the measured zeta potential values of the viruses, latex NPs, and sand for the various IS and temperature conditions. Zeta potentials of all surfaces were negatively charged at the pH of the experiments (5.5–5.8) and as expected, become less negative with increasing IS. Note that the zeta potential values for a given surface and IS were nearly identical (± 4 mV) at the two temperature of 4 and 20 °C (Table 4). Hence, an increase in the temperature from 4 to 20 °C did not significantly influence the electrokinetic properties of the viruses, latex NPs and sand. It is worth mentioning that temperature has been reported to have variable effects on the electrokinetic properties of solid surfaces (Castro and Tufenkji, 2007; García-García et al., 2009; Ishido et al., 1983; Reppert and Morgan, 2003; Rodríguez and Araujo, 2006). A few studies reported that zeta potentials of various materials become more negatively charged with increasing temperature from 4 to 50 °C (0.012–0.5 per °C) (Kim and Walker, 2009; Rodríguez and Araujo, 2006). Other researchers, however, found that increasing temperature from 4 to 40 °C resulted in a decrease in the magnitude of the zeta potentials (0.16–0.25 per °C) (Dhont and Briels, 2008; Freitas and Müller, 1998; Galisteo et al., 1990). (Castro and Tufenkji, 2007) reported that the dissociation constant of certain acidic and basic groups can be sensitive to temperature, whereas other functional groups such as –COOH are insensitive to temperature. Variations in the surface functional groups present on the various colloid surfaces may explain the observed discrepancies in zeta potential value with temperature. The average size of the

Table 4. The measured values of zeta potential for latex NPs (50 and 100 nm), viruses (ΦX174 and PRD1) and quartz sand in a given electrolyte solution at temperature 4 and 20 °C. The average zeta potential values were used for the XDLVO interaction energy calculation

Particle	IS	Temperature	Zetapotential	Average Zetapotential
	[mM]	[°C]	[mV ± STDV[a]]	[mV ± STDV[a]]
50 nm (NP)	1	4	-47 ± 1.7	-48 ± 1.5
		20	-49 ± 1.0	
	10	4	-41 ± 1.2	-40 ± 1.7
		20	-40 ± 2.4	
	30	4	-35 ± 1.5	-35 ± 1.3
		20	-35 ± 1.3	
	50	4	-25 ± 1.3	-25 ± 0.9
		20	-25 ± 0.5	
100 nm (NP)	1	4	-51 ± 2.1	-51 ± 1.4
		20	-51 ± 0.6	
	10	4	-48 ± 1.0	-47 ± 1.8
		20	-46 ± 2.4	
	30	4	-39 ± 1.5	-40 ± 2.5
		20	-41 ± 3.1	
	50	4	-32 ± 1.1	-31 ± 2.6
		20	-30 ± 3.3	
PRD1 (63 nm)	1	4	-38 ± 1.1	-37 ± 1.7
		20	-35 ± 1.4	
	10	4	-31 ± 2.0	-33 ± 2.2
		20	-34 ± 1.0	
	50	4	-21 ± 3.6	-20 ± 3.1
		20	-19 ± 2.5	
ΦX174 (27 nm)	1	4	-36 ± 1.5	-36 ± 1.6
		20	-35 ± 2.0	
	10	4	-29 ± 2.0	-30 ± 1.8
		20	-30 ± 1.5	
	50	4	-17 ± 1.6	-17 ± 1.7
		20	-16 ± 2.2	
Quartz	1	4	-39 ± 1.5	-38 ± 2.4
		20	-38 ± 3.3	
	10	4	-28 ± 2.2	-27 ± 1.5
		20	-27 ± 0.8	
	30	4	-23 ± 1.5	-23 ± 1.2
		20	-24 ± 1.1	
	50	4	-15 ± 0.5	-15 ± 0.7
		20	-16 ± 0.4	

[a] STDEV = Standard deviation

viruses and the latex NPs for the various IS and a temperature conditions was very stable; $\Phi X174 = 27 \pm 3.5$ nm, PRD1 = 63 ± 3.9 nm, 50 nm latex = 50 ± 3.6, and 100 nm latex = 100 ± 4.9 nm. This data indicates that the colloidal suspensions were not aggregating under the considered experimental conditions. Measured average zeta potentials at both temperatures (Table 4) and average particle sizes were therefore used for subsequent XDLVO calculations.

The interaction energy profile of latex NPs and viruses on approach to a physically and chemically homogeneous quartz surface was calculated using XDLVO theory. The height of the energy barrier to attachment in the primary minimum ($\Delta\Phi_a = \Phi_{max} - \Phi_{2^0min}$) is given in Table 5 for all the IS and temperature conditions. As expected, the height of $\Delta\Phi_a$ decreased with increasing IS and decreasing particle size. At IS = 50 mM, the energy barrier is completely eliminated because of the relatively low zeta potentials of the sand and particles. The magnitude of $\Delta\Phi_a$ slightly decreased with increasing temperature when the IS < 50 mM due to the increase in the attractive van der Waal interaction; i.e., the Hamaker constant was greater at a higher temperature (Yan et al., 2015) and the electrostatic repulsion was reduced due to the decrease in Debye-length (κ^{-1}) with temperature ($\kappa^{-1} = 3.06$ nm at 4 °C and $\kappa^{-1} = 3.04$ nm at 20 °C). However, a sizable $\Delta\Phi_a$ (> 7 kT) was predicted for all particles at both temperatures when IS < 50 mM, which, in principle, should inhibit primary minimum attachment of the particles to sand surfaces (Torkzaban and Bradford, 2016; Tufenkji and Elimelech, 2005a). It should be mentioned that the depth of the Φ_{2^0min} was smaller than ~0.5 kT under all conditions (Table 6), indicating that attachment in the Φ_{2^0min} was highly unlikely (Tufenkji and Elimelech, 2005a).

Table 5. Calculated values of the energy barrier to attachment in primary minimum $(\Delta\Phi_a = \Phi_{max} - \Phi_{2\ min}^{0})$ for 50 and 100 nm latex NPs and viruses (ΦX174 and PRD1).

Particle	IS	Temperature	$\Delta\Phi_a = \Phi_{max} - \Phi_{2\ min}^{0}$ Homogeneous[a]	$\Delta\Phi_a = \Phi_{max} - \Phi_{2\ min}^{0}$ Physically and chemically heterogeneous[b]
	[mM]	[°C]	[kT ± STDV[c]]	[kT ± STDV[c]]
50 nm (NP)	1	4	33 ± 0.7	13 ± 0.2
		20	29 ± 0.5	11 ± 0.4
	10	4	23 ± 0.6	1.0 ± 0.06
		20	20 ± 0.1	0.9 ± 0.03
	30	4	14 ± 0.1	0.5 ± 0.09
		20	11 ± 0.6	0.4 ± 0.08
	50	4	2.0 ± 0.07	0.1 ± 0.09
		20	1.1 ± 0.09	0
100 nm (NP)	1	4	101 ± 0.8	27 ± 0.8
		20	88 ± 0.9	24 ± 0.9
	10	4	59 ± 0.1	2.6 ± 0.03
		20	50 ± 0.7	2.2 ± 0.02
	30	4	31 ± 0.8	1.2 ± 0.06
		20	26 ± 0.4	1.0 ± 0.03
	50	4	6.1 ± 0.05	0.2 ± 0.01
		20	4.0 ± 0.07	0.1 ± 0.03
PRD1 (63 nm)	1	4	40 ± 0.9	13 ± 0.2
		20	35 ± 0.7	11 ± 0.4
	10	4	28 ± 0.8	1.3 ± 0.09
		20	24 ± 0.6	1.1 ± 0.07
	50	4	2.1 ± 0.09	0.1 ± 0.01
		20	2.0 ± 0.02	0.07 ± 0.001
ΦX174 (27 nm)	1	4	11 ± 0.1	5.3 ± 0.02
		20	10 ± 0.3	5.1 ± 0.01
	10	4	8.8 ± 0.02	0.5 ± 0.03
		20	7.5 ± 0.01	0.4 ± 0.05
	50	4	1.3 ± 0.02	0.06 ± 0.001
		20	1.2 ± 0.02	0.04 ± 0.001

[a] smooth sand surface.

[b] physically and chemically heterogeneous sand surface. The physical and chemical heterogeneity parameters used for calculations are f_r = 5%, h_r = 20 nm, f_+ = 10% and ζ_+ = 1 mV

[c] STDV = Standard deviation

Table 6. The calculated values of depth of secondary minimum to attachment ($\Phi_2{}^0{}_{min}$) for latex NPs (50 and 100 nm) and viruses (ΦX174 and PRD1) using the zeta potential values presented in Table 4.

Particle	IS	Temperature	Depth of $\Phi_2{}^0{}_{min}$ Homogeneous[a]	Depth of $\Phi_2{}^0{}_{min}$ Physically and chemically heterogeneous[b]
	[mM]	[°C]	[kT]	[kT]
50 nm (NP)	1	4	0	-0.0001
		20	0	-0.0009
	10	4	0	-0.025
		20	-0.0005	-0.026
	30	4	-0.113	-0.049
		20	-0.121	-0.051
	50	4	-0.321	-0.075
		20	-0.345	-0.077
100 nm (NP)	1	4	0	0
		20	0	-0.001
	10	4	-0.055	-0.049
		20	-0.058	-0.050
	30	4	-0.277	-0.097
		20	-0.291	-0.099
	50	4	-0.638	-0.142
		20	-0.675	-0.146
PRD1 (63 nm)	1	4	0	0
		20	0	0
	10	4	-0.008	-0.018
		20	-0.009	-0.019
	50	4	-0.233	-0.554
		20	-0.249	-0.057
ΦX174 (27 nm)	1	4	0	0
		20	0	0
	10	4	0	-0.008
		20	0	-0.008
	50	4	-0.069	-0.023
		20	-0.077	-0.024

[a] smooth sand surface

[b] physically and chemically heterogeneous sand surface. The physical and chemical heterogeneity parameters used for calculations are $f_r = 5\%$, $h_r = 20$ nm, $f_+ = 10\%$ and $\zeta_+ = 1$ mV

3.4.2. Retention of Viruses and latex NPs in Column Experiments

Figure 7 shows representative observed and fitted BTCs for PRD1 and ΦX174 when $v = 0.1$ m day^{-1}, IS = 10 and 50 mM, and temperature = 4 and 20 °C. Here, the relative effluent concentrations (C/C_0; where C is the effluent and C_0 is the

Chapter 3

influent concentration) were plotted on a logarithmic scale as a function of PV. Tables 7 and 8 presents values of mass retained for the viruses (log scale) and replicate experimental results, respectively. The BTCs showed negligible virus retention when the viruses were suspended in 1 mM solution at both temperatures (Table 8). Figure 7 shows that virus retention dramatically increased with increasing IS at a given temperature. For example, more than 2 logs (> 99%) of the injected viruses were retained in the column when IS was 10 mM. Furthermore, the BTCs exhibited a plateau during the 10 PVs of virus injection, implying that filling of available attachment sites was minimal and, therefore, did not affect the kinetic of the attachment process in these experiments. It is interesting to observe that increasing temperature from 4 to 20 °C did not have much of an effect on the BTCs when the IS was 50 mM. In contrast, the BTCs were dependent on temperature when the IS was 10 mM. Notably, about one log (90%) more virus retention occurred at 20 °C than 4 °C when the IS was 10 mM.

Fitted values of the model parameters (i.e., k_{att1}, k_{att2}, and k_{det2}) and the Pearson's correlation coefficient (R^2) for the two viruses in each experiment are given in Table 7. The low detection limit for viruses (~30 viruses mL^{-1}) facilitated the accurate determination of model parameters. Values of k_{att1} were found to be more than one order of magnitude greater than those of k_{att2} ($p < 0.0007$) and, therefore, interaction with site 1 accounted for almost 100% of the virus retention (see Table 7). Hence, the values of k_{att1} were used to compare the kinetics of virus attachment at various conditions. Table 7 shows that the average value of k_{att1} for

Table 7. Experimental conditions and the values of fitted parameters for viruses

Virus	Temperature	IS	Mass retained	k_{att1}	Percentage increase of k_{att1}	k_{att2}	k_{det2}	R^2	η	Percentage increase of η	α	Percentage increase of α
	[°C]	[mM]	[log]	[day⁻¹]	[%]	[day⁻¹]	[day⁻¹]	[%]		[%]		[%]
ΦX174	20 4	10	3.3 1.8	16 ± 0.7 9 ± 0.2	80.8	0.5 ± 0.09 1.6 ± 0.02	0.9 ± 0.03 0.5 ± 0.05	78.3 74.1	0.71 0.65	8.3	0.07 0.05	47.1
	20 4	50	4.7 4.7	25 ± 0.2 25 ± 0.1	0.63	1.6 ± 0.2 1.7 ± 0.03	1.4 ± 0.4 0.5 ± 0.04	87.1 80.4	0.71 0.65	8.3	0.11 0.11	0
PRD1	20 4	10	3.1 1.3	17 ± 0.3 8 ± 0.2	109.7	3.8 ± 0.09 0.4 ± 0.03	1.4 ± 0.08 0.6 ± 0.04	80.2 83.4	0.60 0.54	12.4	0.10 0.04	117.4
	20 4	50	4.6 4.6	24 ± 0.7 23 ± 0.8	3.9	9.2 ± 0.03 7.9 ± 0.09	2.3 ± 0.01 2.1 ± 0.01	82.7 84.4	0.60 0.54	12.4	0.16 0.16	0

Table 8. The mass balance data for the experiment conducted at IS = 1 mM and selected replicate experiment for viruses (ΦX174 and PRD1).

Virus	Velocity	IS	Temperature	Mass Retained
	[m day^{-1}]	[mM]	[°C]	[log]
ΦX174	0.1	1	20	0.09
			4	0.1
		10	20	3.6
				3.3
			4	1.7
				1.8
PRD1	0.1	1	20	0.05
			4	0.04
		10	20	2.9
				3.1
			4	1.5
				1.3

ΦX174 **(A)**

PRD1 **(B)**

Figure 7. Observed effluent concentrations (marker) and corresponding model fits (solid line) for representative effluent concentrations of viruses (A) ΦX174 and (B) PRD1 for experiments conducted at temperature = 4 and 20 °C, IS = 10 and 50 mM Na^+ and flow velocity = 0.1 m day^{-1}. Table 7 provides the values of fitted parameters ($k_{att\ 1}$, $k_{att\ 2}$ and k_{det2}). The BTCs showed negligible virus retention when the viruses were suspended in a solution with IS = 1 mM (Mass balance data is presented in Table 8).

both viruses increase with IS, suggesting that electrostatics dominated virus attachment. The average value of k_{att} for ΦX174 was regularly greater than those of PRD1 over the range of IS, consistent with the isoelectric point value of 6.6 for ΦX174 compared with that of 3.4 for PRD1 (Sasidharan et al., 2016). Similar to the observed BTCs, values of k_{att1} only showed a significant sensitivity ($p < 0.0001$) to

temperature when the IS was 10 mM. Specifically, the average values of k_{att1} at 20 °C were 80 and 109% higher than those at 4 °C for ΦX174 and PRD1, respectively. Our experimental observations were consistent with previous studies (Chrysikopoulos and Aravantinou, 2014; Gharabaghi et al., 2015; Kim and Walker, 2009; McCaulou et al., 1995). For example, (Kim and Walker, 2009) reported that the k_{att} value for latex microspheres increased by 173% when the temperature increased from 10 to 25 °C. Values of η are presented in Table 7 to show the contribution of temperature on mass transfer. It is observed that the increase in temperature from 4 to 20 °C resulted in an increase in η by only ~8–12% (Table 7). This increase in η with temperature, therefore, cannot fully explain the observed increase in the value of k_{att1} (80–109%) when the IS = 10 mM. As a result, it is concluded that the value of α should have also increased with temperature. Indeed, Eq. (4) predicts that α increased by ~47 and 117% for ΦX174 and PRD1, respectively, when the temperature increased from 4 to 20 °C. This substantial increase in α at higher temperature suggests that the probability of overcoming the energy barrier was higher for viruses when the temperature increased from 4 to 20 °C. It should be mentioned that the survival test of viruses at the experimental conditions and duration confirmed a stable virus concentration (i.e., negligible inactivation, Figure 8). There was a slight difference between the measured virus concentration between the 4 and 20 °C but the difference was less than 0.02 log. Therefore, it is confirmed that the observed enhanced retention was due to the influence of temperature on k_{att} rather than on inactivation rate coefficient.

In order to understand the effect of temperature on the retention of abiotic colloids, additional transport experiments were conducted using the latex NPs (50
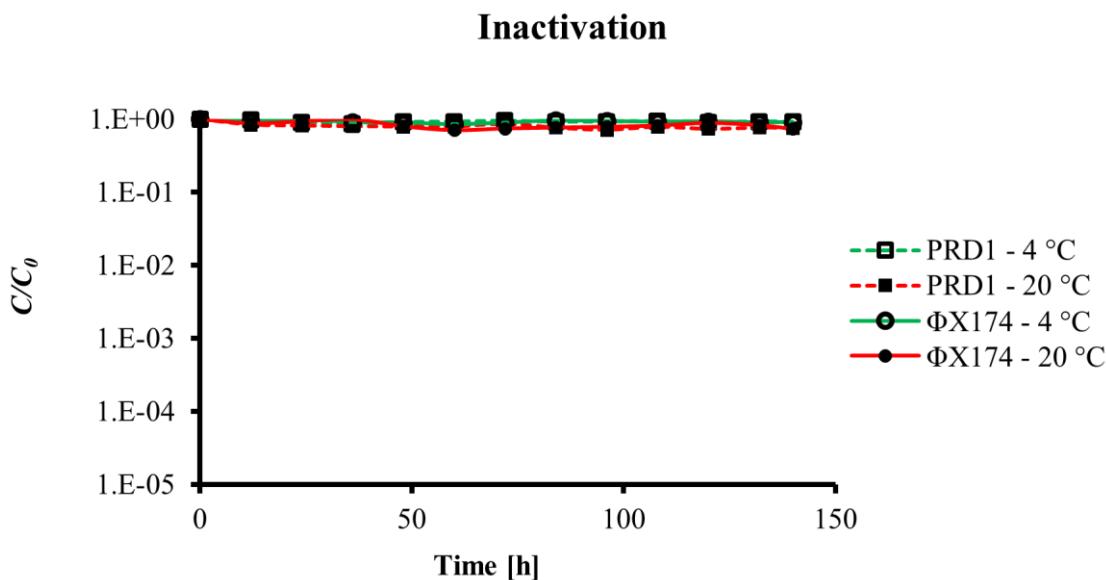
Inactivation

Figure 8. The figure shows the measured inactivation of viruses (ΦX174 & PRD1) in the representative electrolyte solution (IS = 50 mM) at temperature 4 and 20 °C for the experiment duration (140 hours).

and 100 nm) at 4 and 20 °C for various IS and flow velocity values. Figure 9 and 10 present the observed and simulated BTCs for these experiments. Tables 9 and 10 provide values of mass percentage of retained particles and replicate information for the latex NPs experiments, respectively. Similar trends to those of viruses were observed in these experiments, that is, an enhanced latex NP retention was only observed at the higher temperature at intermediate IS conditions (i.e., when the IS was 10 and 30 mM). Comparison of Figures 9 and 10 at the IS of 10 and 30 mM and the corresponding values of PR (Table 9) indicates that the relative importance of temperature on particle retention was also a function of the flow velocity. Results show that the increase in the PR with temperature for the IS of 10 and 30 mM was greater when the flow velocity was lower. These observations collectively demonstrate a coupled effect of IS, flow velocity, and temperature on latex NP retention in porous media.

50 nm **(A)**

50 nm **(B)**
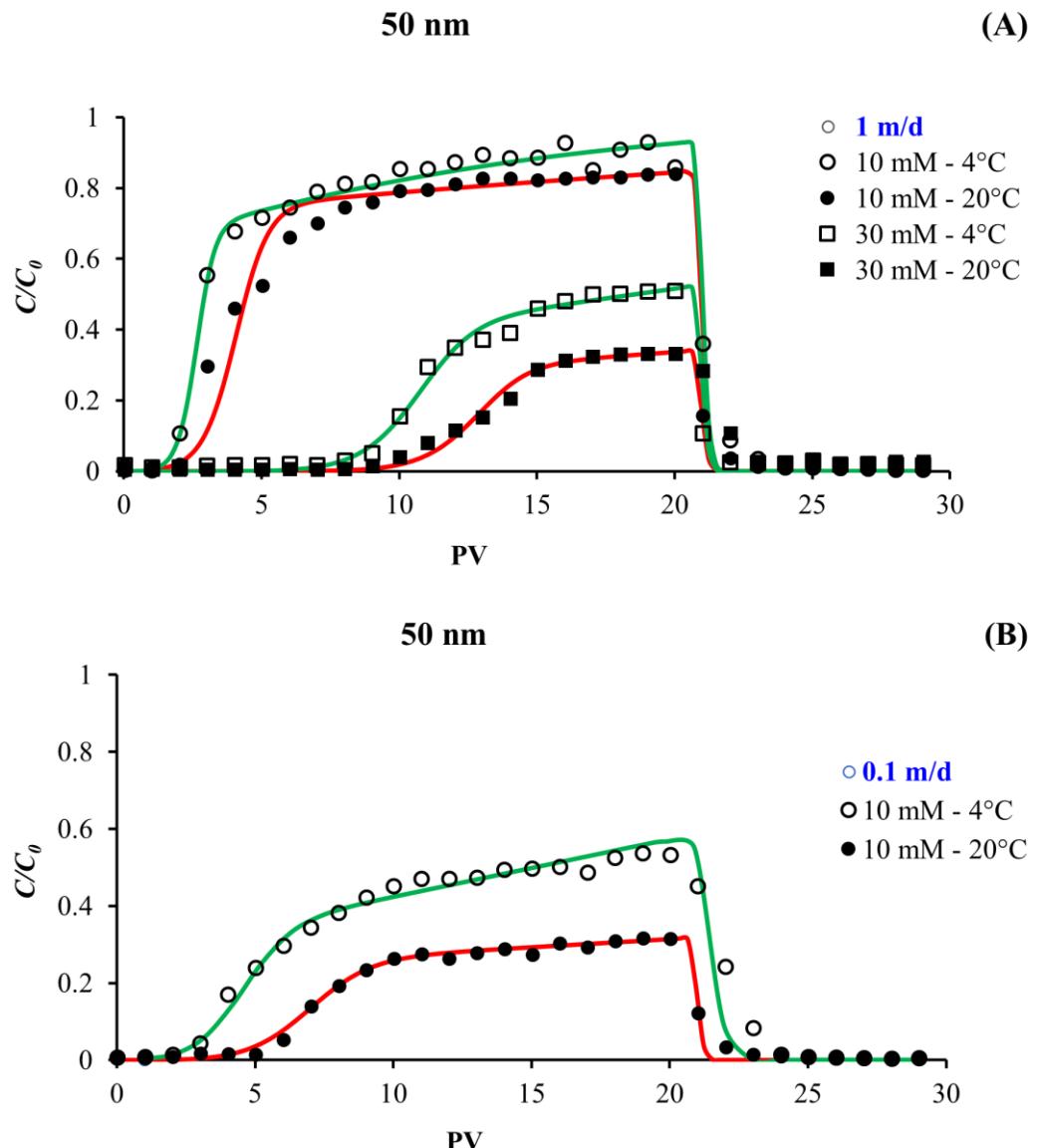
Figure 9. Observed effluent concentrations (marker) and corresponding model fits (solid line) for representative effluent concentrations of 50 nm latex NPs for experiments conducted flow velocity (A) 1 m day^{-1} and (B) 0.1 m day^{-1}, temperature = 4 and 20 °C, and IS = 10 and 30 mM Na$^+$ and. Table 9 provides the values of fitted parameters ($k_{att\ 1}$, $k_{att\ 2}$ and S_{max}).
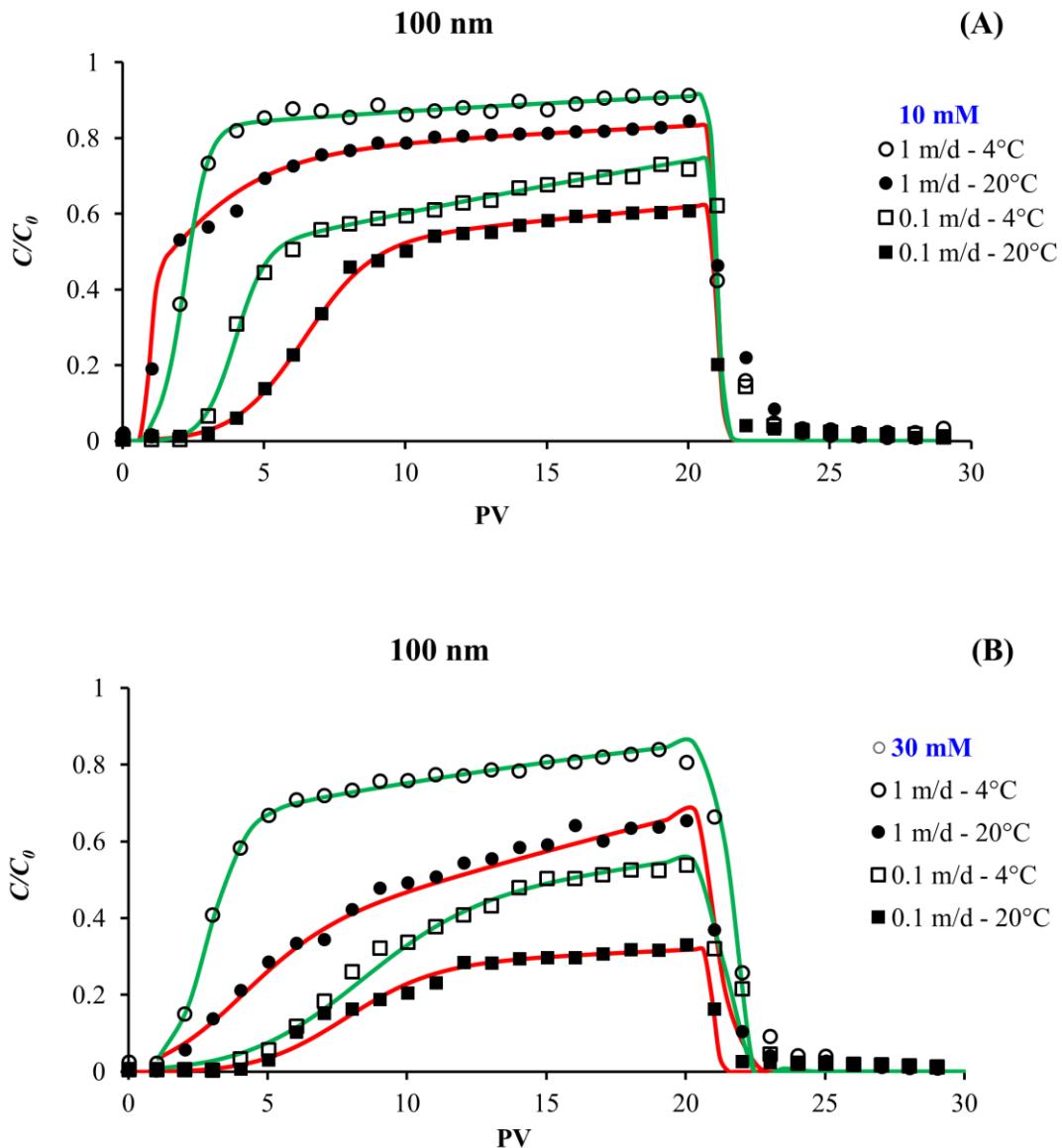
Figure 10. Observed effluent concentrations (marker) and corresponding model fits (solid line) for representative effluent concentrations of 100 nm latex NPs for experiments conducted at IS (A) 10 mM and (B) 30 mM Na^+, temperature = 4 and 20 °C, and flow velocity = 0.1 and 1 m day^{-1}. Table 9 provides the values of fitted parameters ($k_{att\ 1}$, $k_{att\ 2}$ and S_{max}).

Fitted values of k_{att1}, k_{att2}, S_{max1}, and S_{max2} for the latex NPs under various experimental conditions are presented in Table 9. Note that the values of fitted parameters are not presented when latex NP retention was negligible (IS = 1 mM) or when breakthrough concentrations were below the detection limit (IS = 50 mM). The goodness of fit for the IS of 10 and 30 mM simulations confirmed the

Table 9. Experimental conditions, the percentage of mass retained (PR) and values of fitted parameters for 50 and 100 nm latex NPs.

NP	Temperature	IS	Velocity	PR	k_{att1}	k_{att2}	S_{max}	R^2	S_f	Percentage increase of S_f	η	Percentage increase of η
[nm]	[°C]	[mM]	[m day^{-1}]	[%]	[day^{-1}]	[day^{-1}]	[No Kg^{-1}]	[%]	[%]	[%]		[%]
50	20	10	1	33 ± 3.2	123 ± 0.4	6 ± 0.2	2.7 × 10^{14}	99.7	5.1	108.5	0.30	25.1
	4			23 ± 1.9	122 ± 0.7	8 ± 0.1	1.3 × 10^{14}	99.5	2.4		0.24	
	20	10	0.1	79 ± 1.5	19 ± 0.4	2 ± 0.8	1.8 × 10^{15}	99.8	33.4	159.6	0.63	11.1
	4			59 ± 2.1	8 ± 0.2	1 ± 0.9	7.0 × 10^{14}	95.2	12.9		0.57	
	20	30	1	84 ± 3.9	442 ± 0.5	27 ± 0.9	1.0 × 10^{15}	95.6	19.0	44.4	0.30	25.1
	4			75 ± 3.1	291 ± 0.1	21 ± 0.3	7.1 × 10^{14}	99.4	13.2		0.24	
100	20	10	1	23 ± 1.8	11 ± 0.1	5 ± 0.7	6.7 × 10^{13}	98.7	4.9	115.8	0.22	28.5
	4			16 ± 1.4	66 ± 0.3	3 ± 0.8	3.1 × 10^{13}	93.7	2.3		0.17	
	20	10	0.1	58 ± 4.1	11 ± 0.4	1 ± 0.4	1.6 × 10^{14}	99.3	11.7	96.9	0.54	15.0
	4			43 ± 3.2	14 ± 0.9	1 ± 0.4	8.0 × 10^{13}	97.8	5.9		0.47	
	20	30	1	53 ± 1.8	49 ± 0.6	22 ± 0.8	8.8 × 10^{13}	98.7	6.5	55.7	0.22	28.5
	4			25 ± 2.5	67 ± 0.9	8 ± 0.9	5.7 × 10^{13}	99.7	4.2		0.17	
	20	30	0.1	79 ± 3.9	14 ± 0.3	2 ± 0.7	2.5 × 10^{14}	98.4	18.5	48.9	0.54	15.0
	4			66 ± 2.8	12 ± 0.2	1 ± 0.9	1.7 × 10^{14}	97.8	12.4		0.47	

Table 10. The mass balance data for the selected replicate experiments for NPs (50 and 100 nm).

NP	Velocity	IS	Temperature	Mass Retained
[nm]	m day^{-1}	mM	[°C]	[%]
50	1	10	20	31 ± 2.2 33 ± 3.2
			4	22 ± 1.9 23 ± 1.9
		30	20	85 ± 2.1 84 ± 3.9
			4	74 ± 1.5 75 ± 3.1
100	1	10	20	24 ± 1.8 23 ± 1.8
			4	17 ± 0.8 16 ± 1.4
		30	20	52 ± 1.4 53 ± 1.8
			4	26 ± 1.9 25 ± 2.5
	0.1	10	20	57 ± 2.1 58 ± 4.1
			4	42 ± 1.3 43 ± 3.2

assumption of Langmuir blocking on both sites 1 and 2, and negligible detachment. Fitted values of k_{att1} and k_{att2} were not always unique because latex NP concentrations in the initial stage of breakthrough were below the detection limit of our measurement equipment. However, the fitted values of S_{max1} and S_{max2} were unique, as the final values of the fitting process were not affected by the initial values of the parameters. In addition, the Akaike Information Criterion (Akaike, 1974) and R^2 values included in Hydrus-1D indicated that the two-site kinetic model with S_{max1} and S_{max2} provides the best model fit for the observed BTCs. Table 9 presents calculated values of $S_{max} = S_{max1} + S_{max2}$ that were used to calculate S_f (Eq. 5). It is noted that only a small fraction of the sand surface contributed to latex NP attachment when the IS was 10 and 30 mM ($< 33.4\%$). Note that increasing IS and temperature and decreasing NP size and flow velocity increased the value of S_f. Interestingly, values of S_f were observed to increase by ~44–160% at the IS of 10 and 30 mM when the temperature increased from 4 to 20 °C. An explanation for the dependence of latex NP retention on IS and flow velocity and the need to use the two-site kinetic model with a Langmuirian blocking function for each site was previously provided by (Sasidharan et al., 2014).

3.4.3. XDLVO Interaction Energy for a Chemically and Physically Heterogeneous Surface

Recall that, XDLVO calculations for viruses and latex NPs interacting with a homogeneous sand surface predicted a large $\Delta \Phi_a$ (> 7 kT) and negligible attachment when the IS was 1, 10, and 30 mM (Table 5). Natural sand surfaces always exhibit some degree of heterogeneity at the nanoscale. For example, Figure 11 shows the presence of micro-nanoscale surface roughness on a river sand grain observed under scanning electron microscopy (Quanta 450, Adelaide microscopy, The University of Adelaide, Australia). Similarly, (Han et al., 2016) measured the
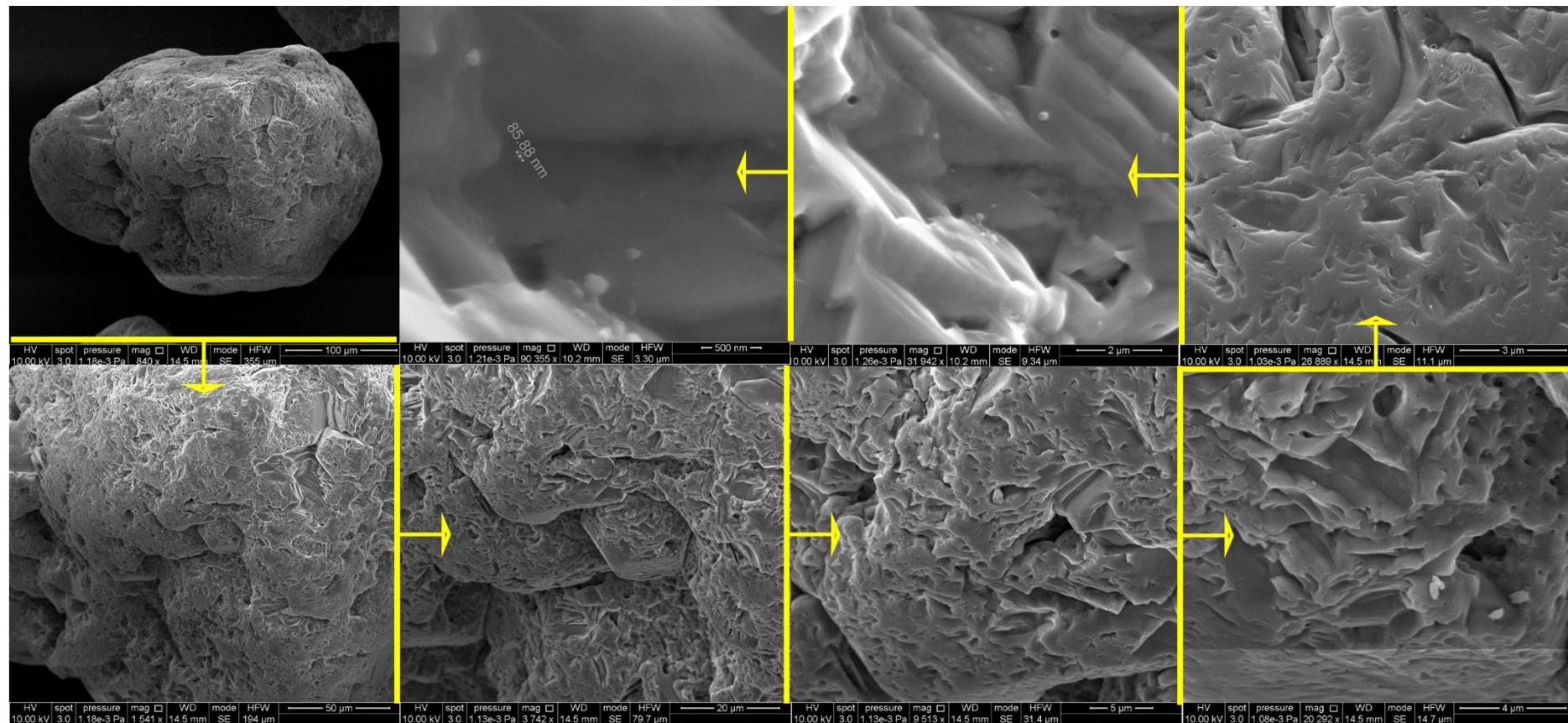
Figure 11. Scanning electron microscopy image of a sand grain

surface roughness of bare quartz sand using atomic force microscopy and reported that the average surface roughness was ~33.4 nm. Nanoscale surface physical heterogeneities (roughness) and chemical heterogeneity (mineral defects, isomorphic substitutions, adsorption of different ions, organic, and/or metal oxides) have been considered in XDLVO calculations to account for observed attachment under unfavourable conditions (Bradford and Torkzaban, 2012; Bradford and Torkzaban, 2013; Hoek et al., 2003; Huang et al., 2009; Shen et al., 2012a). Additional XDLVO calculations on physically and chemically heterogeneous sand were, therefore, conducted in an attempt to explain the observed temperature dependency of virus and latex NP retention. We acknowledge that the virus exhibits chemical (protein coat and lipid membrane) (Meder et al., 2013) and physical heterogeneity (spikes) (Huiskonen et al., 2007; Kazumori, 1981) on their surface but this has been not characterised very well. Similar to many previous studies, we therefore only consider XDLVO calculations on a hypothetical solid-water-interface (Castro and Tufenkji, 2007; Loveland et al., 1996; Wong et al., 2014).

Previous studies have demonstrated that roughness height (h_r), roughness density (f_r), density of chemical heterogeneity (f_+), and zeta potential of the chemical heterogeneity (ζ_+) at a particular location on the collector surface can have a significant influence on the magnitude of $\Delta\Phi_a$ (Bradford and Torkzaban, 2013; Torkzaban and Bradford, 2016). The values of $\Delta\Phi_a$ calculated for the viruses and latex NPs interacting with a chemically and physically heterogeneous sand surface for all the IS and the two temperatures are given in Table 5. Specific heterogeneity parameter values used in these calculations included $f_r = 5\%$, $h_r = 20$ nm, $f_+ = 10\%$ and $\zeta_+ = 1$ mV. The magnitude of $\Delta\Phi_a$ was significantly reduced ($p < 0.0002$) for the heterogeneous surface compared to the homogeneous surface (Table 5). For

Chapter 3

example, Table 5 shows that the value of $\Delta\Phi_a$ for the PRD1 virus at IS = 10 mM

decreased from 28 and 24 kT on the homogeneous surface to 1.3 and 1.1 kT on the

heterogeneous surface at 4 and 20 °C, respectively.

Temperature had a relatively minor (< 3 kT) influence on $\Delta\Phi_a$ in comparison to

physical and chemical heterogeneity. Nevertheless, the Maxwellian kinetic energy

model predicts that a small reduction in $\Delta\Phi_a$ can significantly increase the

probability for particles to attach in a primary minimum when $\Delta\Phi_a < 7$ kT

(Torkzaban and Bradford, 2016). Consequently, the increase in attachment (k_{att} and

S_f) with an increase in temperature depends on the overall value of $\Delta\Phi_a$.

Temperature variations did not have a significant influence on the attachment when

the IS = 1 mM because the value of $\Delta\Phi_a$ was greater than 11 kT even on a nanoscale

heterogeneous surface and this always produced unfavourable attachment

conditions. Similarly, the influence of temperature on attachment was also not

important when the IS = 50 mM. In this case, $\Delta\Phi_a$ was nearly completely eliminated

for both latex NPs and viruses on both homogeneous and nanoscale heterogeneous

surfaces. In contrast, temperature had a large influence on attachment (k_{att} and S_f)

at intermediate IS conditions (10 and 30 mM) because small changes in $\Delta\Phi_a < 7$ kT

drastically increased the probability for particles to diffuse over $\Delta\Phi_a$ into the

primary minimum.

3.4.4. Coupled Effect of IS, Water Velocity, and Temperature on α and S_f Values

Numerical simulations were conducted to better understand the coupled

influence of IS and temperature on α and S_f values. The model of (Bradford and

Torkzaban, 2015) was employed for this purpose. These simulations considered a

homogeneous particle interacting with a physically and chemically heterogeneous

collector surface at 10,000 random A_Z locations. The mean values of physical and

Chapter 3

chemical heterogeneity parameters in these simulations included: $f_+ = 10\%$, $\zeta_+ = 1$ mV, $f_r = 10\%$, $h_r = 20$ nm, and zeta potential values from Table 4. It should be noted that the simulations shown below are a representative example to show the effect of collector surface heterogeneity on α (virus) and S_f (latex NPs) values. Natural surfaces are more complex and determining the accurate heterogeneity parameter distributions is likely to be impossible. Theoretical values of α and S_f were denoted below as α_T and S_{fT}, respectively.

Figure 12 presents the percentage increase of α_T values for viruses and S_{fT} values for latex NPs as a function of IS when the temperature was increased from 4 to 20 °C. It is observed that the percentage increase of α_T values rapidly increased from a minimum value at IS = 1 mM to a maximum at IS = 10 mM, and then slowly decreased with IS and became negligible at IS ≥ 40 mM. Similar behaviour was observed for the percentage increase of S_{fT} values. These results were consistent with our experimental observations; e.g., an increase in temperature from 4 to 20 °C produced an increase in attachment (α and S_f) when the IS = 10 and 30 mM, but had a negligible influence at IS = 1 and 50 mM. In addition, Figure 12 and experimental observations (Table 7 and 9) also indicate that the effect of temperature on attachment was more evident for bigger particles (PRD1 virus or 100 nm latex NP). The larger particles had $\Delta\Phi_a$ values (< 7 kT) that were in the range of the greatest sensitivity to particle diffusion. A small reduction of $\Delta\Phi_a$ at 20 °C allowed more particles to overcome the shallow energy barrier to attachment in a primary minimum, and substantially enhanced α and S_f.

Figures 8 and 9 indicate that a decrease in flow velocity enhanced the retention of latex NPs at a given ionic strength. Experimental and theoretical results have shown that colloidal particles weakly associated with solid surfaces via a
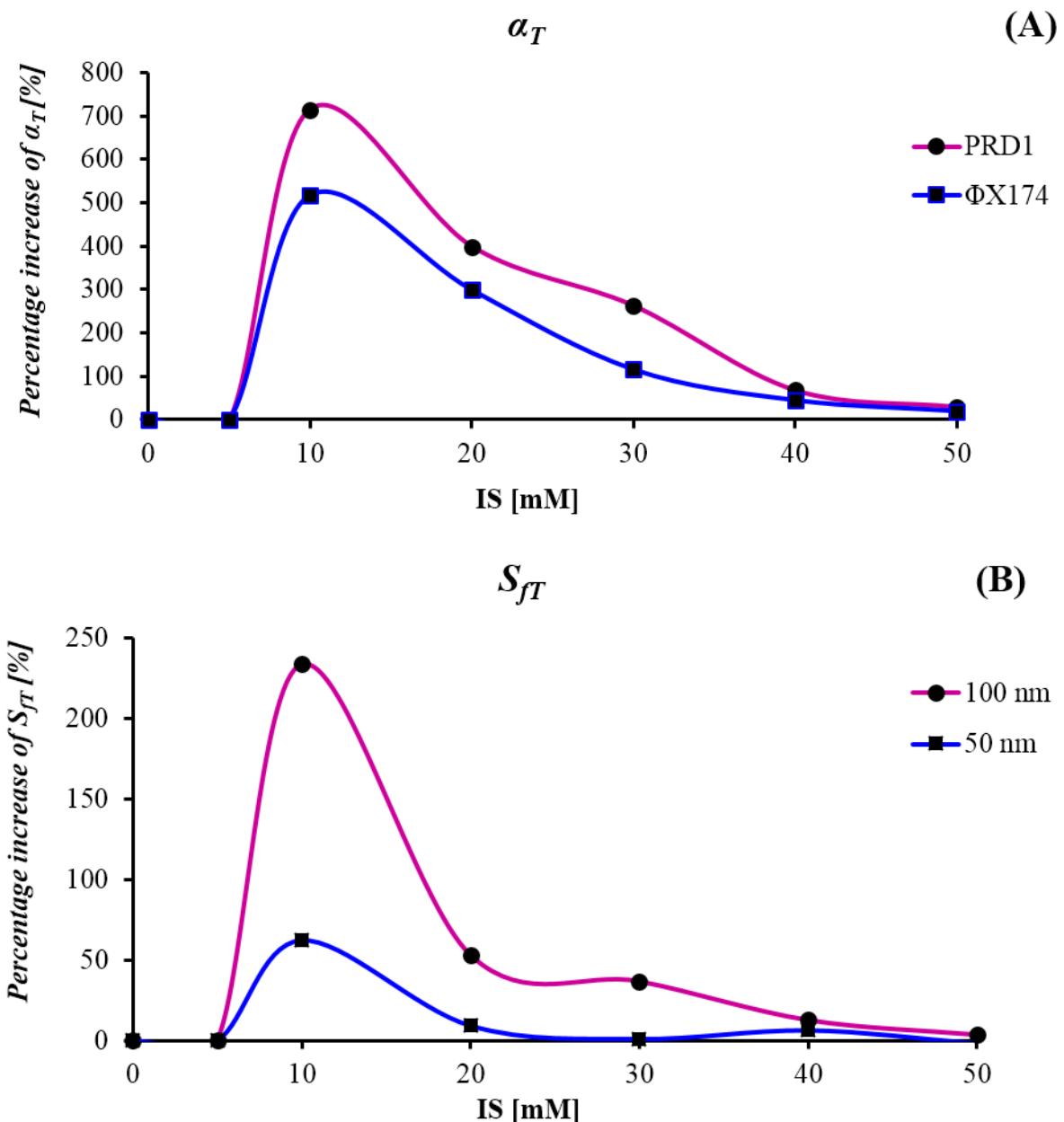
Figure 12. The percentage increase of (A) theoretical attachment efficiency (α_T) of viruses (PRD1 and ΦX174) and (B) theoretical maximum solid fraction contributed to attachment (S_{fT}) of latex NPs (50 and 100 nm) interacting with a heterogeneous sand surface when the temperature increased from 4 to 20 °C. The mean values of parameters used for the simulations are $f_r = 10\%$, $h_r = 20$ nm, $f_+ = 10\%$ and $\zeta_+ = 1$ mV. Zetapotential values used in the calculations are given in Table 4.

shallow secondary minimum may translate over the surface by hydrodynamic forces to reach some locations where the attachment is favourable (Kuznar and Elimelech, 2007; Sasidharan et al., 2014; Torzaban et al., 2010). (Bendersky et al.,

2015) reported that Brownian motion is more significant than or comparable to DLVO interactions and hydrodynamic forces for small particles (< 200 nm) at low flow velocities. Consequently, it is expected that particles with more residence time on the solid surface due to a lower fluid velocity would have an increased probability to diffuse over a shallow $\Delta\Phi_a$ and become attached in the primary energy minimum (Bendersky et al., 2015).

The data from groundwater sources across the world show that the temperature may range from 4 to 32 °C (Vanderzalm et al., 2010) (Kar et al., 2010; Yates et al., 1985). We acknowledge that only two temperatures that correspond to average groundwater extremes were considered in the laboratory experiments in this study. However, the simulated value of α_T and S_{fT} at various temperatures were consistent with our experimental observation. Figure 13 shows the percentage increase of α_T for viruses (PRD1 and ΦX174) and S_{fT} for latex NPs (50 and 100 nm) interacting with a heterogeneous sand surface when the temperature increases from 0 to 25 °C as an increment of 5 °C at IS = 10 mM. Results show a systematic nonlinear increase in α_T and S_{fT} with increasing temperature, with greater increases occurring for the larger virus (PRD1) and latex NP (100 nm).

3.5. Conclusion

This study showed that an increase in temperature from 4 °C to 20 °C increased the retention of viruses and latex NPs in porous media under intermediate IS (10 and 30 mM) conditions. In particular, the value of k_{att}, α (for the virus), and S_f (for the latex NPs) calculated from fitted model parameters showed an increase up to 109, 117, and 160%, respectively, at intermediate IS conditions. Conversely,
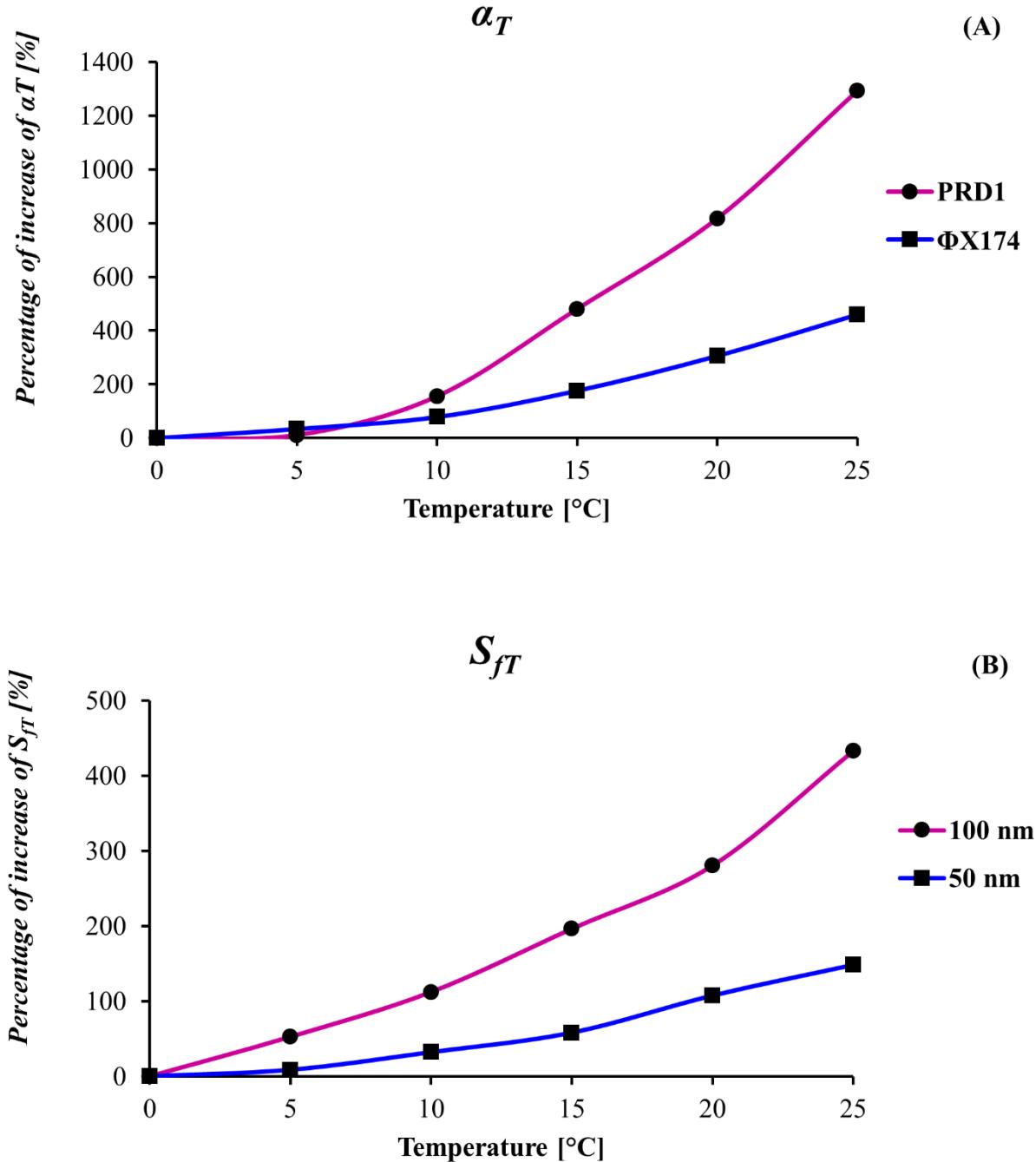
Figure 13. The percentage increase of (A) theoretical attachment efficiency (α_T) for viruses (PRD1 and ΦX174) and (B) theoretical maximum solid fraction contributed to attachment (S_{fT}) for NPs (50 and 100 nm) interacting with a heterogeneous sand surface when the temperature increases from 0 to 25 °C as an increment of 5 °C. The mean values of parameters used for the simulations are IS = 10 mM, f_r = 10%, h_r = 20 nm, f_+ = 10% and ζ_+ = 1 mV. Zetapotential values used in the calculations are given in Table 4.

temperature had negligible influence on k_{att}, α, and S_f values when IS was 1 mM or 50 mM. These results could not be explained by differences in η with temperature.

Chapter 3

An explanation was obtained from XDLVO calculations on sand surfaces that included nanoscale roughness and chemical heterogeneity. The temperature had a relatively minor (< 3 kT) influence on the magnitude $\Delta\Phi_a$ in comparison to physical and chemical heterogeneity. However, a small reduction in $\Delta\Phi_a$ at a higher temperature significantly increased the probability for particles to attach in the primary minimum under intermediate IS conditions. Numerical model predictions conducted to understand the coupled effect of IS, temperature, and colloid size were consistent with the experimental observation.

The experiments presented here were conducted in a simple electrolyte solution at pH 5.5–5.8 and using a clean a quartz sand. Whereas, natural groundwater can have different chemical compositions (presence of mono or divalent ions, high pH, and/or organic matter) and aquifer sediment can have various mineral properties, clay fractions, and/or grain size distributions. Ongoing research in our laboratory aims at extending this work to examine the transport of viruses and NPs in aquifer sediments and ground water over a wide range of environmentally relevant conditions. A better understanding of the effect of temperature on pathogen and engineered NP transport has significant implications for management of potential health and environmental risks associated with groundwater and water reuse. Surface water-groundwater mixing via recharge and seasonal changes in water temperature may significantly affect virus and NP attachment to porous media. Drinking water produced by domestic wells in cold climate regions might be at a higher risk of virus and NP contaminant exposure. Therefore, the influence of temperature should be considered in predictive models in order to accurately assess risks of groundwater contamination.

Chapter 3

Acknowledgements

CHAPTER 4

Transport and Retention of Bacteria and Viruses in Biochar-Amended Sand

| Batch Experiment | Column Experiment |

| Virus | Bacteria | Virus | Bacteria |

$$\frac{C}{C_i} = \frac{Effluent\ concentration}{Input\ concentration}$$

Attachment of bacteria and virus to biochar or sand surface

Amount of virus recovered in effluent

Amount of *E. coli* recovered in effluent

HIGHLIGHTS

• Negligible attachment of bacteria and viruses to biochar particles

• Enhanced transport of virus in the biochar-amended sand

• Enhanced retention of bacteria in biochar-amended sediment

This Chapter is based on the following publication: S. Sasidharan, S. Torkzaban, S. A. Bradford, R. Kookana, D. Page and P. G. Cook (2016). Transport and retention of bacteria and viruses in biochar-amended sand. *Science of the Total Environment* 548–549: 100-109.

Chapter 4

Abstract

The transport and retention of *Escherichia coli* and bacteriophages (PRD1, MS2, and ΦX174), as surrogates for human pathogenic bacteria and viruses, respectively, were studied in sand that was amended with several types of biochar produced from various feedstocks. Batch and column studies were conducted to distinguish between the role of attachment and straining in microbe retention during transport. Batch experiments conducted at various solution chemistries showed negligible attachment of viruses and bacteria to biochar before or after chemical activation. At any given solution ionic strength, the attachment of viruses to sand was significantly higher than that of biochar, whereas bacteria showed no attachment to either sand or biochar. Consistent with batch results, biochar addition (10% w/w) to sand reduced virus retention in the column experiments, suggesting a potential negative impact of biochar application to soil on virus removal. In contrast, the retention of bacteria was enhanced in biochar-amended sand columns. However, elimination of the fine fraction (< 60 μm) of biochar particles in biochar-amended sand columns significantly reduced bacteria retention. Results from batch and column experiments suggest that land application of biochar may only play a role in microbe retention via straining, by alteration of pore size distribution, and not via attachment. Consequently, the particle size distribution of biochar and sediments is a more important factor than type of biochar in determining whether land application of biochar enhances or diminishes microbial retention.

Keywords

Biochar, Porous media, *E. coli* bacteria, Bacteriophages MS2, PRD1, ΦX174, Straining, Attachment

Chapter 4

Abbreviations

DLVO   Derjaguin–Landau–Verwey–Overbeek theory

C_i Initial microbial concentration

C_f Final microbial concentration (batch)

C Effluent concentration (column)

PV   Pore volumes

Φ_{max} Energy barrier against primary minimum attachment

$\Phi_{1}{}^{0}{}_{min}$ Depth of the primary minimum

T_H Applied hydrodynamic torques

T_A Resisting adhesive torques

PRT   Percentage of microbes retained.

4.1.   Introduction

Biochar is a stable form of carbon that is produced by pyrolysis of biomass (e.g., grass, crop or woody residue) under a limited supply of oxygen (Kumari et al., 2014; Wang et al., 2013b). Recently, biochar has gained interest due to its use as a soil amendment to simultaneously mitigate anthropogenic climate change whilst improving soil fertility and enhancing crop production (Lehmann et al., 2006; Mukherjee and Lal, 2014). Extensive studies on benefits of biochar application have been reported related to soil fertility (Doan et al., 2015; Glaser et al., 2002), physical properties (Mukherjee, 2013), microbial community and biota (Jindo et al., 2012;

Lehmann et al., 2011), carbon sequestration and greenhouse gas emissions (Lehmann and Joseph, 2015; Mukherjee et al., 2014). In addition, a number of studies have shown certain biochars are very effective sorbents, especially for chemical contaminants such as pesticides and heavy metals (Cui et al., 2016; Kearns et al., 2014; Kookana, 2010; Macdonald, 2015). Literature also indicates that biochar application to natural porous media (e.g., soil) may enhance pathogen retention (Abit et al., 2012; Abit et al., 2014; Mohanty and Boehm, 2014; Mohanty et al., 2014).

Mechanisms that control retention of microbes, and in general colloids, in porous media include attachment to and detachment from solid (collector) surfaces and physical entrapment (straining) in small pore spaces (Torkzaban and Bradford, 2016; Torkzaban et al., 2015). Colloid interactions with solid surfaces have been explained using Derjaguin-Landau-Verwey-Overbeek (DLVO) theory (Derjaguin, 1941; Verwey and Overbeek, 1955). DLVO theory states that the interaction energy can be quantified as the sum of van der Waals and electrostatic double layer interactions, which can be either attractive or repulsive. The strength of interaction is therefore controlled by various physical and chemical factors such as pH, ionic strength (IS), temperature, presence of organic matter, metal oxides, and multivalent-ions like calcium (Bales et al., 1991a; Bradford et al., 2014; Chu et al., 2003; Da Silva et al., 2011; Foppen et al., 2008; Foppen et al., 2006; Furiga et al., 2010; Kim and Walker, 2009; McCaulou et al., 1995; Redman et al., 2004; Sadeghi et al., 2013; Schijven and Hassanizadeh, 2000; Torkzaban et al., 2013; Wong et al., 2013; Zhang et al., 2012). For example, an increase in pH, which is commonly observed in biochar-amended porous media (Mosley et al., 2015), may increase electrostatic double layer repulsion and consequently enhance transport of microbes

in the porous media. Recently, nanoscale surface roughness and chemical heterogeneity on the collector (e.g., sand grains) and colloid surfaces have been shown to play a significant role in the interaction energy between a colloid and collector (Bradford and Torkzaban, 2013). It is expected that biochar particle size and their physical and chemical surface properties will be similarly important factors influencing the extent of microbial retention in biochar-amended soil.

Straining is another potential mechanism for retention of pathogens. It involves retention of colloids in smallest regions of pore space such as those formed near grain-to-grain contact points and microscopic roughness locations. Straining may also occur in pore throats that are too small to allow passage of single or multiple colloids (Torkzaban et al., 2015). It is expected that the presence of micro and macro-porous structure on the surface of biochar particles and micro-sized biochar particles (e.g., a few micrometres) can lead to an enhanced retention of colloids in biochar-amended porous media (Bradford et al., 2014; Hale et al., 2014). For example, the existence of microscale porous structures on the surface of biochar particles can create low-velocity regions where microbes can be retained via a shallow secondary energy minimum (Mohanty and Boehm, 2014). The relative importance of colloid retention by attachment and straining depends on properties of colloid (both in size and concentration), porous medium (porosity, grain size, and roughness), the hydrodynamic conditions, and the solution chemistry (Bradford and Torkzaban, 2013; Bradford and Torkzaban, 2015).

Batch and column experiments are common methods to study colloid retention in porous media. These experimental techniques offer the advantage that retention mechanisms can be examined under well-defined laboratory conditions. The solid phase in batch systems is continuously mixed and, therefore, the flow direction

changes over time. This agitation facilitates collision of colloids to solid surfaces and possibly increases the attachment rate. However, this agitation also eliminates pore structure and continuously changes the applied and adhesive torques that contribute to colloid retention, especially at microscopic roughness locations on the solid phase (Treumann et al., 2014). Hence, attachment controls colloid retention in batch systems. Conversely, packed-column experiments are commonly utilised to analyse colloid breakthrough curves (BTCs) and the retention profiles. The solid phase in column experiments is stationary, colloids that are retained at locations associated with microscopic roughness, and grain-grain contacts always experience a low applied torque and a greater adhesive torque. The solid surface area contributing to microbe retention is therefore expected to be greater in the column than batch systems because of attachment and straining processes (Treumann et al., 2014). Comparison of retention results from batch and column studies can, therefore, be utilised to determine the relative importance of attachment and straining processes.

Recently, a few column studies have been undertaken to investigate transport of various types of bacteria in biochar-amended porous media (Abit et al., 2012; Abit et al., 2014; Bolster and Abit, 2012; Chung et al., 2014; Mohanty and Boehm, 2014; Mohanty et al., 2014). Abit et al. (2012) reported that *Escherichia coli* retention was enhanced in a high temperature pyrolysed biochar amended-soil compared to a low temperature pyrolysed biochar amended-soil or soil only columns (Abit et al., 2012). Increasing the amount of biochar in soil increased the extent of bacteria retention (Abit et al., 2012). (Chung et al., 2014) reported an enhanced retention of *E. coli* in sand-packed columns containing a potassium hydroxide activated (93%) or raw maize (72%) hydrochar compared to unamended

sand (~30%). To understand the retention mechanism, a backwashing test was performed following the retention phase. A considerable fraction of the retained bacteria was recovered in this phase implying that straining might have been the underlying retention mechanism (Chung et al., 2014). (Mohanty and Boehm, 2014) reported an enhanced removal (~96%) of *E. coli* in a biochar-amended sand compared to unamended sand (~37%). However, it was observed that elimination of fine biochar particles (< 125 μm) in the biochar-amended column considerably decreased the retention capacity (~62%) (Mohanty and Boehm, 2014). This limited number of studies on the efficacy of biochar on bacteria removal indicates that mechanisms and factors controlling bacteria retention in the presence of biochar are still poorly understood. Moreover, to date, no study has been published on the transport and retention of viruses in biochar-amended porous media.

The aim of this study was to gain a better understanding of the underlining mechanisms that control transport and retention of microbes (bacteria and viruses) in the biochar-amended sand. To achieve this, systematic experiments were conducted by using various types of biochars, ultra-pure quartz sand, and *Escherichia coli* and phages (PRD1, MS2, and ΦX174). First, batch experiments with biochars or sand were conducted under varying solution chemistries. Batch experiments were used to specifically examine the extent of microbial attachment to biochar and sand surfaces. In addition, the impact of chemical activation of biochars on microbial attachment was examined in the batch experiments. Then, a series of column experiments using sand amended with various types of biochar were conducted to understand the combined effect of attachment and straining on the microbe retention. Comparison between batch and column experiments using viruses and bacteria helped us identify the controlling retention mechanism in the

biochar-amended sand.

4.2. Materials and Methods

4.2.1. Porous Media Characterization

Biochar samples employed in this research were obtained from feedstocks of Macadamia Shell (MS), Oil Mallee (OM), Phragmites Reed (PR), Rice Husk (RH) and Wheat Chaff (WC). These biochars are currently being assessed for their potential applications, including: sorption of active pharmaceutical ingredients (Williams et al., 2015), mycorrhizal root colonization, growth and nutrition of wheat (Solaiman et al., 2010), immobilization of soil cadmium (Zhang et al., 2013), pH neutralization (Mosley et al., 2015), and efficiency to decrease N volatilization (Mandal et al.). Specific characteristics (feedstock type, pyrolysis temperature, pH, specific conductivity, and density) of the biochar samples are given in Table 11. Biochar samples were crushed and sieved (under running water) to a size < 2 mm and > 60 μm. Therefore, we expect the presence of fine particles smaller than 60 μm was negligible in our batch tests. Particle size distribution information for the biochar samples is given in Table 12. Scanning electron microscopy (SEM) imaging (FEI Quanta 450 FEG Environmental SEM, US) was conducted on biochar samples was conducted on biochar samples to observe their structure before and after washing (Figure 17).

Activation of biochar has received considerable research attention to enhancing its adsorption capacity (Chung et al., 2014). Chemical activation of biochar may affect its physical and chemical characteristics (e.g., surface area, porosity, micro-pore volume, the presence of surface charge group and iso-electric point) and, therefore, influence its efficiency for contaminant removal (Molina-Sabio and Rodríguez-Reinoso, 2004; Trakal et al., 2014). Wheat Chaff (WC) and Oil Mallee

Table 11. Characteristics of Biochar samples.

Feed Stock	Feedstock Type	Genus Name	Pyrolysis Temperature	§pH	§Electric Conductivity	Density	Specific Surface Area
			$^\circ$C		[μS cm^{-1}]	g cm^{-3}	m^2 g^{-1}
Macadamia Shell (MS)	Shell	Macadamia	450	9.67 ± 0.8	2,800	0.341	202.5 ± 0.28[a]
Oil Mallee (OM)	Wood	Eucalyptus	450	7.33 ± 0.7	305	0.369	197 ± 1.2[d]
Phragmites Reed (PR)	Grass	Phragmites	460	7.72 ± 0.4	1,595	0.177	101[b]
Rice Husk (RH)	Grass	Oryza	650	8.62 ± 0.8	375	0.212	400.77[c]
Wheat Chaff (WC)	Grass	Triticum	550	9.14 ± 0.2	3,460	0.195	190 ±0.9[d]

[a] (Mandal et al., 2015); [b] (Zeng et al., 2013); [c] (Yavari et al., 2014); [d] measured in the lab
§ The pH and electric conductivity (EC) of biochar samples in Milli-Q water (1:10 w/v ratio) were measured.

Table 12. The table shows the particle size distribution of biochar fine fraction ≤ 60 μm. 0.1 gr of Oil Mallee (OM) biochar fine fraction was mixed in 500 mL of Milli-Q water. The particle size distribution was measured using Malvern Mastersizer 2000 (UK).

Size	Volume
[μm]	[%]
0.55 - 1.09	1.97 ± 0.8
1.26 - 10.00	17.22 ± 2.3
11.48 - 19.95	20.53 ± 1.6
22.91 - 30.20	16.28 ± 2.5
31.67 - 45.71	21.08 ± 3.9
46.13 - 60.26	22.21 ± 1.8

Chapter 4

(OM) biochars were activated using the steps reported in (Azargohar and Dalai, 2008), which is briefly described in below.

(i) 10 g of raw biochar was mixed in 50 mL of various activating agents (i.e., 0.1 M NaOH, 0.05 M NaOH, 0.1 M HNO_3, or 0.05 M HNO_3) and stirred continuously for 2 h ; (ii) excess solution was then decanted and samples were dried at 100 °C for 24 h ; (iii) dried samples were washed using deionized water (DI) water; (iv) samples were mixed with 0.01 M HCl for 2 h and washed with DI water until the pH stabilized to 7; and (v) samples were ground and wet sieved (under running water) to < 2 mm and > 60 μm in size and kept at 40 °C until dry. Hereafter, these samples are designated as $WC_{0.1\ M\ NaOH}$, $WC_{0.05\ M\ NaOH}$, $WC_{0.1\ HNO3}$, $WC_{0.05\ M\ HNO3}$, $OM_{0.1\ M\ NaOH}$, $OM_{0.05\ M\ NaOH}$, $OM_{0.1\ HNO3}$ and $OM_{0.05\ M\ HNO3}$.

Ultra-pure quartz sand (Charles B. Chrystal CO., Inc., NY, USA) with size ranging from 125 to 300 μm was cleaned as described by (Sasidharan et al., 2014) and used in the experiments. All five biochar samples were used for batch experiments, whereas only WC and OM biochars were used in the column studies because of the limited availability of the other biochar samples. Raw WC or OM biochar particles (grounded and dry sieved < 2 mm) were mixed with sand (biochar-amended sand) to achieve a 0.1 w/w ratio (10%) for column experiments. This corresponds to a volume percentage of 50% for the biochar and sand mixture. Hereafter, these biochar-sand mixtures were designated as 'WC-Sand' and 'OM-Sand'.

4.2.2. Microbe Preparation

Escherichia coli 13706 (ATCC 13706) was used as a surrogate for pathogenic bacteria. The bacteria sample preparation method is explained in detail in the Appendix A. Phages (MS2, ΦX174, and PRD1) used in this study are surrogates

Chapter 4

for human pathogenic viruses (Schijven and Hassanizadeh, 2000). Characteristics of phages and their respective host bacteria are given in Table A.1. The detailed methodology for bacteriophage preparation and enumeration is given in the Appendix A and B.

4.2.3. Interaction Energy Calculations

The biochar was mixed in a selected electrolyte solution and filtered through a < 5 μm filter. The size and zeta potential for the fine biochar fraction that passed through the filter was measured (Nano ZS, Malvern Instruments Ltd., UK). Zeta potentials for crushed sand grains, phages, and bacteria in electrolyte solutions were also measured with this instrument. Measured zeta potentials in the various pH and electrolyte solutions were used to calculate the interaction energy profile for phages and bacteria upon their close approach to sand and biochar surfaces. Sphere-plate interaction energy calculations were conducted by assuming that microbes were spherical and collector surfaces were smooth. The van der Waals interaction (V_{vdW}) was determined from the expression of Gregory (Gregory and Wishart, 1980). The combined Hamaker constant was estimated from the Hamaker constant of individual materials (Israelachvili, 1992). An individual value of 3.70×10^{-20} for water (Israelachvili, 1992), 6.50×10^{-20} for sand (Israelachvili, 1992), 6.19×10^{-20} for biochar (Wang et al., 2013b), 7.00×10^{-19} for *E. coli* (Capco, 2014) and 6.60×10^{-20} for viruses (Kavanaugh, 1980) were used in this study. The combined Hamaker constant was calculated to be 4.03×10^{-20} for *E. coli*-Water-Sand, 3.64×10^{-20} for *E. coli*-Water-Biochar, 4.04×10^{-21} for Virus-Water-Sand, and 3.64×10^{-21} for Virus-Water-Biochar systems. Electrostatic double layer interaction (V_{EDL}) was calculated using the Hogg-Healy-Fuerstenau expression (Hogg et al., 1966) with zeta potentials in place of surface potentials. Born repulsion was considered using the expression given by (Ruckenstein and Prieve, 1976). Hydrophobic

interactions were not considered in these calculations because needed contact angle and surface tension information for the various biochar samples were not available.

4.2.4. Batch Experiments

Batch experiments were conducted to determine the attachment behaviour of phages and bacteria to sand and biochar surfaces at selected electrolyte concentration (5, 10 and 20 mM NaCl) in the absence of pore structure (e.g., the entire system is in motion). All electrolyte solutions in this study were prepared using 1 mM Tris buffer and the pH was adjusted to pH 7.2 using 0.1 M HCl. A detailed step by step method for the batch experiment is given below.

1 g of Rice Husk (RH), Oil Mallee (OM), Wheat Chaff (WC), Phragmites Reed (PR) and Macadamia Shell (MS) biochar or ultra-pure quartz sand was placed into 10 mL PP tubes containing 9.5 mL of bacteriophage or bacteria suspension with a selected electrolyte (5, 10 and 20 mM NaCl) and initial microbe concentration (C_i). Tubes were filled completely to avoid the presence of an air-water interface. To provide a complete mixture of the system, tubes were rotated at a 45° angle on a tube rotator (Scilogex, Mx-Rd-Pro LCD) at a speed of 10 rpm at 18 °C. The tubes were shaken for 2 h and then the final concentration (C_f) of phages and bacteria in the aqueous phase was measured. Triplicate measurements were performed for all experiments. Additionally, a set of control tubes with only phage or bacteria suspension were prepared to ensure the viability of these microbes over the course of experiments.

Additional batch experiments were performed to test the effect of calcium ion (5 mM $CaCl_2$ at pH 7.2) on microbe attachment to biochar samples (RH, OM, WC, and PR). The efficiency of activated WC and OM biochar to adsorb microbes was also tested using various electrolyte solutions (5, 10 and 20 mM NaCl & 5 mM

Chapter 4

CaCl$_2$).

The water samples from virus experiments were centrifuged at $1000 \times g$ for 10 min at 4 ˚C followed by filtrating the supernatant through a 0.45 μm syringe filter (Merck Millipore, Germany) to remove any biochar fine particles. The filtrate was enumerated for virus concentration using the method explained in section 2 of the Appendix A. This filtration step ensured that any possible interference of particle-associated viruses did not affect our results. Similarly, water samples from bacteria experiments were centrifuged at $100 \times g$ for 5 min at 4 ˚C, the supernatant was filtered through a 5 μm syringe filter (Merck Millipore, Germany), and the absorbance at 460 nm using a UV-Vis spectrophotometer was measured. In addition, 100 μl of the filtrate was serially diluted and spread plated to determine the CFU mL^{-1}. In both cases, the final concentration was statistically the same. Both absorbance and spread plate analysis were conducted for all the samples and the average concentration obtained from both methods was used in the determination of the cell concentration for each sample.

4.2.5. Column Preparation

Sterilised polycarbonate columns (1.9 cm inside diameter 5 cm height) were dry-packed by slowly pouring 1 cm increments of sand or sand–biochar mixture (WC-Sand and OM-Sand) into the column while the column was being vibrated. Separate columns were packed for each microbe (phage or bacteria), porous medium (sand or sand-biochar mixture), and solution. After dry-packing the column, a three-way valve at the column inlet was used to flush pressurised CO$_2$ through the column at a flow rate of 10 mL min^{-1} for 30 min. The column outlet tubing was submerged in water to prevent atmospheric air from entering the column. Next, the packed column was saturated and preconditioned with > 10 pore

volumes (PV) of electrolyte solution prepared in 1 mM Tris buffer at pH 7.2 using a syringe pump (Model 22, Harvard Apparatus) at a flow rate of 0.394 mL min^{-1}.

4.2.6. Column Transport Experiment

An electrolyte solution (1, 5, 10 or 20 mM NaCl in 1 mM Tris Buffer with pH 7.2) with suspended phage (PRD1 and ΦX174) or *E. coli* of a known initial concentration (C_i) was introduced into the column at a flow rate of 0.08 mL min^{-1} (corresponding to the pore water velocity of 1 m day^{-1}) for 1,500 min (20 PV - Phase 1). This Phase was followed by injection of ~10 PV of microbe-free solution (Phase 2). Effluent samples were collected every 72 minutes (1 PV) by a fraction collector (CF-2, Spectrum, USA). The effluent samples for both microbes were processed and concentration (C) was measured using the methods explained in Sections 1 & 2 in the Appendix A. Selected samples were also analysed for pH and EC using a pH meter (EC-PH700-42S, Eutech).

The effluent breakthrough concentrations (BTCs) were plotted as dimensionless concentrations (C/C_i) of microbes as a function of the number of pore volumes (PVs). The total number of retained microbes during Phase 1 and 2 (N_{1+2}) was determined by calculating the difference between the number of injected microbes into the column in Phase 1 (N_{in}) and the number of microbes that was recovered in the effluent during Phase 1 and 2 (N_{out}). This information was used to calculate the percentage of retained microbes in each experiment. The survival of phages and bacteria over a 38.4 h interval was determined in the effluent from the preconditioning phase.

The statistical differences of mean removal efficiencies were identified by one-way ANOVA. The mean removal efficiencies were separated by Tukey's honestly significant difference (HSD) test ($p < 0.05$). All statistical analyses were performed

using IBM SPSS Statistics for Windows Version 22.0 (SPSS, 2013).

4.3. Result and Discussion

4.3.1. Zeta Potentials and Interaction Energies

Table 13 presents zeta potentials for the microbes, biochars, and quartz sand at pH 7.2 and IS of 20 mM NaCl and 5 mM CaCl$_2$. Surfaces of sand were less negatively charged than those of biochar particles at both solution chemistries. It has been reported that biochar can contain negatively charged functional groups such as carboxyl, hydroxyl, phenolic groups on its surface (Mandal et al., 2015; Mosley et al., 2015; Nartey and Zhao, 2014; Wang et al., 2013a). These functional groups are ionised and contributed to the net negative charge on the biochar surface under the tested pH conditions (Wang et al., 2013a). All microbes, sand, and biochar surfaces were more negatively charged in the presence of Na$^+$ than Ca^{2+} ions. Divalent cations, such as Ca^{2+}, more effectively decrease the absolute magnitude of the zeta potential than monovalent cations, like Na$^+$. This has been attributed to the combined effects of charge screening and binding of Ca^{2+} to anionic functional groups on natural surfaces (Sasidharan et al., 2014).

Table 14 presents interaction energy parameters, namely the height of the energy barrier against primary minimum attachment (Φ_{max}) and the depth of the primary minimum ($\Phi_1{}^0{}_{min}$), for all the microbes interacting with sand and biochars at IS = 20 mM NaCl or 5 mM CaCl$_2$. A high value of Φ_{max} existed for both *E. coli* and viruses in the presence of 20 mM Na$^+$. The height of Φ_{max} tended to decrease with the microbe size (*E. coli* > PRD1 > ΦX174 > MS2, with *E. coli* being 30 times larger than MS2). Hence, the value of Φ_{max} was considerably larger for the *E. coli* than viruses. The value of Φ_{max} and $\Phi_1{}^0{}_{min}$ considerably decreased and

Table 13. Measured zeta potential (ζ-) values of bacteria, bacteriophages, biochar and sand in electrolyte solution (IS = 20 mM NaCl and 5 mM CaCl$_2$ at pH = 7.2).

Microbe	Porous Material	Electrolyte	ζ-Microbe [mV]	ζ-Porous material [mV]	Electrolyte	ζ-Microbe [mV]	ζ-Porous material [mV]
E. coli	Sand		-42.2 ± 2.1	-31.5 ± 3.1		-35.0 ± 0.1	-20.5 ± 1.1
PRD1	Macadamia Shell		-30.8 ± 1.1	-40.2 ± 1.5		-25.0 ± 0.9	NM[§]
ΦX174	Oil Mallee	20 mM NaCl	-29.8 ± 0.9	-48.1 ± 1.3	5 mM CaCl2	-22.2 ± 0.4	-43.1 ± 1.1
MS2	Phragmites Reed		-27.5 ± 1.2	-69.7 ± 2.4		-20.0 ± 1.1	-64.7 ± 1.4
	Rice Husk			-45.3 ± 1.9			-41.1 ± 0.9
	Wheat Chaff			-53.8 ± 2.8			-50.2 ± 1.8

[§] NM – Not measure

Table 14. Calculated XDLVO interaction energies between Virus-Water-Sand, Virus-Water-Biochar, Bacteria-Water-Biochar and Bacteria-Water-Sand systems. Parameters for calculation IS = 20 mM NaCl and 5 mM CaCl$_2$, pH = 7.2. Hamaker constant values of 4.03 × 10^{-20} for *E. coli*-Water-Sand, 3.64 × 10^{-20} for *E. coli*-Water-Biochar, 4.04 × 10^{-21} for Virus-Water-Sand and 3.64 × 10^{-21} for Virus-Water-Biochar System were used. The Macadamia Shell (MS), Oil Mallee (OM), Phragmites Reed (PR), Rice Husk (RH) and Wheat Chaff (WC) biochar samples were used in this study.

Colloid-Solution-Collector System	Φ_{max}	$\Phi_{1}{}^{0}_{min}$	Φ_{max}	$\Phi_{1}{}^{0}_{min}$
	[kT]	[kT]	[kT]	[kT]
	20 mM NaCl		5 mM CaCl$_2$	
E. coli - Water - Sand	215.24	-8738.65	77.62	-9373.78
E. coli - Water - MS	432.46	-7374.46	-	-
E. coli - Water - OM	604.15	-7103.96	483.93	-7584.12
E. coli - Water - PR	1037.36	-6874.42	820.86	-7651.52
E. coli - Water - RH	543.78	-7188.41	448.39	-7620.85
E. coli - Water - WC	726.47	-6970.84	605.30	-7512.54
PRD1 - Water - Sand	26.9	-10.3	12.4	-31.3
PRD1 - Water - MS	36.1	-2.7	-	-
PRD1 - Water - OM	41.8	-4.4	27.9	-16.9
PRD1 - Water - PR	50.4	-16.6	32.8	-52.1
PRD1 - Water - RH	39.9	-4.4	27.1	-15.8
PRD1 - Water - WC	44.9	-2.5	30.2	-23.7
ΦX174 - Water - Sand	8.9	-6.9	3.4	-15.1
ΦX174 - Water - MS	12.0	-2.5	-	-
ΦX174 - Water - OM	13.9	-2.6	7.2	-13.8
ΦX174 - Water - PR	16.5	-12.9	8.3	-31.9
ΦX174 - Water - RH	13.3	-2.3	7.1	-12.9
ΦX174 - Water - WC	14.8	-3.8	7.7	-17.9
MS2 - Water - Sand	7.2	-7.8	2.6	-14.5
MS2 - Water - MS	9.5	-4.7	-	-
MS2 - Water - OM	10.8	-5.6	5.3	-15.9
MS2 - Water - PR	12.7	-17.4	5.9	-34.8
MS2 - Water - RH	10.4	-5.11	5.2	-14.9
MS2 - Water - WC	11.5	-7.2	5.6	-20.4

increased, respectively, in the presence of Ca^{2+} compared to Na^{+} electrolyte. This behaviour is attributed to both microbes and collector surfaces being less negatively charged in the presence of Ca^{2+} (Table 13). Table 14 shows that the value of Φ_{max} was always greater than the average kinetic energy of diffusing microbes (1.5 kT) at all of the examined solution chemistry conditions. The Maxwellian kinetic energy model predicts that the probability for primary minimum attachment is small when $\Phi_{max} > 1.5$ kT, and approaches zero when $\Phi_{max} > 8$ kT (Chandrasekhar, 1943;

Chapter 4

Shen et al., 2007).

4.3.2. Batch Experiments

Batch experiments over a wide range of chemical conditions were conducted to examine the extent of attachment of three different viruses (MS2, PRD1, and ΦX174) and *E. coli* to quartz sand and various types of biochars. Figure 14 shows the normalised virus concentrations in equilibrated solutions (C_f/C_i; where C_i is the initial concentration and C_f is the final concentration) after 2 h mixing in tubes containing sand or various types of biochar at different concentrations of NaCl solution. Control tubes (without biochar or sand) confirmed stable virus concentration (i.e., no loss due to inactivation or attachment to tube wall) during the course of experiments (data not shown). It was observed that C_f/C_i reduction was negligible for all three viruses reacting with biochars in all solution chemistries. These observations clearly demonstrate negligible attachment of viruses to biochar particles. In comparison, values of C_f/C_i of the three viruses significantly decreased in tubes containing quartz sand, indicating significant ($p < 0.0002$) attachment to sand surfaces. The amount of attachment to sand grains increased with increasing IS.

Figure 15 shows the results of batch experiments with *E. coli* reacting with various types of biochar or sand at different NaCl solution concentrations. The results show negligible *E. coli* attachment to both biochars and sand surfaces under all test conditions. It should be mentioned that all electrolyte solutions in this study were prepared using 1 mM Tris buffer and the pH was adjusted to pH 7.2 using 0.1 M HCl. Our preliminary tests, in which 20 mM unbuffered solution (without Tris) was used and the pH was lowered to 7.3 after several washing steps, showed negligible virus and *E. coli* attachment to biochar surfaces (data not shown). This
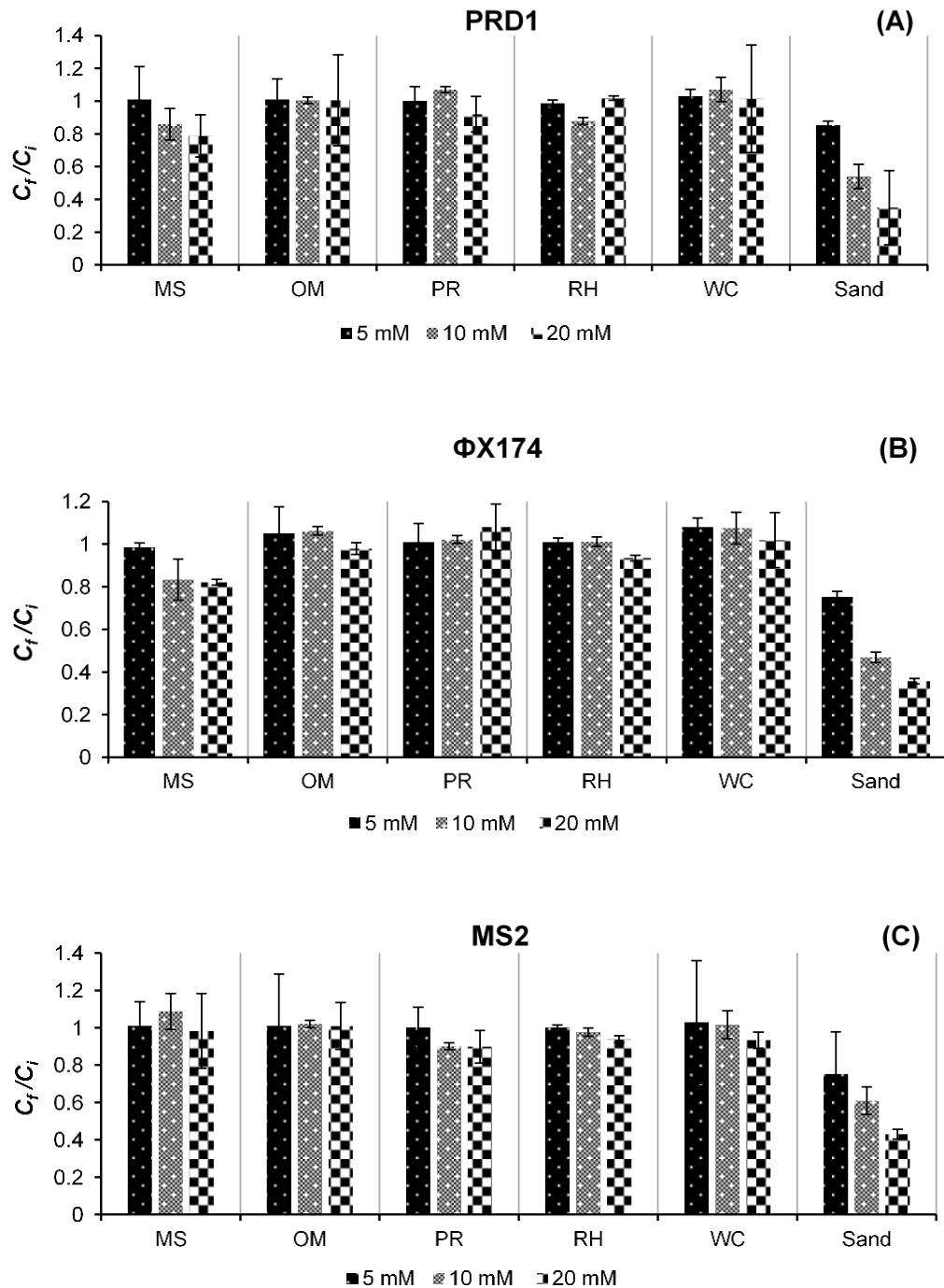
Figure 14. Representative bar chart plot with error bar for bacteriophages: (A) PRD1 (B) ΦX174 and (C) MS2 obtained from batch experiments conducted using sand and five different biochar samples; Macadamia Shell (MS), Oil Mallee (OM), Phragmites Reed (PR), Rice Husk (RH) and Wheat Chaff (WC); as adsorbing media. The parameters for experiment are IS = 5, 10 and 20 mM NaCl; pH = 7.2 (Tris buffer); and temperature = 18 °C. The Y-axis shows the normalized concentration C_f/C_i (C_i = initial concentration & C_f = final concentration) values. Error bars represent the standard error (n = 3).

result confirmed that the presence of 1 mM Tris in our buffered solution did not affect the adsorption process to biochar surfaces. Figure 16 shows the results of batch experiments for viruses and *E. coli* in which the electrolyte solution was 5 mM $CaCl_2$. It was observed that the attachment of viruses to biochars (Figure 16) only slightly increased ($p < 0.001$) in the presence of 5 mM Ca^{2+} in comparison with that of Na^+ solution (Figure 14). However, virus attachment to quartz sand increased by more than 1 order of magnitude ($C_f/C_i < 0.1$) in the presence of 5 mM Ca^{2+} ($p < 0.0006$). In addition, it was observed that C_f/C_i values for *E. coli* showed little attachment to both sand and biochars under this high calcium concentration. Each of these observations will be further discussed in detail below.

Negligible attachment of *E. coli* and viruses to biochars in the various Na^+ solution chemistries were consistent with interaction energy parameters presented in Table 14. These calculations predict the presence of a sizable energy barrier against microbe attachment in a primary minimum. However, biochar surfaces are known to contain micropores of various sizes (micropores $< 2 \times 10^{-3}$ µm, mesopores 2–50×10^{-3} µm and macropores $> 50 \times 10^{-3}$ µm) (Downie et al., 2009; Shen et al., 2014). Figure 17 shows representative SEM images of OM biochar confirming the presence of a large number of micro-hollow pores (1–50 µm), accessible for viruses and even *E. coli*, on the surface of biochar particles. The water velocity, and, therefore, hydrodynamic forces, is expected to be negligible in these micropores. Thus, a considerable amount of microbe attachment is expected in micropores when the adhesive energy (e.g., even a shallow secondary energy minimum) is larger than the thermal energy of diffusing microbes (1.5 kT). However, the secondary energy minimum was negligible for microbial interaction with biochar in Na^+ solutions, suggesting that the entire surface of biochar particles was unfavourable for

attachment.

Negligible attachment of *E. coli* to sand surfaces agrees with previous batch studies using *E. coli* O157:H7 and *E. coli* D21g, and Ottawa and quartz sands (Bradford et al., 2015a; Bradford et al., 2015b). Another study with carboxyl modified latex colloids (1 and 2 μm) also showed very little colloid attachment (< 25%) on sand surfaces in batch systems, even when the IS was as high as 800 mM (Treumann et al., 2014). This small amount of colloid attachment was attributed to the continuous motion of sand in batch systems that altered the applied
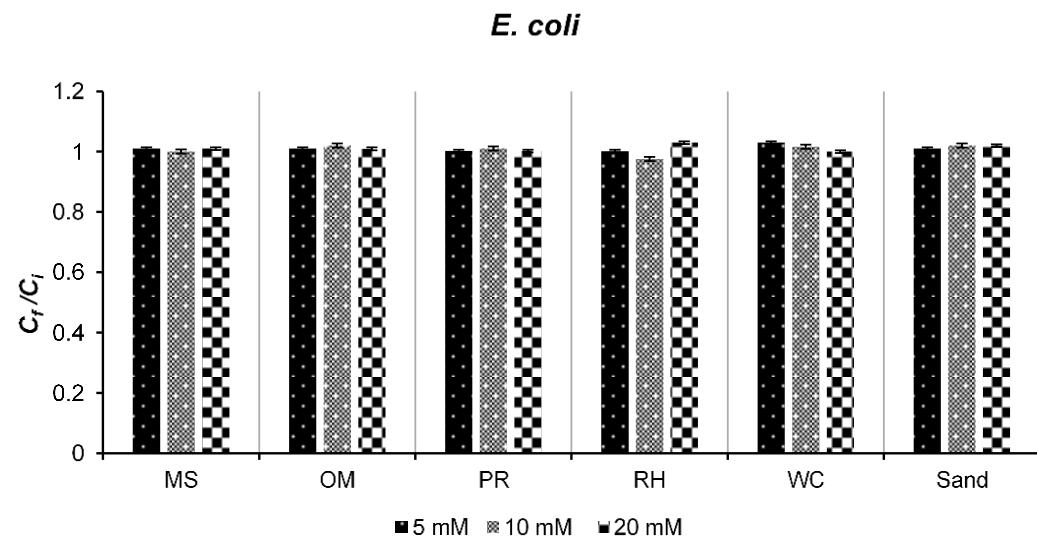
Figure 15. Representative bar chart plot with error bar for *E. coli* obtained from batch experiments conducted using sand and five different biochar; Macadamia Shell (MS), Oil Mallee (OM), Phragmites Reed (PR), Rice Husk (RH) and Wheat Chaff (WC); as adsorbing media. The parameters for experiment are IS = 5, 10 and 20 mM NaCl; pH = 7.2; and temperature=18 $^{\circ}$C. The Y-axis shows the normalized concentration C_f/C_i (C_i= initial concentration & C_f= final concentration) values. Error bars represent the standard error (n = 3).
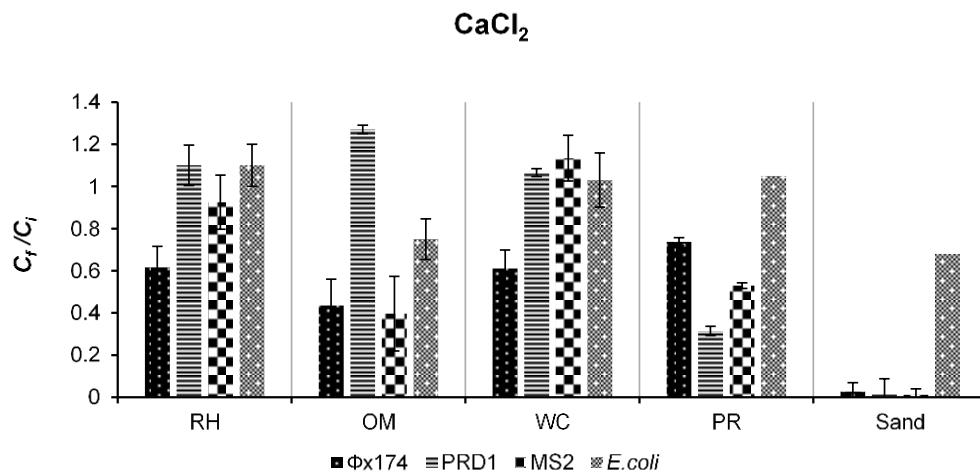
Figure 16. Representative bar chart plot with error bar for bacteriophages PRD1, MS2 and ΦX174; and bacteria *E. coli* obtained from batch experiments conducted using sand and four different biochar; Oil Mallee (OM), Phragmites Reed (PR), Rice Husk (RH) and Wheat Chaff (WC); as adsorbing media. The parameters for experiment are IS = 5 mM $CaCl_2$, pH = 7.2 and temperature = 18 °C. The Y-axis shows the normalized concentration C_f/C_i (C_i = initial concentration & C_f = final concentration) values. Error bars represent the standard error (n = 3).
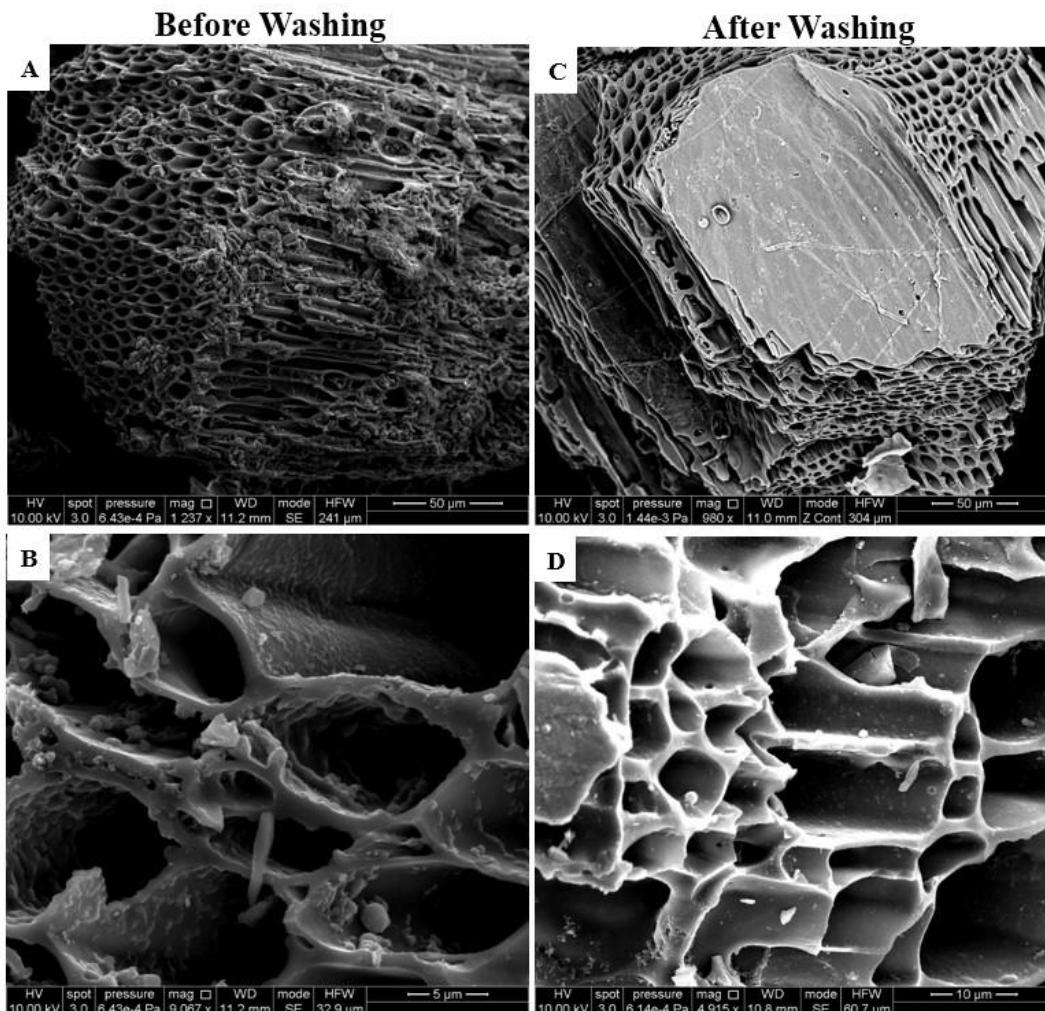
Figure 17. SEM image of Oil Mallee biochar samples and their distinctive structure (A-B) before washing and (C–D) after washing with DI water.

hydrodynamic (T_H) and resisting adhesive (T_A) torques with time. Both T_A and T_H are functions of the colloid radius (r_c), but T_H decreases more rapidly (proportional to r_c^3) than T_A with r_c. Consequently, nanoparticles such as viruses show higher attachment than micro-sized colloids (e.g., *E. coli*), provided the strength of the adhesion force is larger than the Brownian force (Bradford and Torkzaban, 2015).

Table 14 shows high values of Φ_{max} and negligible secondary minimum for virus interactions with sand surfaces in NaCl solutions. However, batch results show a considerable amount of virus attachment to sand grains (Figure 14). A detachment experiment was conducted to better understand the nature of this virus-sand interaction. Following completion of a virus-sand batch experiment, the excess solution was removed and replaced with virus-free solution of the same chemical composition. The tubes were subsequently shaken for another 2 h, and the final virus concentration in the aqueous phase was measured. The virus concentration was again found to be negligible (data not shown), demonstrating that the detachment rate was very low and that attachment most likely occurred in a primary energy minimum. Recent studies have demonstrated that primary minimum attachment may occur even at low solution IS when nanoscale surface roughness is incorporated into XDLVO calculations (Argent et al., 2015; Bradford and Torkzaban, 2013). Nanoscale roughness has been shown to reduce (or even eliminate) Φ_{max}, such that colloids can diffusive over the energy barrier. Hence, nanoscale roughness on viruses and sand surfaces provide a plausible explanation for the discrepancy in interaction energy parameters (Table 14) and batch results. Note that Φ_{max} was greater for biochar than sand (Table 14). Nanoscale roughness apparently did not reduce Φ_{max} enough to produce primary minimum interaction for microbes on the biochar.

Chapter 4

Colloids such as Cryptosporidium parvum oocysts, viruses, and engineered nanoparticles have been observed to strongly attach to mineral surfaces in the presence of Ca^{2+}, even when DLVO theory predicted a substantial energy barrier (Janjaroen et al., 2010; Sadeghi et al., 2013; Torkzaban et al., 2013). In this study, the presence of Ca^{2+} only slightly enhanced attachment of *E. coli* to sand and biochar surfaces in comparison to Na^+ (Figures 15 and 16). In contrast, the presence of calcium in solution significantly enhanced the attachment of viruses (by more than one order of magnitude) to quartz surfaces (Figures 14 and 16). However, much smaller amounts of virus attachment occurred on biochar samples than sand, and only slight attachment ($C_f/C_i = 0.5$) of MS2 and ΦX174 occurred on OM biochar. These differences in the influence of Ca^{2+} on attachment with microbe size and the solid surface can be explained in terms of nanoscale chemical heterogeneity. In particular, multivalent cations (e.g., Ca^{2+}) have been shown to strongly bind to negatively charged mineral surfaces and anionic functional groups of microbes (Greenland, 1971; Sposito, 2008; Torkzaban et al., 2013). This adsorption can create nanoscale chemical heterogeneity as a result of charge neutralisation and/or reversal (De Kerchove and Elimelech, 2008; Sasidharan et al., 2014). Consistent with the experimental observations, the influence of nanoscale chemical heterogeneity on attachment has been shown to become more important for smaller colloids (such as viruses) and higher IS (Bradford and Torkzaban, 2013; Bradford and Torkzaban, 2015; Duffadar et al., 2009). Furthermore, the influence of nanoscale heterogeneity is expected to be diminished when the solid surface exhibits a greater net negative charge (biochars) because it is more difficult to eliminate a higher energy barrier (Table 14). It should be mentioned that nanoscale chemical heterogeneity may be related to bridging complexation or "cation bridging" (Greenland, 1971). Bridging complexation occurs when anionic or polar

functional groups (typically carboxylate-terminated molecules) bind with multivalent cations that are adsorbed on negatively charged surfaces (Sposito, 2008).

Additional experiments were conducted to examine the role of biochar activation on microbial attachment. A few studies have suggested that chemical activation of biochar improved its retention capacity of various contaminants (Azargohar and Dalai, 2008; Chung et al., 2014; Molina-Sabio and Rodríguez-Reinoso, 2004; Trakal et al., 2014). For example, activation with HCl led to the generation of more available sites on the surface for nutrient retention (Li et al., 2014). Activation of hydrochar with a 1 M KOH also showed an increase in *E.coli* removal by 21% in column experiments compared with that of raw hydrochar (Chung et al., 2014). Figure 18 and 19 show batch results for *E. coli* and three viruses, respectively, on activated WC and OM biochars in the presence of 20 mM NaCl solution. The four different activation solutions (0.1 M NaOH, 0.05 M NaOH, 0.1 M HNO_3 and 0.05 M HNO_3) did not show a large influence on virus and bacteria attachment to the biochars. For example, activation of WC and OM biochar with 0.1 M NaOH did show a very slight improvement in attachment of PRD1 and ΦX174, and 0.1 M NaOH activation of OM enhanced the attachment of ΦX174 by 37% compared to the unactivated OM (Figure 14). However, differences in microbe attachment to either activated or non-activated biochar samples were not statistically different ($p < 0.11$), and microbe attachment was always significantly ($p < 0.0001$) lower on activated biochar than quartz sand.

4.3.3. Column Experiments

The addition of 10% w/w biochar to sand resulted in a considerable increase in total organic carbon and a negligible change in effluent pH in the biochar-amended

column because of the high buffering capacity of the influent (Tris Buffer, pH 7.2) solution. Moreover, no detectable change in other water quality parameters (e.g., specific conductivity, phosphate, dissolved organic carbon) was observed in the effluent after flushing the column with 10 PVs of the background solution.
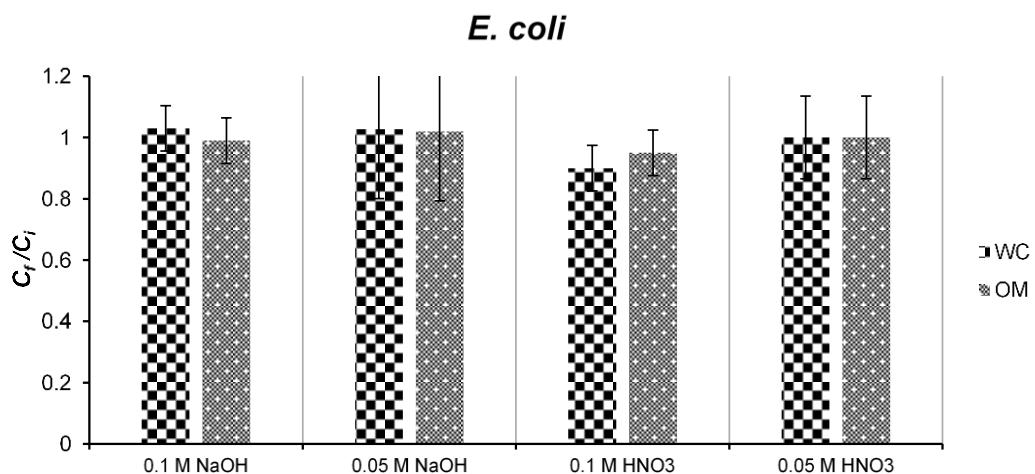
Figure 18. Representative bar chart plot with error bar for *E. coli* obtained from batch experiments conducted using activated biochar. The Wheat Chaff (WC) and Oil Mallee (OM) biochar was activated using 0.1 M NaOH, 0.05 M NaOH, 0.1 M HNO3 and 0.05 M HNO3. The parameters for experiment are IS = 20 mM NaCl, pH = 7.2 and temperature = 18 °C. The Y-axis shows the normalized concentration C_f/C_i (C_i= initial concentration & C_f = final concentration) values. Error bars represent the standard error (n = 3).

Figure 20 presents representative effluent BTCs for PRD1 and ΦX174 from biochar-amended and unamended (sand) packed columns when the solution contained 10 mM Na$^+$. Here the normalised effluent concentration (C/C_i) is plotted against the number of PVs. Table 15 shows the percentage of retained (PRT) viruses for similar column experiments for the various IS levels and biochar types. Virus retention was significantly lower ($p < 10^{-7}$) in biochar-amended than unamended sand columns. Notably, the unamended (only sand) column retained ~2 log of PRD1 (~98.7%) and ΦX174 (97.4%) when the IS was 10 mM Na$^+$. However, always < 50% of the input viruses were retained in the column when the sand was
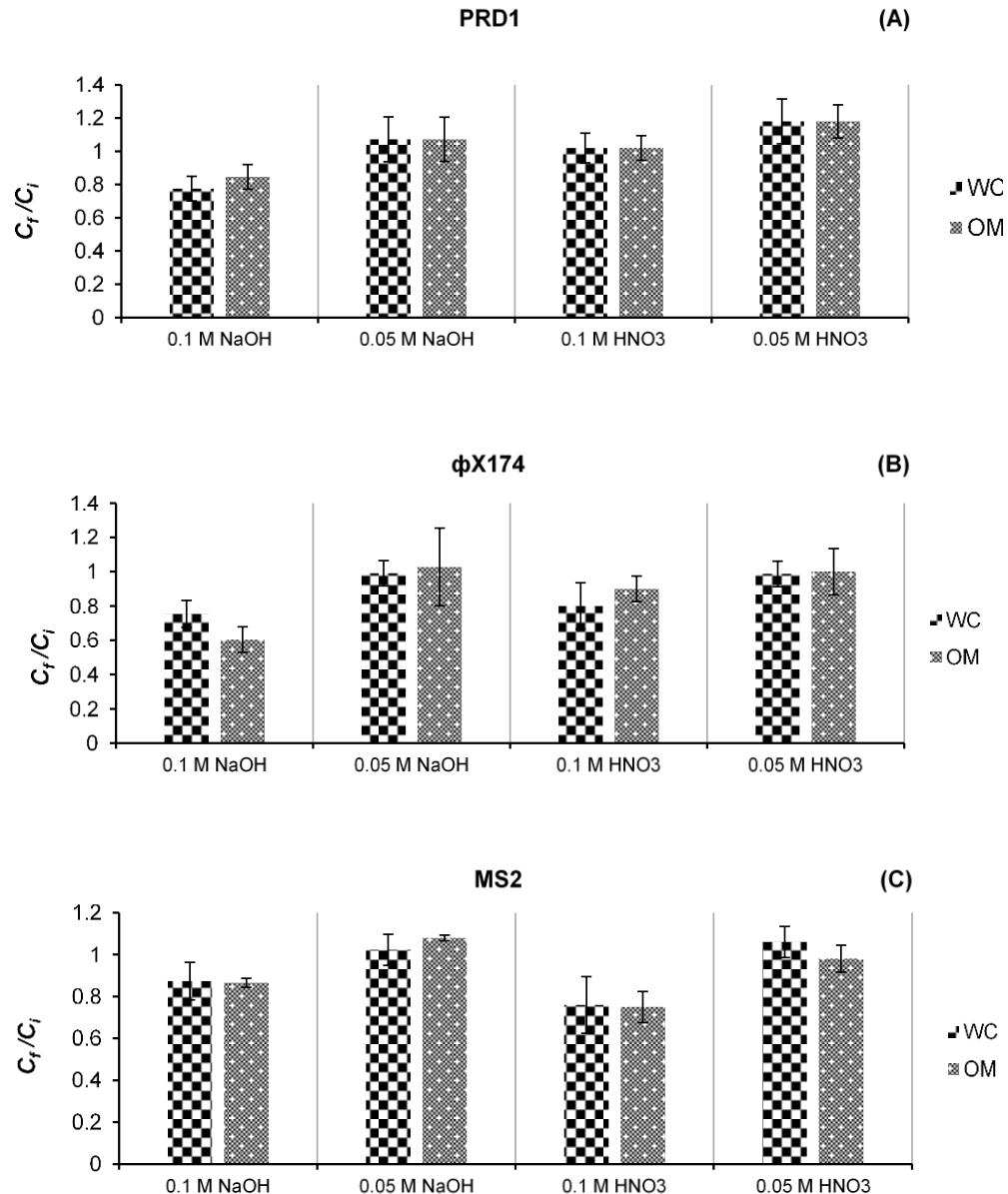
Figure 19. Representative bar chart plot with error bar for bacteriophages PRD1, MS2 and ΦX174 obtained from batch experiments conducted using activated biochar. The biochar was activated using 0.1 M NaOH, 0.05 M NaOH, 0.1 M HNO_3 and 0.05 M HNO_3. (A) PRD1 (B) ΦX174 and (C) MS2 for activated biochar. The parameters for experiment are IS = 20 mM NaCl, pH = 7.2 and temperature = 18 °C. The Y-axis shows the normalized concentration C_f/C_i (C_i= initial concentration & C_f= final concentration) values. Error bars represent the standard error (n = 3). The Wheat Chaff (WC) and Oil Mallee (OM) biochar samples were used in this study.

PRD1 (A)

ΦX174 (B)
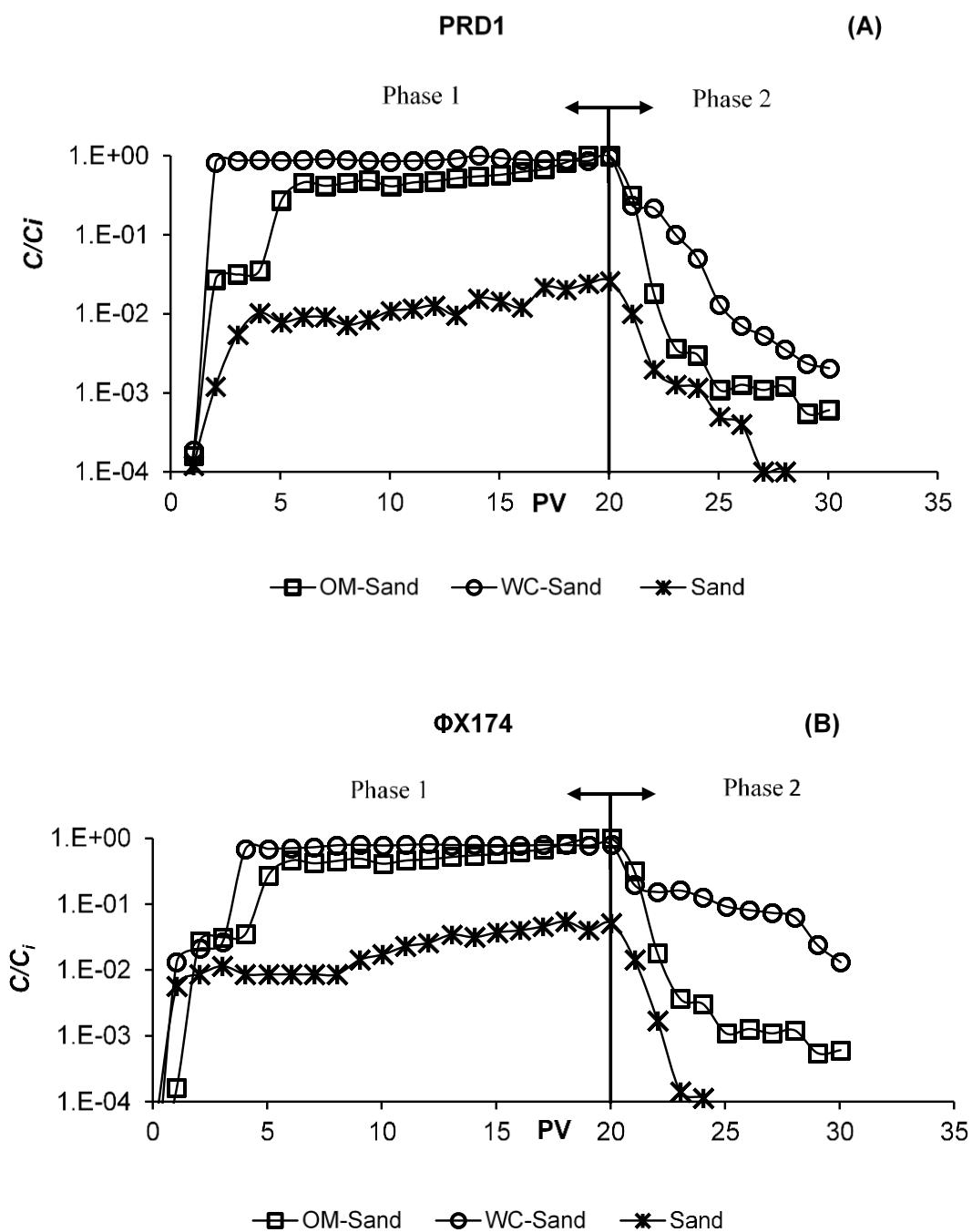
Figure 20. Representative measured BTCs for bacteriophages (A) PRD1 and (B) ΦX174 obtained from column experiments using biochar-amended and non-amended porous media (WC-Sand, OM-Sand and Quartz sand only) at IS = 10 mM, pH = 7.2, flow velocity = 1 m day^{-1} and temperature = 18 $^{\circ}$C. The Wheat chaff (WC) and Oil Mallee (OM) biochar samples were used in this study.

amended with biochar (Table 15). These results also show that the tailing of BTCs

approached zero after a few PV injection of the virus-free solution, indicating that

the detachment rate of the retained viruses was very low. Therefore, virus retention

in these experiments was primarily attributed to irreversible attachment to sand surfaces. These results are consistent with those obtained from the batch experiments that showed a negligible virus attachment to biochar particles and a considerable attachment to sand surfaces.

Figure 21 presents representative BTCs for *E. coli* in biochar-amended and unamended sand columns when the solution IS = 20 mM NaCl. Table 15 provides PRT values for other biochar experiments at different IS conditions. In contrast with the results obtained for viruses, higher bacteria retention was observed in biochar-amended than unamended sand columns. For example, the addition of OM or WC biochar to sand increased retention of *E. coli* by ~60%. This result is consistent with previous studies which reported an enhanced bacteria retention after biochar addition to porous media (Abit et al., 2012; Abit et al., 2014; Mohanty and Boehm, 2014; Mohanty et al., 2014). The amount of bacteria retention in biochar amended sand was not dependent on the solution IS, as the PRT values were practically the same for 5 and 10 mM experiments (Table 15). Conversely, an increase in bacteria retention was observed with increasing IS in experiments with unamended sand (Table 15). Other researchers have reported a similar dependence of bacteria retention on IS in packed sand columns (Li et al., 2004; Tufenkji and Elimelech, 2004b; Tufenkji and Elimelech, 2005a). It should be mentioned that negligible *E. coli* retention occurred in the unamended sand column when deionized water (IS = 0) was used as the background solution (data not shown), implying that physical straining was negligible.

Table 15. Percentage of retention (PRT) for bacteriophages (PRD1 and ΦX174) and *E. coli* in various experiments (sand, sand + biochar or sand + coarse biochar). The experiment parameters are IS = 5, 10 and 20 mM NaCl, pH = 7.2, injection pore volume = 20 PV, flow velocity = 1 m day^{-1} and temperature = 18 °C. The Wheat Chaff (WC) and Oil Mallee (OM) biochar samples were used in these studies.

Colloid	Porous Media	IS	Percentage of retention
		[mM]	[%]
PRD1	Sand		98.7 ± 0.2
	WC-Sand	10	11.3 ± 2.1
	OM-Sand		50.1 ± 1.9
ΦX174	Sand		97.4 ± 0.4
	WC-Sand	10	25.9 ± 2.5
	OM-Sand		45.1 ± 2.1
E. coli	Sand	5	10.2 ± 1.9
	Sand	10	26.6 ± 1.7
	Sand	20	32.8 ± 1.2
	WC-Sand	5	64.5 ± 1.2
	WC-Sand	10	67.1 ± 1.3 [1] a
	WC-Sand	20	67.8 ± 1.3 a
	OM-Sand	5	65.2 ± 1.7 b
	OM-Sand	10	66.0 ± 1.4 b
	OM-Sand	20	67.4 ± 2.9
	WC coarse textured-Sand	5	5.3 ± 1.1
	WC coarse textured-Sand	10	9.6 ± 1.5
	WC coarse textured-Sand	20	12.1 ± 1.1
	OM coarse textured-Sand	5	8.5 ± 2.8
	OM coarse textured-Sand	10	16.5 ± 1.9
	OM coarse textured-Sand	20	18.5 ± 1.1

[1] Within the column, the mean percentage of retention (PRT) values followed by the same letter are not significantly different using Turkey's HSD test at *p < 0.05*.

As noted previously, interaction energy calculations presented in Table 14 indicated that attachment in the primary or secondary minimum was not expected for *E. coli* interacting with biochar and sand particles under the current experimental conditions. In addition, batch experiments showed negligible bacteria attachment to sand and biochar particles in the considered solution chemistries. The batch results demonstrated that the adhesive interaction energy between the bacteria and surfaces of sand and biochar particles was not strong enough to produce attachment.
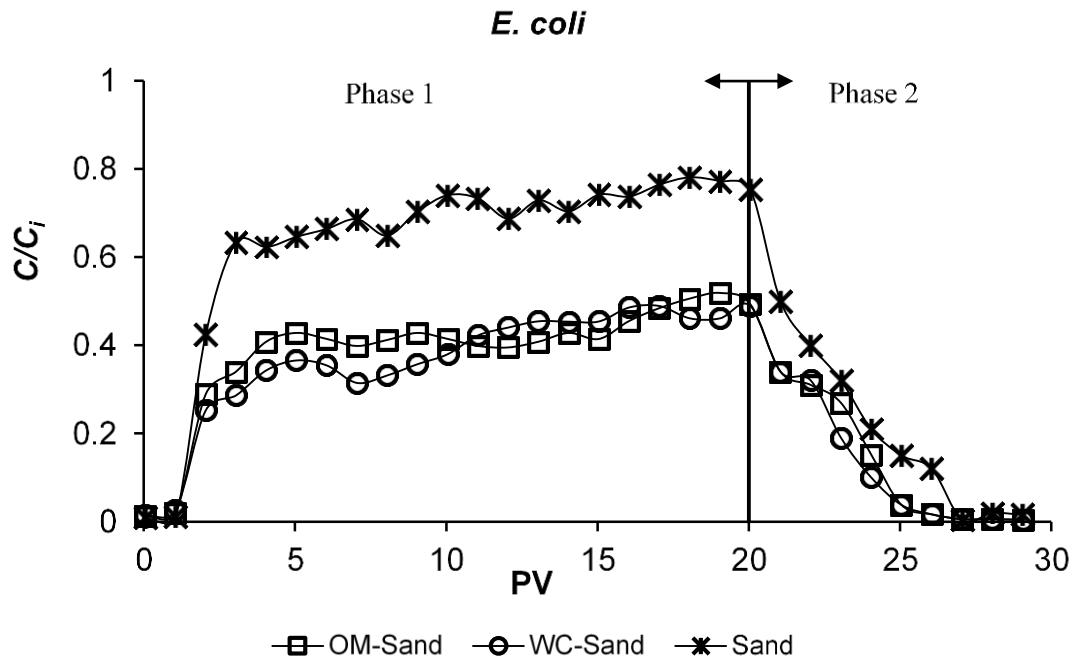
E. coli

Figure 21. Representative measured BTCs for *E. coli* bacteria obtained from column experiments using biochar-amended and non-amended porous media (WC-Sand, OM-Sand and Quartz Sand only) at IS = 20 mM NaCl, pH = 7.2, flow velocity = 1 m day^{-1} and temperature = 18 °C. The Wheat Chaff (WC) and Oil Mallee (OM) biochar samples were used in this study.

This inconsistency between the results of batch and column experiments with unamended sand (without biochar) can be attributed to the coupled effect of hydrodynamic forces and microscopic roughness on retention. In particular, colloid retention is well-known to depend on the balance of T_H and resisting adhesive T_A at a particular location on a solid surface (Bradford and Torkzaban, 2015). Colloid retention is expected to predominantly occur at locations associated with large scale roughness, ridges, and valleys on sand grains because these locations are associated with larger T_A and lower T_H (surface topography influences the lever arms). In batch experiments, however, the direction and magnitude of T_H and T_A at a particular location on the grain surface are continuously altered with time (Treumann et al., 2014). Thus, the torque balance criterion is not being satisfied in a batch system. In contrast, the direction and magnitude of T_H and T_A are constant at a particular location on the sand surface in the static column system under steady-state

conditions. Consequently, the negligible colloid attachment in batch experiments and the significant retention in the column experiments with sand demonstrate the importance of microscale surface roughness on bacteria retention in porous media.

In previous experiments conducted with biochar-amended porous media, enhanced bacteria retention was ascribed to increases in the specific surface area leading to increased attachment sites after the biochar addition (Mohanty and Boehm, 2014). Biochar is highly porous relative to sand, thus, the surface area of biochar is at least 5 orders of magnitude larger than sand (Mohanty et al., 2014). Moreover, the enhanced bacteria retention has been attributed to stronger attachment of bacteria to surfaces of biochar particles than that of sand surfaces. Non-DLVO forces including hydrophobic and steric interactions were suggested to cause the strong attachment of bacteria to biochar particles (Mohanty et al., 2014). Hydrophobic attraction is expected to be much greater between bacteria and biochar than bacteria and sand due to the high organic carbon content of biochar (Abit et al., 2012). Thus, it has been proposed that biochar may retain *E. coli* at the primary minimum due to the increased hydrophobic interactions (Abit et al., 2012). However, strong attachment or increased attachment sites are unlikely to be the dominant mechanisms causing the enhanced bacteria retention in the biochar-amended sand in this study. If attachment was the dominant mechanism, then bacteria attachment would have been observed in the batch experiments with biochar. However, cell attachment in the batch experiments was not observed. Moreover, no attachment to biochar was observed for the three different viruses, that encompass a wide range of hydrophobicity and isoelectric points (Aronino et al., 2009; Chrysikopoulos and Syngouna, 2012; Dika et al., 2015; Schijven and Hassanizadeh, 2000).

Chapter 4

Another explanation for the observed enhanced bacteria retention in the biochar-amended sand is physical straining. This explanation seems to be more reasonable given that biochar addition did not cause an increase in virus retention in the column experiments. Note that straining increases with the microbe size, and *E. coli* is more than 30 times larger than a virus (e.g., ΦX174). Additional column experiments were conducted to investigate whether physical straining was responsible for the effect of biochar amendment on bacteria retention. These experiments were conducted in a similar manner to others, with the exception that the crushed biochar materials were sieved to remove the fine fraction (< 60 μm); e.g., only the coarse biochar fraction (60 μm–2 mm) was used to amend the sand. Figure 22 presents BTCs for *E. coli* in coarse-textured biochar amended sand at different solution IS. Retention of *E. coli* was significantly lower ($p < 10^{-7}$) in coarse (60 μm–2 mm) than fine (< 2 mm) biochar amended sand. Note that the PRT in the coarse-textured biochar-amended sand was even smaller (~12–18%) than that of unamended sand (~33%), indicating the importance of sand surface area for bacteria retention (Table 15). A recent study found that considerable amounts of biochar micro-particles (in the order of a few micrometres) were retained at pore constrictions when a stable biochar micro-particle suspension was injected into a packed sand column (Wang et al., 2013a; Zhang et al., 2010). These results demonstrate that the fine fraction in the experiments was the dominant fraction responsible for the enhanced bacteria retention.

Pore straining is the trapping of colloidal particles, in this case, bacterial cells in the down-gradient pore throats that are too small to allow colloid passage (McDowell-Boyer et al., 1986). The magnitude of colloid retention by straining

131

WC

OM
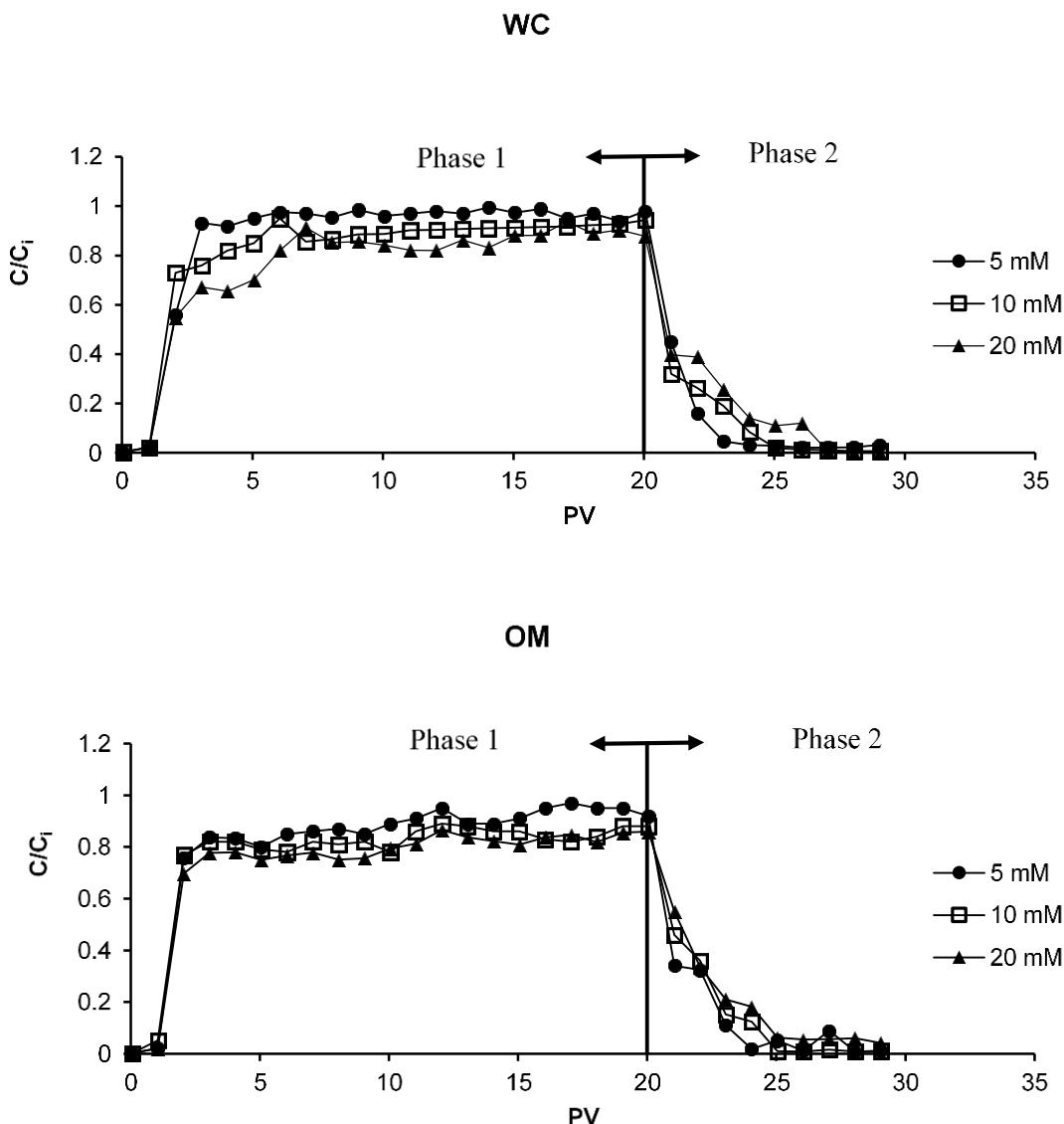
Figure 22. Representative measured BTCs for *E. coli* bacteria obtained from column experiments using biochar-amended porous media (WC coarse [texture]-Sand and OM coarse [texture]-Sand) at IS = 5, 10 and 20 mM NaCl, pH = 7.2, flow velocity = 1 m day^{-1} and temperature = 18 °C. The Wheat chaff (WC) and Oil Mallee (OM) biochar samples were used in this study.

depends on both the colloid and porous medium properties (Bradford and Torkzaban, 2013). Natural porous media (e.g., soil) typically exhibit a wide range in pore sizes due to variations in grain size, orientation, and configuration. Biochar also exhibits a wide range of particle sizes varying from a fraction of micrometres to a few millimetres. Recall that the results from unamended sand suggested that little straining occurred when the IS was very low (~0 mM). In contrast, when the

sand was amended with biochar, a fraction of fine particles in the biochar was retained in small pores during the packing or equilibration phase. This process will decrease the effective pore sizes of the porous media and may, therefore, increase the likelihood of subsequent bacteria retention in the narrow pores. When the colloid size is considerably smaller than the sand pore sizes (e.g., viruses), straining becomes a less dominant mechanism of colloid retention. Pore and surface (microscopic roughness and grain-grain contacts) straining of bacteria in uniformly sized sands has been shown to be an important factor affecting bacterial retention when the ratio of bacteria diameter to sand grain diameter is > 0.007 (Bradford et al., 2014). In this current study, the flow velocity was constant and there was no detectable permeability reduction in the biochar-amended sand as the overall permeability was very high (50 m day^{-1}).

The effect of biochar amendment on the extent of bacterial retention has been observed to be dependent on the type of biochar and soil. For instance, (Abit et al., 2014) examined the effect of biochar addition on the transport of bacteria in sand and soil columns. They found that bacteria retention decreased (13%) when a low-temperature poultry litter (LTPL) was added to a sandy loam soil. Conversely, the addition of the LTPL biochar had no major effect on the retention in a fine sand medium (7%). Moreover, the addition of a high-temperature poultry litter (HTPL) biochar to the fine sand increased the *E. coli* retention and had no discernible effect in the sandy loam (Abit et al., 2014). Note that biochar produced at higher pyrolysis temperature generally have a much greater fraction of fine particles, specific surface area and hydrophobicity (McBeath et al., 2015; Wang et al., 2013a). These observations were attributed to differences in hydrophobicity values for bacteria suspended in leachates collected from the fine sand and sandy loam amended with

biochar. However, based on the results of the current study, a more likely explanation for some of the observed changes in bacteria retention after biochar addition is the potential for increasing or decreasing straining of bacteria in porous media. For example, given the size distribution of loamy sand, it is likely that LTPL biochar addition resulted in a coarser-textured porous media compared to the unamended media and, therefore, the contribution of straining was diminished. In another study by (Chung et al., 2014) when the column was flushed with DI water after the retention phase, only a minor fraction (~3%) of the retained *E. coli* was released. Conversely, when the column was flushed in the reversal mode (backwashing), a considerable fraction (~22%) of the retained bacteria was released, implying that straining was the underlying retention mechanism in the biochar-amended column.

4.4. Conclusion

In this study, batch experiments showed negligible attachment of viruses and bacteria to biochar surfaces before and after chemical activation. At a given chemical condition, the attachment of viruses to sand was much higher than to biochar surfaces. In this study, the column experiments demonstrated that the biochar-amendment of sand enhanced the transport of viruses. In contrast, retention of bacteria was enhanced in a biochar-amended sand column. In this study, the particle size of biochar was found to be important in retention of bacteria. The removal of a fine fraction of biochar particles (< 60 μm) enhanced the transport of bacteria during column experiments. Together these results demonstrate that the enhanced retention of bacteria in the biochar-amended sand is a result of straining of bacteria in pore constrictions, grain-grain contact points, and/or microscopic roughness locations.

Chapter 4

This study was conducted using pure quartz, which is an example of worst case scenario of microbial attachment to a collector surface. Even though the interaction energy calculations showed that experimental conditions were unfavourable for attachment, batch and column experiments showed significant ($p < 0.0001$) retention of bacteriophages to quartz surface. Natural soil and sediments typically contain metal oxides and clay particles, which will enhance the number of favourable sites available for attachment and thus increase the potential of microbial retention (Tong et al., 2012; Truesdail et al., 1998). Biochar contains a large number of nano- and micro-size biochar particles. These particles can compete for favourable attachment sites (metal oxides, clay) available on the soil surface. This process may further reduce the removal of colloids like pathogenic viruses or toxic nanoparticles, which have less negative charges than biochar particles. In addition, biochar generally tends to increase the pH of the background solution (Table 11). This effect may further reduce the retention efficiency of soil or sediments upon amendment with biochar.

Biochar application has received wide research attention, especially in agriculture and environmental fields. This study showed that the application of biochar to sediments could enhance the transport of viruses and nanoparticles. This may increase the risk of pathogen contamination in nearby drinking water wells. This study provides an important insight into the retention processes of microbes in sediments upon biochar amendment and the potential impact of biochar in facilitating microbial transport in the subsurface environment.

for providing guidance in bacteriophage analysis. We like to thank Mr Harold Rankine for assisting in the laboratory works and Mr Toney Hirnyk for helping in a laboratory set up. We also like to thank Ms Martin Sheridan (CSIRO, Adelaide), Dr Luke Mosely (University of Adelaide), and Mr Naser Khan (University of South Australia) for supplying the Biochar samples for us. We also thank the internal (Dr Mike Williams and Dr Lynne Macdonald) and external reviewers who have contributed ideas and suggestions to improve this manuscript.

Funding Sources

CHAPTER 5

Major Findings, Conclusions and Future Recommendations

5.1. Major Results and Conclusions

In chapter 2, the long-term breakthrough concentrations (BTCs) of nanoparticles (NPs) from the column experiments exhibited a bimodal shape i.e., an initial delay, then they rapidly increased, and then slowly approached the influent concentration. A one-site kinetic model with a Langmuirian (Adamczyk et al., 2013) or random sequential adsorption (Johnson and Elimelech, 1995) blocking function reasonably simulated the first few PVs of BTC, however, failed to adequately describe the deposition kinetics at later stages of deposition conducted at various physiochemical conditions. The fitted parameters showed that the initial time delay in BTC was determined by the values of attachment coefficient (k_{att1}) and maximum solid phase concentration of attached NPs (S_{max1}) on site 1, and the rising portion of the BTC was strongly determined by the values of attachment coefficient (k_{att2}) and maximum solid phase concentration of attached NPs (S_{max2}) on site 2. This observation was attributed to the variations of mass transfer rates of NPs to deposition sites affected by the variations in sand surface topography (Bradford et al., 2011a). The k_{att1} was controlled by the direct Brownian diffusion of NPs to the favourable attachment sites and the mass transfer of NPs over unfavourable regions via a shallow secondary minimum to the favourable attachment sites (Kuznar and Elimelech, 2007; Torkzaban et al., 2010). The presence of microscale surface roughness or previously deposited NPs can create a shadow region downgradient to the protrusion (Ko and Elimelech, 2000; Meinders

et al., 1992). The attachment of NPs at favourable attachment sites present in this shadow region is only possible by direct diffusive transport to this site, not by rolling or translating of NPs over the surface. Therefore, this study concluded that the value of k_{att2} will be impacted by the shadow effect (Sasidharan et al., 2014).

The study in chapter 2 also demonstrated that the fraction of the solid surface area that was available for deposition, S_f, was very small ($< 9\%$) and controlled by the coupled effect of flow velocity, solution chemistry, and particle size. The value of S_f increased with increasing ionic strength (IS), with the larger values were associated with smaller particles. This observation was attributed to the presence of physical and/or chemical heterogeneity on the sand surface, which completely eliminated the energy barrier to attachment and created a finite primary minimum interaction relative to the solution IS and colloid size (Bradford and Torkzaban, 2013; Shen et al., 2012b). The value of S_f was greater in the presence of Ca^{2+} than Na^+, suggesting that the complexation of Ca^{2+} ions to the silanol and carboxylic acid groups on the solid surface created nanoscale chemical heterogeneity that was favourable for attachment (Israelachvili, 1992). The value of S_f increased with decreasing flow velocity and was attributed to the increase in adhesion strength with increasing residence time at lower velocities (Dabroś and van de Ven, 1983; Meinders and Busscher, 1993; Xu et al., 2005).

In chapter 3, the influence of temperature on viruses and NPs attachment was examined under various physiochemical conditions. The experimental BTCs showed that the retention of viruses and NPs increased when the temperature increased from 4 to 20 °C, at intermediate ionic strength (IS) conditions (10 or 30 mM). The experimental results also demonstrated that the increase in the NPs retention with temperature for the IS of 10 and 30 mM was greater when the flow

velocity was lower. When the IS equalled 10 and 30 mM, an increase in the temperature from 4 to 20 °C produced an increase of up to 109% in fitted k_{att} value. However, the observed increase in k_{att} failed to be explained by the increase in single-collector efficiency, η, alone (only ~8–28%). The value of sticking efficiency, α, (up to 117%) and therefore, the value of S_f (up to 159%) significantly increased with temperature at intermediate IS conditions (10 or 30 mM). Conversely, the temperature had negligible influence on k_{att} and S_f values when IS was too low (1 mM) or too high (50 mM).

The results were explained by incorporation of nanoscale surface roughness and chemical heterogeneity on the sand surfaces in extended Derjaguin-Landau-Verwey-Overbeek (XDLVO) calculations (Bradford and Torkzaban, 2015; Huang et al., 2009; Shen et al., 2012a; Torkzaban and Bradford, 2016). The temperature had a relatively minor (< 3 kT) influence on the magnitude of the energy barrier to attachment ($\Delta\Phi_a$) in comparison to physical and chemical heterogeneity. However, a small reduction in $\Delta\Phi_a$ at a higher temperature significantly increased the probability for particles to attach in the primary minimum under intermediate IS conditions (Torkzaban and Bradford, 2016). Whereas, the temperature had negligible influence on the value of k_{att} and S_f at low IS (1 mM) due to the presence of a very large $\Delta\Phi_a$, and at high IS (> 50 mM) due to the complete absence of $\Delta\Phi_a$. Numerical simulations were conducted to better understand the coupled effect of IS, flow velocity, temperature, and colloid size by employing the (Bradford and Torkzaban, 2015) model. Consistent with the experimental observation, the simulated value of α and S_f increased from a minimum value at IS = 1 mM to a maximum at IS = 10 mM, and then slowly decreased with IS and became negligible at IS $\geq$ 40 mM. Therefore, this study concluded that an increase in temperature

from 4 °C to 20 °C increases the retention of viruses and NPs in porous media under intermediate IS conditions, representing fresh to brackish groundwater. The increase in k_{att} value with temperature can be only explained by the increase in α and, therefore, S_f by incorporating nanoscale surface physical and chemical heterogeneity on collector surface in interaction energy calculation.

In chapter 4, the transport and retention of *E. coli* bacteria and viruses were studied in the sand amended with several types of biochar from various plant material based feedstocks. Batch experiments over a wide range of chemical conditions demonstrated negligible adsorption of microbes to the biochar surface before and after chemical activation. At any given solution ionic strength, the attachment of viruses to sand was significantly higher than that of biochar, whereas bacteria showed no attachment to either sand or biochar. Column experiments conducted using biochar amended-sand demonstrated an enhanced transport of viruses compared to unamended sand experiments. In contrast, the retention of bacteria in biochar-amended columns was enhanced regardless of the solution chemistry. In this study, the particle size of biochar was found to be the underlining factor controlling the bacteria retention mechanism. The removal of the fine fraction of biochar (< 60 μm) was found to increase the transport of bacteria in biochar-amended experiments (Sasidharan et al., 2016). Therefore, this study concluded that the enhanced retention of bacteria in the biochar-amended sand was a result of straining of bacteria in pore constrictions, grain-grain contact points, and/or microscopic roughness locations (Bradford et al., 2014). This study has major implications for biochar application in environmental and agricultural fields. Biochar application to sediments may enhance the transport of nano colloids such as pathogenic viruses and toxic NPs, which can contaminate drinking water wells

Chapter 5

(Sasidharan et al., 2016).

As demonstrated by chapter 2, 3 and 4, the experiments conducted on pure quartz sand or river sand represent the worst-case scenario for microbe and NP attachment to a collector surface. Even though the XDLVO interaction energy calculation showed unfavourable conditions for NPs and microbe attachment to a solid surface, all the experimental results presented in this thesis showed significant retention for both NPs and microbes in the saturated sand porous media. The natural soil sediments typically contain metal oxides and clay particles, which will enhance the number of favourable sites available for attachment (Bradford and Torkzaban, 2013). Moreover, natural surfaces contain nanoscale physical heterogeneities (roughness) and chemical heterogeneities (mineral defects, isomorphic substitutions, adsorption of different ions, organic, and/or metal oxides) (Bradford and Torkzaban, 2012), which can significantly reduce the energy barrier to attachment and enhance the attachment of NPs and microbes to the collector surface (Bhattacharjee et al., 1998; Hoek et al., 2003; Shen et al., 2012a). Therefore, this thesis concluded that the transport and retention of NPs and microbes in saturated porous media is a coupled effect of solution chemistry (pH, IS, presence of divalent ion Ca^{2+}), system hydrodynamics, temperature, colloid size, and collector surface (chemical and physical heterogeneity) properties.

Chapter 3 and 4 showed that negligible inactivation of viruses was observed under various physiochemical conditions (electrolytes composition and temperature) during the experimental duration. Therefore, this thesis concluded that the observed enhanced deposition of viruses and NPs (abiotic particles, therefore, no inactivation) at various physiochemical conditions was purely due to the attachment of colloids to the solid grain surface. Thus, this thesis acknowledges the

141

solid-phase attachment of colloids as the very significant primary mechanism that contributes to the efficient removal of colloidal contaminants from treated wastewater or stormwater during natural porous media filtration applications.

5.2. Future Research Directions

5.2.1. Theoretical Aspects

This study specially acknowledged the importance of nanoscale chemical and physical heterogeneity on collector surface to include in the XDLVO interaction energy calculations to account for the observed NPs and microbe deposition in saturated porous media at unfavourable conditions. However, natural colloids such as viruses and bacteria contain nanoscale surface chemical (functional groups, extracellular polymers, and amino acid charge distribution) and physical (flagella, pili, and capsid structure) heterogeneities (Hori and Matsumoto, 2010; Jiang et al., 2004; Seth, 1994; Tsuneda et al., 2003). Future colloid deposition studies could attempt to quantify the colloid surface heterogeneities and include it in the interaction energy calculation to more accurately predict the microbial transport and deposition in saturated porous media.

5.2.2. Experimental Aspects

This thesis mainly focused on gaining a mechanistic understanding of the effect of individual factors (physical and chemical) on NPs and microbes deposition in a clean and controlled environment. The natural sediment contains a distribution of grain size (Bui et al., 1989), clay fractions, metal oxides on sediment surface (Chao and Zhou, 1983), and different mineral composition (Barber et al., 1992). These complex sediment properties and mineralogy may have a significant role in determining colloid deposition. Additionally, the stormwater, groundwater or wastewater contains organic matter such as humic materials (Artinger et al., 2000;

Tan, 2014) polysaccharides (Pi and Wang, 2006), proteins, and lipids (Fujita et al., 1996) with highly variable concentrations. The organic matter may block the attachment sites or may act as a competitor to NPs and microbes for favourable attachment sites on sediment surface (Franchi and O'Melia, 2003; Pham et al., 2009). Therefore, future research could be conducted in a more complex system that mimics natural conditions in order to assess the influence of sediment mineralogy and organic compounds on the transport and retention of NPs and microbes in subsurface environments.

The pore scale distribution of natural aquifer systems is more complex and contains fractures, macropores, and preferential flow (Cook et al., 2005; Gelhar et al., 1992; Igbal and Krothe, 1995). This could be the reason for observed discrepancies in field data where microorganisms were detected in drinking water wells (Malard et al., 1994). Therefore, laboratory scale studies with fractured system could be conducted to investigate the effect of fractures in colloid transport and retention, which will help to develop transport models to account for fractures in field studies.

This thesis mainly aimed to understand the factors controlling the irreversible attachment of colloids to collector surface. Interestingly, attempts to release viruses followed by deposition through transient changes in solution chemistry and system hydrodynamics showed negligible release of viruses implying irreversible attachment of viruses to the collector surface. However, it is speculated that once attached the presence of a strong adhesive force may lead to the capsid fracturing, escape of nucleic acid, structural deformation and changes in host reorganization sites, and nucleic acid degradation of viruses, which make them inactive or non-infectious (Harvey and Ryan, 2004). Therefore, it is very important to distinguish

between irreversible attachment and surface inactivation to acknowledge the virus removal through attachment and subsequent inactivation in natural filtration systems. Future research could be focussed on developing methods to distinguish between irreversible attachment and surface inactivation by employing techniques such as reverse transcriptase-polymerase chain reaction (RT-PCR) to detect viable microbes (Tsai et al., 1993; Yaron and Matthews, 2002).

In the managed aquifer recharge (MAR) guidelines (NRMMC-EPHC-NHMRC, 2009), the removal mechanism of microbes is primarily attributed to the inactivation in the aqueous phase during the aquifer storage period and the removal by attachment to solid grain (sediment) surface is completely neglected (Page et al., 2015a). In this research, virus samples kept at various physiochemical conditions during the course of experiments showed negligible virus inactivation (Sasidharan et al., 2016). Therefore, this thesis concluded that irreversible attachment is the primary mechanism that accounted for the observed removal of viruses and NPs at various physiochemical conditions in the saturated porous media. However, in order to incorporate the contribution of attachment as a removal mechanism and make necessary changes in the MAR guidelines, regulators would demand more field scale evidence. Therefore, future research could be focussed to conducting field scale virus (bacteriophage) transport studies in order to validate the laboratory scale experimental observations.

5.3. Applications in a Specialised Area of Research.

This thesis developed a significant understanding of mechanisms that control the interfacial interaction of colloids at SWI. Specific focus has given on incorporating nanoscale surface physical and chemical heterogeneity to determine the interaction energy between colloids and solid grain surface. Interestingly, colloids are present

in a wide variety of systems such as soil, the human body, atmosphere, food, and marine environment. Therefore, the knowledge gained in this thesis can be applied not only in water recycling or reuse technologies but also into many other research areas where an understanding of colloids and SWI interactions are important.

In biomaterial engineering applications such as the development of human body implants e.g., dental implant, knee implant or contact lenses, the surface nanotopography and chemistry of the implants surface found to have a significant role in determining the cell responses (Choi et al., 2007; Yim et al., 2010). A significant number of studies are attempting to develop biomaterials by introducing surface nanotopography of various size, shape, and density to study their effects on various biological processes such as immunological response, host cell-biomaterial surface interactions, cell adhesion and proliferation, and protein adsorption (Christo et al., 2016; Dalby et al., 2002; Deligianni et al., 2000; Goreham et al., 2013; Mendonça et al., 2008).

Marine biofouling, the colonisation of marine microbial organisms on submerged marine surfaces (e.g., ship, submarines) is a huge problem for the marine industry and cost millions of dollars for the maintenance (Callow and Callow, 2011). A significant number of bioinspired research showed that the surface nanotopography of marine surfaces has a significant role in preventing fouling organisms from attaching to the surface or promoting their easy detachment from the surface (Carman et al., 2006; Emily and Geoffrey, 2009; Genzer and Marmur, 2008). Schumacher et.al. demonstrated that the presence of a nanoforce gradient caused by the topographical features such as nanoscale surface roughness and chemistry has a significant role in determining the attachment of fouling organisms. The development of a predictive model will help to design unique non-

fouling surfaces for marine applications (Schumacher et al., 2008).

In the food industry, the contamination of the surfaces such as stainless steel by spoilage and pathogenic microbes, and subsequent biofilm formations are a major concern (Hilbert et al., 2003; Jullien et al., 2003). A significant number of studies have looked into the role of random irregular surface topographical features (peaks and valleys with varied height and spacing) (Flint et al., 2000) or surfaces with defined topographies on adsorption of various bacteria on steel surfaces (Whitehead et al., 2005). The results showed that the size, width and depth of the nanotopography, and size and shape of the bacteria have a significant role in determining the deposition of bacteria on the surface (Whitehead and Verran, 2006).

The above examples demonstrate that many research areas have acknowledged the importance of nanoscale surface topography and chemistry in developing surfaces that either enhance or reduce the colloidal attachment to the solid surface depends upon the end use. Therefore, understanding the factors and the fundamental mechanisms that control the deposition of colloids to solid surfaces is necessary, and this thesis contributes significant knowledge into these broad areas of colloid interface research.

APPENDIX A

Methodology

A.1. Bacteria Preparation

The day prior to each experiment, a bacterial colony from a pure culture plate was inoculated in 50 mL of Tryptic Soya Broth (TSB) (CM0129, Oxoid) and grown at 37 °C for 15–18 h while mixing on an orbital shaker (Incu-Shaker Mini, Benchmark Scientific, USA) at 100 rpm. Cells were pelleted using a centrifuge at 3,500 g for 30 minutes at 4 °C. The pellet was re-suspended in 1 mM NaCl and centrifuged again. Bacterial cells were twice washed with this electrolyte solution to ensure removal of the growth medium. The bacterial pellet was then diluted into the desired electrolyte solution to get a final absorbance of 0.45 at a wavelength of 460 nm, which corresponds to a bacterial influent concentration of ~10^8 cells mL^{-1}. Samples from batch and column experiments were analysed by measuring the absorbance at 460 nm using UV-vis spectrophotometry (SpectraMax Plus 384, US) and/or by counting colony forming units (CFUs) from the spread plate method (Wise, 2006).

Chapter 6

A.2. Bacteriophage Preparation

Phages (MS2, ΦX174, and PRD1) were used in this study as surrogates for human pathogenic viruses (Schijven and Hassanizadeh, 2000). Characteristics of phages and their respective host bacteria are given in Table A.1. The detailed methodology for bacteriophage preparation and enumeration is given below.

Phages were grown overnight on their host bacteria and cleaned following published protocols (10705-1-1995; 10705-2-2000). Concentrated phage suspension (10^9 to 10^{11} Plaque Forming Unit (PFU) mL^{-1}) was diluted in the electrolyte solution to obtain a final concentration of 10^7 PFU mL^{-1} for batch and column experiments.

The double-layer agar method was used to determine the concentration of viable viruses in aqueous samples. In brief, a host bacterial colony from a pure culture plate was inoculated into 10 mL of TSB in a sterile polypropylene (PP) 10 mL tube. For host *E. coli* ATCC 700891, 150 μg mL^{-1} Ampicillin and Streptomycin antibiotics were added into the broth. The bacterial culture was grown overnight (16–18 h) at 37 °C in a shaking incubator at 100 rpm. Overnight host cultures were stored in an ice bucket until use. A 3 mL aliquot of autoclaved half strength Tryptone Soya Agar (hsTSA) (CM0131, Oxoid) containing $CaCl_2$ (10 mM) was added to a glass test tube sitting on a 50 °C heat block (Dri-Block heater DB-4D, Techne, UK). Then 500 μl of host bacteria and 100 μl of sample were added to the hsTSA test tube, mixed well, and poured over a Tryptone Soya agar (TSA) plate containing $CaCl_2$ (10 mM). The TSA plate contained 150 μg mL^{-1} Ampicillin and Streptomycin antibiotics when the host was *E. coli* ATCC 700891. The agar plate was gently swirled to evenly distribute the soft agar, and once the soft agar dried (5 min) the plate was incubated at 37 °C. The ΦX174 plates were analysed for PFU

after 3.5-5 h incubation. MS2 and PRD1 plates were analysed after 18–20 h incubation. Only plates with 30–300 PFU were considered for analysis (10705-1-1995, 1995).

Table A.1. Characteristics of bacteriophages MS2, PRD1, and ΦX174 used in this study

Phage	Host	Phage type	Family	Isoelectric point	Size	Protein coat	Reference
				[pH]	[nm]		
MS2 [§](15597-B1)	*E. coli* HS(pFamp)R (700891)	F-specific (ssRNA)	Leviviridae	~2.2–3.9	24–26	partially hydrophobic	(Chrysikopoulos and Syngouna, 2012), (Schijven and Hassanizadeh, 2000)
PRD1 (BAA769-B1)	*E. coli* (BAA 769)	Somatic (dsDNA)	Tectiviridae	~3.4–4	62–65	partially hydrophobic	(Thomson, 2005), (Schijven and Hassanizadeh, 2000)
ΦX174 (13706-B1)	*E. coli* (13706)	Somatic (ssDNA)	Microviridae	~2.6–6.8	25–27	hydrophilic	(Chrysikopoulos and Syngouna, 2012), (Dika et al., 2015)

§All bacteria and bacteriophage strains were purchased from American Type Culture Collection

APPENDIX B

A systematic methodology for bacteriophage analysis

B.1. Virus

The word virus originally came from the Latin word referring to poison or venomous subject (Grafe, 2012). A virus is the most abundant biological entities on the planet and the smallest infectious agent, which can infect all types of organisms from large eukaryotic organisms like animals and plants to small prokaryotic organisms such as bacteria and archaea (Mutsaers, 2016) (Koonin et al., 2006). In scientific world there are still arguments are going on viruses, whether they are a form of life or organic structures that interact with living organisms. They are considered as the "organism at the edge of the life" as they have genes, they can reproduce, and evolve by natural selection (Rybicki, 1990). However, viruses do not have a cellular structure which is considered as the basic unit of life and lack metabolism, therefore, depend on host cell mechanism to reproduce or to carry out life-sustaining functions (Holmes, 2007; Wimmer et al., 2009). They can produce multiple copies of their progeny by a mechanism called self-assembly, where they use host mechanism to translate the genetic material and eventually produce their building blocks include lipids, amino acids, and capsid protein (Lodish et al., 2000).

B.2. Bacteriophage

A virus that attacks a bacteria or uses bacteria as a host is known as

bacteriophage (Orlova, 2009). The size of the bacteriophage can be ranged from 20–200 nm (Sulcius et al., 2011). For e.g., MS2 has a size of 26 nm (Sasidharan et al., 2016) and lambda bacteriophage roughly measure 200 nm (Mayer, 2016). Bacteriophages are considered as a surrogates for enteric viruses and are widely used in the transport studies due to their non-pathogenicity to human and animals, and easiness to work with them (Schijven and Hassanizadeh, 2000). The bacteriophage MS2, PRD1, and ΦX174 were used in this study and their characteristics are given in Table A.1 and (Sasidharan et al., 2016).

B.3. Virus Structure

B.3.1. Capsid

The capsid is the outer proteinaceous coat of the virus, which encloses the nucleic acid, and called the nucleocapsid (Davidson, 2015; Lodish et al., 2000). This capsid is made up of multiple copies of one or different protein subunits structures called capsomeres (Steven et al., 1976). The shape and arrangements of capsid protein subunit are determined by single or multiple gene products, which gives it's a rod-shaped helix, polygon-shaped sphere or elongated icosahedrons prolate structure (Prasad and Schmid, 2012). The viral capsid serves several functions, such as protect the virus genetic material from enzymatic digestion, virus attachment to host cells through specific protein sites, facilitate the entry of virus genomic material into the cell, and packing of newly formed viral particles (Davidson, 2015; Lucas, 2001).

B.3.2. Envelope

Many types of viruses have the envelope, a lipid bilayer surrounding the nucleocapsid consists of glycoproteins and sometimes lipid materials from

the host cell plasma membrane originated during the budding process (Lenar, 1978). Many viruses also develop a spike-like structure made of one or more types of a glycoprotein on the envelopes that facilitate their attachment to specific host cell surfaces (Davidson, 2015; Lenar, 1978).

B.3.3. Nucleic Acid

The genetic information of viruses is encoded in DNA (Deoxyribonucleic acid) or RNA (Ribonucleic acid). The genome of a virus can be single-stranded (ss) RNA, double-stranded (ds) RNA, ss DNA, dsDNA or a combination of DNA and RNA. Most viruses like MS2 has plus stand (+) ssRNA, which can act as a messenger RNA and can translate to produce proteins (Sugiyama et al., 1967). Based on the genetic material type and replication path the viruses are classified as six classes called Baltimore classification (Baltimore, 1971).

B.4. Life Cycle of Virus

The virus infection to bacteria can occur by two mechanisms called lytic or lysogenic cycle (Bertani, 1951; Lodish et al., 2000; Wang et al., 1996). A typical lytic cycle occurs as follows: 1) adsorption – the virus will adsorb to the host cell surface, 2) latent period – the virus will inject its genetic material, and various components for the final maturation of phage progeny are synthesised within the host cell using the materials of parental phage, host, and medium surrounding the host. This period is called eclipse period and at the end of it, the phage particles will assemble, and 3) lysis – lysis of host cells via enzymatic degradation or autolysis and release of virus progeny into the surrounding environment (Wang et al., 1996). Depends upon the species and condition a parent phage would able to produce 50–200 daughter phages

per lytic cycle (Raghu et al., 2012).

In a lysogenic cycle, the bacteriophage genetic material will stably associate into the host cell DNA in such a way the viruses remain dormant (prophage) and transferred to other cells via successive replication of infected host cell (Bertani, 1951; Lodish et al., 2000). However, prophage can sometimes activate via chemical or UV radiation and can undergo lytic cycle (Hartl, 2009). The viruses (MS2, PRD1, and ΦX174) used in this study undergo lytic cycle for their replication. The lysis of bacteria by the viruses can be observed as a cell destruction region is known as plaque (or clear zone) (Abedon and Yin, 2009) which is the basic principle of double layer agar method.

B.5. Inactivation of Virus

Viral inactivation makes viruses inactive (die), unable to replicate, or unable to infect the cell (Kumar, 2012). It is very important to understand the mechanism of virus inactivation to develop methods to improve the water quality level to safe drinking water. The virus may destruct by strong chemicals, exposure to UV, sunlight, temperature, or high pressure (Bertrand et al., 2012; Schijven and Hassanizadeh, 2000; Spire et al., 1984; Wommack et al., 1996). Various mechanisms of virus inactivation include capsid, lipid envelope, or genetic material destruction (Cordova et al., 2003; Gerba, 1984), mutation of genetic material and subsequent alteration or removal of its proteins (Fleischmann, 1996), induced conformational change of proteins, breakage of covalent bonds such as peptide and disulphide bonds (Wolbarsht, 1971), modification of virus surface protein which prevents virus adsorption and subsequent replication cycle (Saeb-Parsy, 1999), enzymatic degradation

of viral surface protein or genetic material and complete denature of virus (Harvey and Ryan, 2004).

B.6. Types of Bacteriophages

The RNA bacteriophages which enter the host cell via primary adsorption to F (fertility) or sex pili (fimbriae) coded by F-plasmid of male bacteria strain is called F-specific RNA bacteriophages (FRNA-phages) (Havelaar et al., 1990). The F-encoded pili are synthesised at a temperature higher than 30 °C and, therefore, FRNA-phages are not likely to replicate in a natural environment with low temperature. Moreover, their close resemblance in structure, composition, morphology, and failure to reproduce in a natural environment makes them a very conservative surrogate for animal viruses (Grabow, 2004). The MS2 used in this study is an FRNA-phage and infect the male *E. coli* ATCC 700891 HS(pFamp)R (Table A.1).

Bacteriophage that infects the host cell via the cell membrane is called somatic phages (Leclerc et al., 2000). The bacteriophages ΦX174 and PRD1 used in this study are an example for somatic coliphage (Table A.1).

B.7. Methods for Detection of Bacteriophages

The detection of bacteriophages in water or environmental samples is important to use them as an indicator of faecal contamination and to employ them as a surrogate for enteric viruses in field or laboratory scale transport studies. The bacteriophage analysis methods are well-developed and often called double-layer agar method or direct plaque assays (10705-1-1995, 1995; 10705-2-2000, 2000; Kropinski et al., 2009). However, this

study slightly modified the existing method to make the procedure more

user-friendly, cross-contamination free, faster, and use of fewer

consumables. The method presented here are for bacteriophages MS2,

PRD1, and ΦX174 using their respective host presented in Table A.1. The

method provides a step-by-step approach in order to establish this

technique in a new institution facility.

B.7.1. Preparation of Growth Media

B.7.1.1. 1 M CaCl2

1. Weigh 11.098 gr of $CaCl_2$ (Sigma-Aldrich–C1016).

2. Dissolve the salt in 100 mL Milli-Q water.

3. Filter sterilise using a 0.22 μm Milex-GP syringe filter Unit (Merck

   Millipore–SLGP033RB) attached to a 10 mL sterile syringe

   (Terumo Syringe Luer Lock–0197).

4. Aliquot 10 mL into the sterile 10 mL tubes.

5. Store in dark (wrap the tube with a foil paper) at 4 °C, for up to 2

   months.

6. Store in freezer at 20 °C for up to 1 year.

B.7.1.2. Antibiotics Stock (Ampicillin and Streptomycin Stock)

1. Weigh 0.15 g of ampicillin sodium salt (Sigma-Aldrich–A9518).

2. Weigh 0.15 gr of streptomycin sulphate (Sigma-Aldrich–S6501).

3. Dissolve the antibiotics in 100 mL Milli-Q water.

4. Mix/vortex, so all the antibiotics go into solution.

5. Filter sterilise using a 0.22 μm Milex-GP syringe filter Unit (Merck

   Millipore–SLGP033RB) attached to a 10 mL sterile syringe

   (Terumo Syringe Luer Lock–0197). [1]

6. Aliquot 10 mL into the sterile 10 mL tubes.

7. Store in dark (wrap the tube with a foil paper) at 4 °C, for up to 1 weeks. [2]

8. Store in freezer at 20 °C for up to 1 year. [3]

   NOTES:

   1) The solution should not be autoclaved.

   2) The stability of ampicillin in solution is a function of pH and temperature. The optimal pH is 3.8–5 and it lost the activity when stored above pH 7.

   3) The solution should not be freeze-thawed multiple times. Once thaw, store in the fridge in dark (wrap the tube with a foil paper) at 4 °C, for up to 1 week and discard.

B.7.1.3. Tryptone Soya Agar without Antibiotic

This media can be used for PRD1 and ΦX174 hosts *E. coli* ATCC BAA769 and *E. coli* 13706, respectively.

1. Weigh 20 gr of Tryptone Soya Agar powder (Oxoid–CM0131) in a weighing dish using a weighing balance.

2. Add the powder into a 1000 mL (1 L) Schott glass bottle. [4]

3. Measure 500 mL Milli-Q water using a measuring cylinder.

4. Add the measured 500 mL Milli-Q water into the bottle.

5. Shake well.

6. Add a heat resistant magnetic stirrer into the agar-water mix.

7. Place the bottle on a hot plate and set the temperature at 100 °C.

8. Continuously stir the media and boil the solution until the agar is completely dissolved and the solution is clear.

9. Label the bottle with an autoclave tape and write TSA, date and the name of the owner.

10. Autoclave at 121° C for 20 min in the autoclave machine. Usually, it takes 75 min to complete a cycle. [5]

11. Once autoclaved, bring the bottles (close the lids to avoid contamination) back to the lab and leave them in the water bath [6] at 50 °C. [7]

12. While waiting for the media to be cooled, switch on the laminar flow cabinet sterilises the surface using 70 % ethanol.

13. Open the petri dish bags [8] and spread the sterile 90 mm petri dishes (SARSTEDT–82.1472) (as five plate stacks) in the laminar flow cabinet.

14. Leave the plates in the laminar flow cabinet under UV lights for 10 min.

15. Switch off the UV light and leave the plates in the laminar flow cabinet.

16. Once the agar medium is cooled down to 50 °C [9], add 5 mL of the 1 M $CaCl_2$ stock (refer step B7.1.1) into the medium to obtain a final concentration of 10 mM mL^{-1} Ca^{2+}. [10]

17. Swirl gently in a circular motion to mix the media [11] and immediately pour ~10 mL per plate, into the sterile petri dishes. [12]

18. Once the plates are completely cooled down (30–60 min), invert the plates upside down in order to avoid the condensation to fall over the plates.

19. Place three prepared TSA plates from the batch in a 37 °C incubator for purity check before storing away and leave the rest of the plates at room temperature in the laminar flow cabinet (keep the cabinet switched off) or in any other sterile surface for overnight.

20. Next day, check for the presence of any bacteria growth on the incubated plates or plates in the laminar flow cabinet.

21. Discard the plates with growth.

22. Stack the plates into 20 (depends on the package size), stripe the side of the plates with a BLACK marker pen (to identify the plates for later use). [13] Pack the plates into the plastic bag (the original sterile package can be used), label the package with name, date, TSA and store at 4 °C in a cold room. [14]

NOTES:

4) Never prepare an agar media as a full bottle. The agar solution boils and can spill into the autoclave. This leads to changes in the composition of the media and may lead to poor results. It may also damage the autoclave.

5) Make sure, while autoclaving, the caps of the bottles are loosened and the bottles are placed in an aluminium tray to avoid any spillage blocking the autoclave.

6) Make sure to use only double distilled or Milli-Q water in the water bath and ensure to clean the water bath every two days in order to avoid the growth of bacteria. The temperature and moisture help microbes to grow, which can contaminate the media. Take care to keep the bottle only submerged enough to keep the bottle content to be warm. Do not let the media-containing bottle to fall over and float, which may lead to the contamination as well.

7) The autoclaved agar media is very hot and can cause severe burns. Therefore, wear appropriate personal protective equipment (PPE) such as heatproof gloves, shoes, and lab coats while handling and transport.

8) Take care to cut the petri dish bag on the top in order to keep it for later storage of the plate.

9) A simple test to check the temperature is to touch the bottle on the wrist for 10 sec. If the temperature is warm, it is ready to proceed. Alternatively, a thermometer can be used to test the temperature. However, make sure to sterilise the thermometer, open the media while it is in the laminar flow cabinet, and work near a Bunsen burner flame to avoid contamination.

10) Use a 5 mL pipette (Socorex 835.05) with autoclaved tips to add the $CaCl_2$ solution to avoid the cross contamination. Work near a Bunsen burner flame. The $CaCl_2$ found to enhance the attachment of bacteriophage to the bacteria surface and helps improve the virus detection limits.

11) Do not shake the media to create bubbles, as it will produce bubbles in the plate, which can lead to poor results.

12) Approximately 50 plates can be prepared from one 500 mL TSA bottle. Therefore, plan the media preparation in order to produce enough plates for the later analysis. Also, make sure to pour the plates fast enough to avoid the formation of clotted agar, which will give a rough surface to the solidified plates and will lead to poor results. If clotting started to occur, stop pouring in order to avoid wastage of prepared media. Place the bottle into a microwave (with loosened cap) and melt the agar completely before pouring the media into the petri dish again.

13) One can label individual plates (at the bottom of the plate not on the lids), but it may laborious and time-consuming. Striping it with specific colour would be easier and faster, but remember that, this will be only useful in lab facilities with a limited number of growth media,

single user facility, or appropriate communication arrangements are in place.

14) The prepared plates can be stored for up to 2 months. However, check for the presence of microbial growth, drying out of media (visible as lines) or excessive condensation in the plates before further use.

B.7.1.4. Tryptone Soya Agar with Antibiotics

This media can be used for the MS2 host *E. coli* 700891. The *E. coli* 700891 contains a conjugative F-plasmid with an antibiotic (Ampicillin and Streptomycin) resistance gene. Therefore, this *E. coli* strain is considered as a genetically modified organism and Biosafety level 2 guidelines are applicable where necessary.

1. Weigh 20 gr of Tryptone Soya Agar powder (Oxoid–CM0131) in a weighing dish using a weighing balance.

2. Add the powder into a 1000 mL (1 L) Schott glass bottle. [4]

3. Measure 500 mL Milli-Q water using a measuring cylinder.

4. Add the measured 500 mL Milli-Q water into the bottle.

5. Shake well.

6. Add a heat resistant magnetic stirrer into the agar-water mix.

7. Place the bottle on a hot plate and set the temperature at 100 °C.

8. Continuously stir the media and boil the solution until the agar is completely dissolved and the solution is clear.

9. Label the bottle with an autoclave tape and write TSA, date and the name of the owner.

10. Autoclave at 121° C for 20 min in the autoclave machine. Usually, it takes 75 min to complete a cycle. [5]

11. Once autoclaved, bring the bottles (close the lids to avoid contamination) back to the lab and leave them in the water bath [6] at 50 °C. [7]

12. While waiting for the media to be cooled, switch on the laminar flow cabinet, and sterilises the surface using 70% ethanol.

13. Open the petri dish bags [8] and spread the sterile 90 mm petri dishes (SARSTEDT–82.1472) (as five plate stacks) in the laminar flow cabinet.

14. Leave the plates in the laminar flow cabinet under UV lights for 10 min.

15. Switch off the UV light and leave the plates in the laminar flow cabinet.

16. Once the agar medium is cooled down to 50 °C [9], add 5 mL of the 1 M $CaCl_2$ stock (refer step B7.1.1) into the medium to obtain a final concentration of 10 mM mL^{-1} Ca^{2+}. [10]

17. Add 5 mL of Ampicillin-Streptomycin antibiotic stock into the 500 mL TSA to obtain a final concentration of 150 μg mL^{-1} antibiotics in the medium.

18. Swirl gently in a circular motion to mix the media [11] and immediately pour ~10 mL per plate, into the sterile petri dishes. [12, 15]

19. Once the plates are completely cooled down (30–60 min), invert the plates upside down in order to avoid the condensation to fall over the plates.

20. Place three prepared TSA plates from the batch in a 37 °C incubator for purity check before storing away and leave the rest

of the plates at room temperature in the laminar flow cabinet (keep the cabinet switched off) or in any other sterile surface for overnight.

21. Next day, check for the presence of any bacteria growth on the incubated plates or plates in the laminar flow cabinet.

22. Discard the plates with growth.

23. Stack the plates into 20 (depends on the package size), stripe the side of the plates with a RED marker pen (to identify the plates for later use). [13] Pack the plates into the plastic bag (the original sterile package can be used), label the package with name, date, TSA and store at 4 °C in a cold room. [14]

NOTES

Follow the notes as explained for TSA preparation at section 7.1.3.

15) If clotting started to occur, stop pouring. However, do not re-melt in the microwave as it will break down the antibiotics and will not be useful. Dispose the clotted agar into the appropriate biological contaminant bin. Do not pour the agar-containing solution through the sink, as it will clog the drainage.

NOTES

If the Oxoid ready-made formulation for TSA is not available, use the below formulation to prepare the Tryptone Yeast agar, a replacement for TSA agar.

Tryptone	5 g
Yeast Extract	0.5 g

NaCl	4 g
Agar	7.5 g
Milli-Q water	500 mL

Follow the procedures explained in section 7.1.3 or 7.1.4

B.7.1.5. Tryptone Yeast Single Strength Agar (ssTYA) Powder

1. Prepare the stock ssTSA powder as follows for 1000 mL.

    a. Tryptone   10 gr

    b. Yeast   1 gr

    c. NaCl   8 gr

    d. Agar   7.5 gr

2. Mix well and store. [16]

    NOTES:

      16) If needed, a bulk volume can be prepared with the same proportion. Mix well the powder by keeping the mixture-containing bottle in an orbiting rotator for 1 h.

B.7.1.6. Tryptone Yeast Single Strength Agar (ssTYA)

1. Weigh 5.3 gr of ssTYA powder. [17]

2. Measure 200 mL Milli-Q water. [17]

3. Add the powder and 200 mL water into a 500 mL Schott glass bottle. [17]

4. Shake well.

5. Add a heat resistant magnetic stirrer into the agar-water mix.

6. Place the bottle on a hot plate set and set at 100 °C.

7. Continuously stir the media and boil the solution until the agar is completely dissolved and the solution is clear.

8. Label the bottle with an autoclave tape and write ssTYA, date and the name of the owner.

9. Autoclave at 121° C for 20 min in the autoclave machine.

10. Once finished the autoclaving, close the lids, and bring the bottles back to the lab.

11. Store on the lab shelf. [18, 19]

   NOTE:

   17) If using a 250 mL Schott glass bottle, weigh 2.65 gr of ssTYA powder, add 100 mL of Milli-Q water, and follow step 4–11.

   18) The ssTYGA agar has a shelf life of 1 month at room temperature.

   19) It can be stored at 4 °C for up to 6 months.

B.7.1.7. Tryptone Soya Broth (TSB)

1. Weigh 30 gr of Tryptone Soya Broth (Oxoid–CM0129) in a weighing dish using a weighing balance.

2. Add the powder into a 1000 mL (1 L) Schott glass bottle.

3. Measure 500 mL Milli-Q water using a measuring cylinder.

4. Add the measured 500 mL Milli-Q water into the bottle.

5. Shake well.

6. Label the bottle with an autoclave tape and write TSB, date, and the name of the owner.

7. Autoclave at 121° C for 20 min in the autoclave machine.

8. Once finished the autoclaving, bring the bottles back to the lab and leave on the lab bench to cool down.

9. Store in the fridge at 4 °C. [20]

NOTE:

20) The TSB can be stored in the fridge for up to 2 months. If any
cloudiness, precipitation, crystallisation, or growth was observed,
autoclave the media immediately, and discard appropriately.

B.7.2. *Escherichia coli* Culture Preparation
Materials

Day 1

a. *Escherichia coli* ATCC 13706 stock

b. *Escherichia coli* ATCC BAA 769 stock

c. *Escherichia coli* ATCC 700891 stock

d. Tryptone Soya Broth

e. Ampicillin-Streptomycin stock

f. 10 mL sterile culture tubes

g. Sterile loop

h. Pipettes

    i. 1 mL   (Socorex 825.1000)   Bacteria

    ii. 200 μL   (Socorex 825.0200)   Antibiotics

    iii. 10 mL   (Socorex 835.02)   TSB Transfer

i. Pipette tips

    i. 1.2 mL   Biosphere®Fil.Tip 1250 μl   Bacteria

    ii. 200 μL   Sterile yellow tips   Antibiotics

j. 10 mL   TSB

k. Incubator at 37 °C

l. Shaking incubator at 37 °C

m. Laminar flow cabinet

Chapter 7

Day 2

    a.   Tryptone Soya Agar Plate

    b.   Tryptone Soya Agar Plate with Ampicillin/Streptomycin

    c.   Items g–l from Day 1

Method

STEP 1: Liquid culturing method

1. Bring out the bacteria culture cryo vial stored at -20 °C or -80 °C freezer.

2. Allow to thaw the tubes to room temperature (20 min).

3. Label three 10 mL culture test tubes with culture name, species name, owner name, and date.

4. Aliquot 5 mL TSB into each of the bottle.

5. Add 50 μl of ampicillin-streptomycin stock into the *E. coli* ATCC 700891 labelled tube.

6. Add 100 μl of appropriate bacteria culture from the cryo vial to the respectively labelled tubes.

7. Place the tubes in a shaking incubator at 37 °C for 16–18 h. [21]

8. Next day observe the tubes for growth.

STEP 2: Plate Method

9. Label the plates with culture name, species name, owner name, and date as follows. [22]

      • Use Tryptone Soya Agar plate (black stripe) for *Escherichia coli* ATCC 13706 and ATCC BAA 769.

      • Use Tryptone Soya Agar Plate with Ampicillin-Streptomycin (red stripe) for *Escherichia coli* ATCC 700891.

10. Take 100 µl of the overnight grown bacterial culture, add it to the corner of the respective bacteria plate, and allow drying for 1 min.

11. Make a streak plate using the sterile loop. [23]

12. Make replicate plates for each of the bacterial species.

13. Incubate the plates by keeping upside down at 37 °C for overnight (16–18 h).

14. Next day, observe the plates for ideal colony size and distribution.

15. Wrap each plate using a parafilm to avoid contamination and longer shelf life.

16. Store in fridge at 4 °C. [24]

NOTES

21) Loosen the lids to allow the airflow into the tubes, as *E. coli* is an aerobic bacterium and require enough oxygen to grow.

22) Always label on the bottom of the plate. Never label the lids as it will lead to mixing up of the lid and thus the bacteria cultures.

23) Make sure to use a new loop after streaking each side of the plate to get a single colony distribution.

24) The *E. coli* bacteria culture can stay in the fridge at 4 °C for up 4 weeks. A new culture plate can be prepared from the mother plate after 4 weeks. However, do not produce more than three generations from a mother culture as the bacteria might lose specific characteristics via mutation. After three generations, go back to the step 1 and repeat the procedures.

B.7.3. *Escherichia coli* Culture Long Term Storage

Materials

a. *60 % Glycerol*

- Make a 60 % glycerol solution by mixing 40 mL Milli-Q water and 60 mL 100% glycerol.

- Autoclave at 121 °C for 20 minutes.

- Store at room temperature for up to 6 months.

b. 2 mL sterile screw cap cryo vials [25]

c. 10 mL sterile tube

d. Pipettes

• 1 mL	(Socorex 825.1000)	Bacteria
• 200 μL	(Socorex 825.0200)	Antibiotics
• 5 mL	(Socorex 835.05)	Glycerol transfer
• 10 mL	(Socorex 835.02)	TSB Transfer

e. Pipette tips

• 1.2 mL	Biosphere®Fil.Tip 1250 μl	Bacteria
• 200 μL	Sterile yellow tips	Antibiotics
• 5 mL		Glycerol
• 10 mL		TSB

Method

1. Prepare bacterial cultures as described in section B7.2, Step 1: Liquid culture.

2. Label three 10 mL culture test tubes with the culture name, species name, owner name, and date.

3. Aliquot 10 mL of TSB into each of the bottle.

4. Add 100 μl of ampicillin-streptomycin stock into the *E. coli* ATCC 700891 labelled tube.

5. Add 100 µl of the overnight grown bacterial culture into the respective tubes.

6. Place the tubes in a shaking incubator at 37 °C for 4–5 h.

7. Remove 2.5 mL of the liquid bacteria culture from the 5 h grown 10 mL culture tube.

8. Add 2.5 mL of 60 % glycerol into the remaining 7.5 mL to obtain a final concentration of 15 % glycerol.

9. Mix very well until glycerol is fully mixed and no layers are present in the tube.

10. Label cryo vials with appropriate bacteria name, owner name, and date. [25]

11. Aliquot 1 mL of the bacteria culture in respective cryo vials.

12. Store at -80 °C for several years. [26]

13. Store at -20 °C for up to a year. [26]

   NOTE:

   25) Snap cap centrifuge tubes are not recommended for glycerol storage as they can open while in the freezer.

   26) Do not freeze-thaw the frozen glycerol stocks multiple times. This may affect the viability of cultures.

B.7.4. Bacterial Host Preparation Prior to Double Layer Agar Method

Materials

a. *Escherichia coli* ATCC 13706 stock plate [27]

b. *Escherichia coli* ATCC BAA 769 stock plate [27]

c. *Escherichia coli* ATCC 700891 stock plate [27]

d. Tryptone Soya Broth

e. Ampicillin-Streptomycin Stock

      f.   10 mL sterile polypropylene culture tubes

      g. Sterile Loop

      h. Pipettes

- 200 µL   (Socorex 825.0200)   Antibiotics

- 10 mL   (Socorex 835.02)   TSB Transfer

      i. Pipette tips

- 200 µL   Sterile yellow tips   Antibiotics

- 10 mL   TSB

      j. Racks for test tube

      k. Mini Shaking Incubator set at 37 °C

Method

1. Label three 10 mL tubes with the name of the bacteria, owner name, and date.

2. Transfer 10 mL Tryptone Soya Broth into each tube. [28]

3. Add 100 µl of ampicillin-streptomycin stock to obtain a final concentration of 150 µg mL^{-1} into the *E. coli* ATCC 700891 tube.

4. Pick a single colony from each host plates using a sterile loop and add it to the respective labelled 10 mL tubes.

5. Mix well.

6. Close the lid and continue the process for all bacteria.

7. Place the tubes in a mini shaking incubator.

8. Loosen the lids slightly.

9. Incubate at 37 °C at 100 rpm for 14–16 hours.

10. Place the host in an ice bucket until ready to use. [29]

NOTES

27) Use fresh bacterial culture plates, which is not older than two weeks. Also, do not use more than three generations from the mother culture.

28) Transfer 50 mL of TSB into a sterile tube and leave it at room temperature for 30 minutes before use. Allocate the 10 mL pipette for handling only sterile solution. This will reduce the chances of cross-contamination. Maintain the pipettes according to the manufacturer's recommendations.

29) The host prepared can be stored in the ice bucket for 4–6 hours and should be used within the same day. The bacteria host kept in the ice bucket are not suitable for next day use.

B.7.5. Preparation of Bacteriophage Samples from the Column Experiments Prior to the Double Layer Agar Method

Material

a. **Phosphate Buffer Saline (PBS)**
   - Weigh 1.44 gr of Na_2HPO_4.
   - Weigh 0.24 gr of KH_2PO4.
   - Mix the salt with 1 L Milli-Q water.
   - Autoclave at 121 °C for 20 min.
   - Store at room temperature for up to 1 year.

b. Sterile 2 mL centrifuge tubes
c. Pipettes

   - 1 mL   (Socorex 825.1000)   Bacteriophage sample
   - 200 µL   (Socorex 825.0200)   Bacteriophage sample
   - 5 mL   (Socorex 835.05)   PBS

d. Pipette tips

   - 1 mL   Biosphere®Fil.Tip 1000 µl   Bacteriophage sample

Chapter 7

- 200 μL   Sterile yellow tips   Bacteriophage sample

- 5 mL   PBS

e. Bacteriophage samples

f. Bacteriophage control

g. Sterile 50 mL falcon tubes

h. Racks for centrifuge tubes

Method

1. Aliquot 1.8 mL of PBS into 2 mL sterile centrifuge tubes. [30]

2. Add 200 μl of the bacteriophage-containing sample into the centrifuge tube.

3. Perform a serial dilution. [31]

4. Label the dilution tubes with samples ID and dilution step.

5. Prepare dilutions of bacteriophage stock with known concentration to use as a control.

6. Store the samples at 4 °C. [32]

NOTES

30) Transfer 50 mL of PBS into the sterile 50 mL falcon tube in order to avoid contaminating the stock solution.

31) You should have an idea on the required number of serial dilution for each sample. This will gain through experience.

32) The sample analysis should be finished within 0–4 days of the experiment. One can conduct inactivation study of a control at given experimental condition if analysis requires longer periods.

B.7.6. Double Layer Agar Method

Material

a. Overnight grown bacteria culture

- *Escherichia coli* ATCC 13706 stock plate

- *Escherichia coli* ATCC BAA 769 stock plate

- *Escherichia coli* ATCC 700891 stock plate

b. Bacteriophage sample

c. Bacteriophage stock (control)

d. Pipettes [33]

- 1 mL   (Socorex 825.1000)   Bacteria

- 1 mL   (Socorex 825.1000)   Bacteriophage sample

- 200 μL   (Socorex 825.0200)   Bacteriophage Sample

- 5 mL   (Socorex 835.05)   sTYGA, $CaCl_2$ and antibiotics

e. Pipette tips

- 1.2 mL   Biosphere®Fil.Tip 1250 μl   Bacteria

- 1 mL   Biosphere® Tip 1000 μl   Bacteriophages

- 200 μL   Sterile yellow tips   Bacteriophage Sample

- 5 mL   ssTYGA, $CaCl_2$ and antibiotics

f. Sterile 8 mL glass test tubes

g. Dri-Block heater DB-4D (Techne)

h. 1 M $CaCl_2$ stock

i. Ampicillin-Streptomycin Stock

j. ssTYA Agar

k. TSA Plates (Black stripe)

l. TSA+Antibiotics plate (Red stripe)

    m. Waste Container

    n. Marker Pen

    o. 70 % Ethanol

    p. Laminar Flow Cabinet

    q. Microwave

    r. Water bath set at 50 °C

Method for PRD1 and ΦX174

1. Melt the 200 mL ssTYA agar in the microwave.

2. Keep the bottle in the water bath at 50 °C for 20 min.

3. Add 2 mL of $CaCl_2$ stock into the ssTYA media.

4. Mix well.

5. Aliquot 3 mL of the ssTSA media into the glass test tube sitting on a 50 °C heat block.

6. Add 500 μl of the host bacteria [34] into the ssTYA media.

7. Add 100 μl of the samples into the ssTSA + bacteria mixture.

8. Mix well.

9. Pour into the previously prepared TSA (black stripe) plate.

10. Gently swirl the plate to evenly distribute the soft agar on the TSA plate.

11. Once dried (5 min), incubate the plates at 37 °C.

12. Analyse the ΦX174 plates after 3.5–5 h incubation.

13. Analyse the PRD1 plates after 16–24 h incubation.

14. Count the plaque forming units (PFU).

15. Only consider plates with 30–300 PFU.

Chapter 7

Method for MS2

1. Melt the 200 mL ssTYA agar in a microwave.

2. Keep the bottle in the water bath at 50 °C for 15 min.

3. Add 2 mL CaCl$_2$ stock into the ssTYA media.

4. Add 2 mL ampicillin-streptomycin antibiotics into the ssTYA media.

5. Mix well.

6. Aliquot 3 mL of the ssTSA media into the glass test tube sitting on a 50 °C heat block.

7. Add 500 μl of the host bacteria [34] into the ssTYA media.

8. Add 100 μl of the samples into the ssTSA + bacteria mixture.

9. Mix well.

10. Pour into the previously prepared TSA + antibiotics (red stripe) plate.

11. Gently swirl the plate to evenly distribute the soft agar on the TSA plate.

12. Once dried (5 min), incubate the plates at 37 °C.

13. Analyse the MS2 plates after 16–24 h incubation.

14. Count the PFU.

15. Only consider plates with 30–300 PFU.

NOTES:

33) It is very important to use the specific pipette for each task. Do not mix up the pipettes for bacteria, bacteriophages, and sterile solution. During the pipetting, nanodroplets can adhere to the wall of the pipette. This could lead to contamination and very poor results in DLA.

34) Bring out the bacteria host culture from the ice bucket and keep it in the room temperature for 30 min before using it for the DLA. The

sudden temperature change from zero to 50 °C may lead to the

bacteria death via heat shock and leads to the poor results. In

addition, it will create clots in the ssTYA media and produce a rough

surface on the DLA plates, which will lead to a poor result.

B.7.7. Plaque Forming Unit Calculation

Sample 1.

You have a sample with unknown concentration. You have diluted the sample

1:1000 times. The volume of sample plated is 1 mL from the 1:1000 dilution.

You have observed 234 plaques on your plates. What is the concentration of

your initial sample?

$$PFU\ mL^{-1} = \frac{Number\ of\ plaques\ (PFU)}{Dilution\ \times Volume\ of\ the\ sample\ plated\ (mL)}$$

Number of plaques   = 234

Dilution   = 1: 1000 = 0.001 or 10^{-3}

Volume plated   = 1 mL

PFU mL^{-1} $= \frac{234}{0.001 \times 1}$ $=$ 2.34×10^5 PFU mL^{-1}

Sample 2.

You have a sample with unknown concentration. You have diluted the sample

1:10,000 times. The volume of sample plated is 100 μL from the 1:10,000

dilutions. You have observed 89 plaques on your plates. What is the

concentration of your initial sample?

Number of plaques   = 89

Dilution $= 1: 10{,}000 = 0.0001$ or 10^{-4}

Volume plated $= 100\ \mu L = 0.1\ mL$

PFU mL^{-1} $= \dfrac{89}{0.0001 \times 0.1}$ $=$ 8.9×10^{6} PFU mL^{-1}

B.7.8. Production of Bacteriophage

Material

a. Overnight grown bacteria culture

- *Escherichia coli* ATCC 13706 stock plate

- *Escherichia coli* ATCC BAA 769 stock plate

- *Escherichia coli* ATCC 700891 stock plate

b. Bacteriophage stock

- ΦX174 ATCC 13706-B1 [35]

- PRD1 ATCC BAA769-B1 [35]

- MS2 ATCC 15597 B1 [35]

c. Sterile autoclaved conical flask

d. Tryptone soya broth

e. Ampicillin-Streptomycin stock

f. Mini shaking incubator set at 37 °C

Method

1. Use standard procedures for phage propagation as described in the literature. The following is an example of a procedure, which has proven to give good results (10705-1-1995, 1995; 10705-2-2000, 2000).

2. Label three conical flasks of 250 mL with the host name, respective bacteriophage name, owner name, and date.

3. Aliquot 25 mL of TSB into each conical flask.

Chapter 7

4. Add 250 μl of ampicillin-streptomycin stock into the *E. coli* ATCC 700891 + MS2 ATCC 15597-B1 conical flask.

5. Inoculate with 1 mL of appropriate overnight grown host strain.

6. Incubate at 37 °C at 100 rpm for 3 h.

7. Add MS2/PRD1/ΦX174 from a stock to a final concentration of 10^7 PFU mL^{-1} to the respective host culture flasks.

8. Incubate at 37 °C at 100 rpm for 6 h.

9. Add 2.5 mL of chloroform ($CHCI_3$), mix well, and place overnight at 4 + 2 °C.

10. Decant the aqueous phase into a 50 mL centrifuge tube (labelled appropriately) and centrifuge at a minimum of 3000 g for 20 min at 4 °C.

11. Carefully pipette out the supernatant containing the bacteriophages into a sterile 50 mL centrifuge tube and store at 4 + 2 °C. [36]

12. Double-layer agar method was used to determine the concentration of viable viruses from the samples. [37]

SAFETY PRECAUTIONS

Chloroform is a carcinogenic substance. Use relevant safety precautions or use a suitable alternative.

NOTES

35) The bacteriophages can be purchased from American Type Culture Collection (ATCC).

36) The titre of the phage stock suspension will slowly decrease over time.

37) The titre of the phage suspension should be above $I0^{10}$ PFU mL^{-1} and may reach up to 10^{13} PFU mL^{-1}. Repeat the culturing step using a higher titre initial stock to increase the final phage concentration.

APPENDIX C

Abstracts Presented in Conference Associated with this Research

1. **Coupled Effects of Hydrodynamic and Solution Chemistry Conditions on Long-Term Nanoparticle Transport and Deposition in Saturated Porous Media**

S. Sasidharan[1, 2], S. Torkzaban[1] and S. A. Bradford[3]

[1]*CSIRO Land and Water, Glen Osmond, SA 5064, Australia*

[2]*NCGRT, Flinders University, SA 5001*

[3]*USDA, ARS, Salinity Laboratory, Riverside, CA 92507*

Oral Presentation: ***The International Conference on Interfaces against Pollution (IAP)***, titled "Interfaces in Water and Environmental Science", organised by Wetsus, Centre of Excellence for Sustainable Water Technology, Leeuwarden, The Netherlands.

Time and location: 25–28 May 2014, De Harmonie, Leeuwarden, The Netherlands

Abstract

This study aims to systematically explore the coupled effects of hydrodynamic and solution chemistry conditions on the long-term transport and deposition kinetics of nanoparticles (NPs) in saturated porous media. Column transport

experiments were carried out at various solution ionic strengths (IS), ion types (monovalent and divalent), and flow velocities utilising negatively charged carboxyl-modified latex NPs of two different sizes (50 and 100 nm) using acid washed medium sized river sand. Most experimental studies of NP deposition in porous media have focused on the initial clean bed deposition. In this study, the experiments were designed to obtain the long-term breakthrough curves (BTCs) in order to unambiguously determine the full deposition kinetics and the fraction of the solid surface area (S_f) that was available for NP deposition. The experimental evidence accessible in the literature on the dependency of S_f on physiochemical and hydrodynamics factors, especially for NP are very narrow. The BTCs exhibited a bimodal shape with increasing solution IS; e.g., BTCs were initially delayed, then they rapidly increased, and then slowly approached the influent particle concentration. Most of the previous research was conducted in the presence of a monovalent electrolyte. In this study, we compared the effect of monovalent (NaCl) and divalent ($CaCl_2$) solution chemistry. NP deposition was much more prominent in the presence of Ca^{2+} than Na^+ at any given solution IS. Deposition dynamics of NPs was successfully simulated using a two-site kinetic model that accounted for irreversible deposition and blocking (e.g., a decreasing deposition rate as the available site filled) on each site. Results showed that S_f values were controlled by the coupled effects of flow velocity, solution chemistry, and particle size. Data analyses further demonstrated that only a small fraction of the solid surface area contributed in NP deposition even at the highest IS (60 mM NaCl and 3 mM $CaCl_2$) and lowest flow velocity (1 m day^{-1}) tested. Consistent with previous studies conducted with clean sand, our results imply that NP deposition occurred because of physicochemical interactions between the negatively charged COOH groups on the NPs and nanoscale physical and/or chemical heterogeneities on the sand

surfaces that produced localised nanoscale favourable sites. Furthermore, our results suggest that the NP interactions with the collector surfaces tended to strengthen with increasing contact time.

Chapter 8

Chapter 8

2. The Impact of Nanoscale Charge Heterogeneity on the Fate and Transport of Viruses: Effects of Solution pH, Ionic Strength, and Phosphate

S. Saidharan[1,2], S. Torkzaban[1], S.A. Bradford[3], and P.G. Cook[2]

[1]CSIRO Land and Water, Glen Osmond, SA 5064, Australia

[2]NCGRT, Flinders University, SA 5001

[3]USDA, ARS, Salinity Laboratory, Riverside, CA 92507

Abstract

Chemical heterogeneity is an intrinsic property of all naturally-occurring mineral surfaces in the subsurface environment. An extensive set of column experiments was conducted to examine the effects of solution chemistry such as ionic strength (IS), pH, and anion type on attachment and inactivation of three bacteriophages (MS2, PRD1, ΦX174), as surrogates for human pathogenic viruses, in a chemically heterogeneous (metal oxides) sand. Patchwise nanoscale chemical

heterogeneity was introduced to the sand surfaces by modifying the surface chemistry of sand grains via reaction with a weak acid. The attachment efficiency of all viruses to the sand surfaces increased with increasing IS and decreasing pH. Attachment of MS2 and PRD1 was found to be more sensitive to the changes in pH and IS than ΦX174 because of their lower isoelectric points. The presence of phosphate (10 mM PO_4^{-2}) in the eluting solution significantly reduced the virus attachment efficiency due to a reduction in the chemical heterogeneity as a result of complexation of phosphate ions with metal oxides. At pH 7.5 about 40% of the attached viruses were released when the columns were eluted using a beef extract solution (pH 9.5) immediately following the attachment phase. Conversely, when the viruses remained attached for about 2 days on the sand surfaces, less than 2% of viruses were recovered following elution with beef extract. This difference in the release was attributed to rapid inactivation of the attached viruses.

Chapter 8

3. Coupled Effect of Flow Velocity and Particle Concentration in the Attachment and Detachment of Nanoparticle in Natural Porous Media

S. Sasidharan[1,2], S. Torkzaban[1] and P.G. Cook[2]

[1]*CSIRO Land and Water, Glen Osmond, SA 5064, Australia*

[2]*NCGRT, Flinders University, SA 5001*

Abstract

Understanding the fate and transport of nanoparticles (NPs) such as engineered NPs and pathogenic viruses in subsurface environment is important to assess contamination potential of groundwater resources. In this study, laboratory column and batch experiments were undertaken to examine the influence of flow velocity, solution ionic strength (IS), and input NP concentration (C_i) on the retention of two different sizes (100 and 50 nm) of carboxyl-modified latex NPs in natural sand. Batch studies showed the effect of input concentration (C_i) on NP retention on sand surfaces was absent over the range of IS conditions tested. In contrast, the results of the column experiments showed that the fraction of sand surface area available

to NP attachment (S_f) at a given IS decreased with increasing flow velocity and C_i. The input concentration effects were dependent on the flow velocity and IS conditions. Results showed that following the NP deposition, negligible detachment occurred when the flow velocity increased to as high as 100 m day^{-1}. This finding demonstrates that the effect of flow velocity was only important during the deposition phase. These observations were explained by diffusion-dependent mass transfer of NPs in the primary minimum of the DLVO interaction energy profile. Theoretical analysis indicated that the nanoscale surface roughness and chemical heterogeneities on sand grains reduce the magnitude of the energy barrier against attachment in the primary minimum and may also produce non-monotonic changes in the interaction energies between the NPs and sand surfaces. Higher values of C_i are believed to reduce the likelihood of NP transfer to the primary energy minimum due to increased numbers of collisions that knock the weakly associated NPs off the sand surface and prevent their transfer into the primary minimum.

Chapter 8

4. Effect of Aquifer Sediment Mineralogy and Stormwater Chemistry on Transport and Removal of Viruses

S. Sasidharan [1,2 & 3,] and S. Torkzaban [1]

[1]*CSIRO Land and Water, Adelaide, Australia*

[2]*Flinders University of South Australia, Adelaide, Australia*

[3]*National Centre for Groundwater Research and Training, Adelaide, Australia*

Poster Presentation: ***Waite Campus Conference & Exhibition***, organised by CSIRO Land and Water and CSIRO Agriculture, Adelaide, Australia

Time and Location: Friday 22nd August 2014, CSIRO, Waite Campus, Urrbrae, Australia

Abstract

Managed Aquifer Recharge (MAR) is the process of storing a water source, such as treated wastewater or stormwater, in aquifers under controlled conditions for withdrawal at a later date. Enteric viruses are one of the major concerns in water reclamation and reuse. Understanding the process of virus attachment to aquifer sediments under various chemical and physical conditions will provide an insight into the selection of appropriate MAR site and helps to assess the risk of contamination of recovered water. In this study, we investigated the fate and transport of three different bacteriophages (ΦX174, MS2 and PRD1), as a surrogate

for human pathogenic viruses, in columns packed with aquifer sediment from the Parafield aquifer, which is a sedimentary limestone aquifer. Stormwater is the rain/runoff water collected and stored in the Urrbrae wetland. The stormwater was either directly used in the experiments or was first equilibrated with the limestone sediments, which resulted in a high calcium concentration. A control experiment was conducted using clean river sand and 10 mM Na^+ electrolyte with a pH adjusted to 7. More than 2 log virus removal due to attachment to the aquifer sediment was observed when the stormwater was directly used in the experiments. Attachment efficiency increased with increasing calcium concentration implying that virus attachment may increase as water travel further away from the injection well. We also observed that the virus attachment was irreversible, that is, negligible detachment occurred when the flow velocity was increased and the pH was increased to 10. This finding suggests that attached viruses might have quickly inactivated or were irreversibly attached to the sediment surfaces. Our results suggest that a limestone sediment has a great capacity to remove viruses. We demonstrated that the sediment mineralogy was the key parameter influencing virus attachment and transport in the sediment.

Chapter 8

5. Antagonistic Effects of Biochar Amendment on Transport of *Escherichia coli* and Bacteriophages in Saturated Sand Porous Media

S. Sasidharan[1,2], S. Torkzaban[1] and P.G. Cook[2]

[1]*CSIRO Land and Water, Glen Osmond, SA 5064, Australia*

[2]*NCGRT, Flinders University, SA 5001*

Oral Presentation: (Best Oral Presentation Award): ***2nd Annual Research Higher Degree Conference,*** organised by School of the Environment, Flinders University, Australia.

Time and Location: Wednesday 30th September – Thursday 1st October 2015, 182 Victoria Square, Flinders University City Campus, Adelaide, Australia

Abstract

Biochar is a stable form of carbon, which is produced by pyrolysis of biomass. There are some potential positive indications that biochar application to natural porous media (e.g., sand) may enhance pathogen retention. However, current understanding of the governing processes that control the transport and retention of various microbes such as bacteria and viruses in porous media-amended with biochar is still limited. This study aims to investigate the underlining mechanism involves in the transport and retention of bacteria and viruses in biochar-amended sand. To achieve this, we have used biochars from various feedstocks and ultra-

pure quartz, as porous media; and *Escherichia coli* and bacteriophages (ΦX174, PRD1, and MS2) as a surrogate for pathogenic bacteria and viruses, respectively. At the first stage, batch studies with biochar or sand were conducted at various chemical conditions. This was the key experiment to differentiate the attachment and straining processes of microbes to biochar and sand surfaces. At next step, packed column transport experiments using various fractions and particle size of biochar-amended sand were conducted to understand the combined retention mechanism (attachment and straining) of microbes. Comparative studies between batch and column experiment show enhanced transport of bacteriophages through biochar-amended sand. Enhanced retention of bacteria in the packed column was the result of straining by fine biochar particles. Our study provides an important breakthrough knowledge regarding the potential negative impact of biochar in land application.

REFERENCE

10705-1-1995, I., 1995. ISO 10705-1-1995 Water quality - Detection and enumeration of bacteriophages - Part 1- Enumeration of F-specific RNA bacteriophage. In: I.O.f. Standardisation (Editor), Geneva, Switzerland.

10705-2-2000, I., 2000. ISO 10705-2-2000 Water quality - Detection and enumeration of bacteriophages - Part 2- Enumeration of somatic coliphages. In: I.O.f. Standardisation (Editor), Geneva, Switzerland.

Abedon, S.T. and Yin, J., 2009. Bacteriophage Plaques: Theory and Analysis. In: M.R.J. Clokie and A.M. Kropinski (Editors), Bacteriophages: Methods and Protocols, Volume 1: Isolation, Characterization, and Interactions. Humana Press, Totowa, NJ, pp. 161-174.

Abit, S.M., Bolster, C.H., Cai, P. and Walker, S.L., 2012. Influence of feedstock and pyrolysis temperature of biochar amendments on transport of Escherichia coli in saturated and unsaturated soil. Environmental Science and Technology, 46(15): 8097-8105.

Abit, S.M., Bolster, C.H., Cantrell, K.B., Flores, J.Q. and Walker, S.L., 2014. Transport of escherichia coli, salmonella typhimurium, and microspheres in biochar-amended soils with different textures. Journal of Environmental Quality, 43(1): 371-388.

Acharya, R.C., Valocchi, A.J., Werth, C.J. and Willingham, T.W., 2007. Pore-scale simulation of dispersion and reaction along a transverse mixing zone in two-dimensional porous media. Water Resources Research, 43(10): n/a-n/a.

Adamczyk, Z., 2006. Particles at interfaces: interactions, deposition, structure, 9. Academic Press.

Chapter 9

Adamczyk, Z. et al., 2009. Colloid particle deposition on heterogeneous surfaces produced by polyelectrolyte adsorption. Colloids and Surfaces A: Physicochemical and Engineering Aspects, 343(1-3): 111-117.

Adamczyk, Z., Nattich-Rak, M., Sadowska, M., Michna, A. and Szczepaniak, K., 2013. Mechanisms of nanoparticle and bioparticle deposition - Kinetic aspects. Colloids and Surfaces A: Physicochemical and Engineering Aspects, 439: 3-22.

Adamczyk, Z., Siwek, B. and Musiał, E., 2003. Latex particle adsorption at heterogeneous surfaces. Colloids and Surfaces A: Physicochemical and Engineering Aspects, 214(1-3): 219-229.

Adamczyk, Z., Siwek, B., Zembala, M. and Belouschek, P., 1994. Kinetics of localized adsorption of colloid particles. Advances in Colloid and Interface Science, 48(C): 151-280.

Ahmad, M. et al., 2014. Biochar as a sorbent for contaminant management in soil and water: A review. Chemosphere, 99: 19-23.

Akaike, H., 1974. A new look at the statistical model identification. Automatic Control, IEEE Transactions on, 19(6): 716-723.

Ali, I., 2012. New Generation Adsorbents for Water Treatment. Chemical Reviews, 112(10): 5073-5091.

Altenor, S. et al., 2009. Adsorption studies of methylene blue and phenol onto vetiver roots activated carbon prepared by chemical activation. Journal of Hazardous Materials, 165(1–3): 1029-1039.

Am Water Works Res, F., Langlais, B., Reckhow, D.A. and Brink, D.R., 1991. Ozone in water treatment: application and engineering. CRC press.

Chapter 9

Ambashta, R.D. and Sillanpää, M., 2010. Water purification using magnetic assistance: A review. Journal of Hazardous Materials, 180(1–3): 38-49.

Anders, R. and Chrysikopoulos, C.V., 2005. Virus fate and transport during artificial recharge with recycled water. Water Resources Research, 41(10): W10415.

Anisuzzaman, S.M., Joseph, C.G., Taufiq-Yap, Y.H., Krishnaiah, D. and Tay, V.V., 2015. Modification of commercial activated carbon for the removal of 2,4-dichlorophenol from simulated wastewater. Journal of King Saud University - Science, 27(4): 318-330.

Argent, J. et al., 2015. Visualization of Micro-Particle Retention on a Heterogeneous Surface Using Micro-models: Influence of Nanoscale Surface Roughness. Transport in Porous Media: 1-15.

Aronino, R. et al., 2009. Removal of viruses from surface water and secondary effluents by sand filtration. water research, 43(1): 87-96.

Artinger, R. et al., 2000. Characterization of groundwater humic substances: influence of sedimentary organic carbon. Applied Geochemistry, 15(1): 97-116.

Asano, T. and Levine, A.D., 1996. Wastewater reclamation, recycling and reuse: past, present, and future. Water Science and Technology, 33(10–11): 1-14.

Asghar, A., Raman, A.A.A. and Daud, W.M.A.W., 2015. Advanced oxidation processes for in-situ production of hydrogen peroxide/hydroxyl radical for textile wastewater treatment: a review. Journal of Cleaner Production, 87: 826-838.

Attinti, R., Wei, J., Kniel, K., Sims, J.T. and Jin, Y., 2010. Virus' (MS2, ϕX174, and Aichi) Attachment on Sand Measured by Atomic Force Microscopy and Their Transport through Sand Columns. Environmental Science & Technology, 44(7): 2426-2432.

Chapter 9

Azargohar, R. and Dalai, A.K., 2008. Steam and KOH activation of biochar: Experimental and modeling studies. Microporous and Mesoporous Materials, 110(2–3): 413-421.

Bales, R.C., Hinkle, S.R., Kroeger, T.W., Stocking, K. and Gerba, C.P., 1991a. Bacteriophage adsorption during transport through porous media: chemical perturbations and reversibility. Environmental Science & Technology, 25(12): 2088-2095.

Bales, R.C., Hinkle, S.R., Kroeger, T.W., Stocking, K. and Gerba, C.P., 1991b. Bacteriophage adsorption during transport through porous media: Chemical perturbations and reversibility. Environmental Science and Technology, 25(12): 2088-2095.

Baltimore, D., 1971. Expression of animal virus genomes. Bacteriological reviews, 35(3): 235.

Barber, L.B., Thurman, E.M. and Runnells, D.D., 1992. Geochemical heterogeneity in a sand and gravel aquifer: Effect of sediment mineralogy and particle size on the sorption of chlorobenzenes. Journal of contaminant hydrology, 9(1): 35-54.

Baron, S. and Yaeger, R.G., 1996. Protozoa: Structure, Classification, Growth, and Development.

Baumann, T. and Werth, C.J., 2004. Visualization and modeling of polystyrol colloid transport in a silicon micromodel. Vadose Zone Journal, 3(2): 434-443.

Bedrikovetsky, P., Siqueira, F.D., Furtado, C.A. and Souza, A.L.S., 2011. Modified Particle Detachment Model for Colloidal Transport in Porous Media. Transport in Porous Media, 86(2): 353-383.

Bendersky, M. and Davis, J.M., 2011. DLVO interaction of colloidal particles with topographically and chemically heterogeneous surfaces. Journal of Colloid and Interface

Science, 353(1): 87-97.

Bendersky, M., Santore, M.M. and Davis, J.M., 2015. The Effects of Brownian Motion On Particle Interactions with Patchy Surfaces Bearing Nanoscale Features. arXiv preprint arXiv:1510.06484.

Berg, J.C., 2010. An introduction to interfaces & colloids: the bridge to nanoscience. World Scientific.

Bergendahl, J. and Grasso, D., 1999. Prediction of colloid detachment in a model porous media: Thermodynamics. AIChE Journal, 45(3): 475-484.

Bertani, G., 1951. STUDIES ON LYSOGENESIS I.: The Mode of Phage Liberation by Lysogenic Escherichia coli1. Journal of bacteriology, 62(3): 293.

Bertrand, I. et al., 2012. The impact of temperature on the inactivation of enteric viruses in food and water: a review. Journal of applied microbiology, 112(6): 1059-1074.

Betancourt, W.Q. and Rose, J.B., 2004. Drinking water treatment processes for removal of Cryptosporidium and Giardia. Veterinary Parasitology, 126(1–2): 219-234.

Bhattacharjee, S., Chen, J.Y. and Elimelech, M., 2000. DLVO interaction energy between spheroidal particles and a flat surface. Colloids and Surfaces A: Physicochemical and Engineering Aspects, 165(1-3): 143-156.

Bhattacharjee, S. and Elimelech, M., 1997. Surface Element Integration: A Novel Technique for Evaluation of DLVO Interaction between a Particle and a Flat Plate. Journal of Colloid and Interface Science, 193(2): 273-285.

Bhattacharjee, S., Ko, C.H. and Elimelech, M., 1998. DLVO interaction between rough

surfaces. Langmuir, 14(12): 3365-3375.

Bhattacharya, P. et al., 2008. Groundwater for sustainable development: problems, perspectives and challenges. CRC Press.

Bolster, C.H. and Abit, S.M., 2012. Biochar Pyrolyzed at Two Temperatures Affects Escherichia coli Transport through a Sandy Soil. Journal of Environmental Quality, 41(1): 124-33.

Bradford, S.A., Bettahar, M., Simunek, J. and van Genuchten, M.T., 2004. Straining and Attachment of Colloids in Physically Heterogeneous Porous Media. Vadose Zone Journal, 3(2): 384-394.

Bradford, S.A. and Kim, H., 2012. Causes and implications of colloid and microorganism retention hysteresis. Journal of Contaminant Hydrology, 138-139: 83-92.

Bradford, S.A., Tadassa, Y.F. and Jin, Y., 2006. Transport of Coliphage in the Presence and Absence of Manure Suspension. Journal of Environmental Quality, 35(5): 1692-701.

Bradford, S.A. and Torkzaban, S., 2012. Colloid adhesive parameters for chemically heterogeneous porous media. Langmuir, 28(38): 13643-51.

Bradford, S.A. and Torkzaban, S., 2013. Colloid interaction energies for physically and chemically heterogeneous porous media. Langmuir, 29(11): 3668-76.

Bradford, S.A. and Torkzaban, S., 2015. Determining parameters and mechanisms of colloid retention and release in porous media. Langmuir, 31(44): 12096-12105.

Bradford, S.A., Torkzaban, S., Kim, H. and Simunek, J., 2012. Modeling colloid and microorganism transport and release with transients in solution ionic strength. Water Resources

Research, 48(9): n/a-n/a.

Bradford, S.A., Torkzaban, S., Leij, F. and Simunek, J., 2015a. Equilibrium and kinetic models for colloid release under transient solution chemistry conditions. Journal of Contaminant Hydrology(0).

Bradford, S.A., Torkzaban, S., Leij, F., Šimůnek, J. and van Genuchten, M.T., 2009. Modeling the coupled effects of pore space geometry and velocity on colloid transport and retention. Water Resources Research, 45(2): n/a-n/a.

Bradford, S.A., Torkzaban, S. and Shapiro, A., 2013. A theoretical analysis of colloid attachment and straining in chemically heterogeneous porous media. Langmuir, 29(23): 6944-52.

Bradford, S.A., Torkzaban, S. and Simunek, J., 2011a. Modeling colloid transport and retention in saturated porous media under unfavorable attachment conditions. Water Resources Research, 47(10): n/a-n/a.

Bradford, S.A., Torkzaban, S. and Walker, S.L., 2007. Coupling of physical and chemical mechanisms of colloid straining in saturated porous media. Water Res, 41(13): 3012-24.

Bradford, S.A., Torkzaban, S. and Wiegmann, A., 2011b. Pore-Scale Simulations to Determine the Applied Hydrodynamic Torque and Colloid Immobilization. Vadose Zone Journal, 10(1): 252.

Bradford, S.A., Wang, Y., Kim, H., Torkzaban, S. and Šimůnek, J., 2014. Modeling microorganism transport and survival in the subsurface. Journal of Environmental Quality, 43(2): 421-440.

Bradford, S.A., Wang, Y., Torkzaban, S. and Šimůnek, J., 2015b. Modeling the release of

E. coli D21g with transients in water content. Water Resources Research, 51(5): 3303-3316.

Brown, L.R., 2000. How Water Scarcity Will Shape the New Century, Stockholm Water Conference. Earth Policy Institute.

Bui, E., Mazzullo, J. and Wilding, L., 1989. Using quartz grain size and shape analysis to distinguish between aeolian and fluvial deposits in the Dallol Bosso of Niger (West Africa). Earth Surface Processes and Landforms, 14(2): 157-166.

Callow, J.A. and Callow, M.E., 2011. Trends in the development of environmentally friendly fouling-resistant marine coatings. Nat Commun, 2: 244.

Camper, A.K., LeChevallier, M., Broadaway, S. and McFeters, G., 1986. Bacteria associated with granular activated carbon particles in drinking water. Applied and environmental microbiology, 52(3): 434-438.

Capco, D.G.C., Yongchen, 2014. Nanomaterial: Impacts on Cell Biology and Medicine. Springer, New York.

Carman, M.L. et al., 2006. Engineered antifouling microtopographies – correlating wettability with cell attachment. Biofouling, 22(1): 11-21.

Castro, F.D. and Tufenkji, N., 2007. Relevance of nontoxigenic strains as surrogates for Escherichia coli O157:H7 in groundwater contamination potential: Role of temperature and cell acclimation time. Environmental Science and Technology, 41(12): 4332-4338.

Centers for Disease Control and Prevention, Waterborne Illnesses. In: V.Sanitation P. National Center for Environmental Health (Editor). CDC.

Chandrasekhar, S., 1943. Stochastic problems in physics and astronomy. Reviews of

modern physics, 15(1): 1.

Chao, T. and Zhou, L., 1983. Extraction techniques for selective dissolution of amorphous iron oxides from soils and sediments. Soil Science Society of America Journal, 47(2): 225-232.

Chatterjee, R., Mitra, S.K. and Bhattacharjee, S., 2011. Particle deposition onto Janus and patchy spherical collectors. Langmuir, 27(14): 8787-8797.

Choi, C.-H. et al., 2007. Cell interaction with three-dimensional sharp-tip nanotopography. Biomaterials, 28(9): 1672-1679.

Christo, S.N. et al., 2016. The Role of Surface Nanotopography and Chemistry on Primary Neutrophil and Macrophage Cellular Responses. Advanced healthcare materials.

Chrysikopoulos, C.V. and Aravantinou, A.F., 2012. Virus inactivation in the presence of quartz sand under static and dynamic batch conditions at different temperatures. Journal of Hazardous Materials, 233-234: 148-157.

Chrysikopoulos, C.V. and Aravantinou, A.F., 2014. Virus attachment onto quartz sand: Role of grain size and temperature. Journal of Environmental Chemical Engineering, 2(2): 796-801.

Chrysikopoulos, C.V. and Syngouna, V.I., 2012. Attachment of bacteriophages MS2 and ΦX174 onto kaolinite and montmorillonite: Extended-DLVO interactions. Colloids and Surfaces B: Biointerfaces, 92: 74-83.

Chu, Y., Jin, Y., Baumann, T. and Yates, M.V., 2003. Effect of Soil Properties on Saturated and Unsaturated Virus Transport through Columns. J. Environ. Qual., 32(6): 2017-2025.

Chu, Y., Jin, Y., Flury, M. and Yates, M.V., 2001. Mechanisms of virus removal during

transport in unsaturated porous media. Water Resources Research, 37(2): 253-263.

Chung, J.W., Foppen, J.W., Izquierdo, M. and Lens, P.N.L., 2014. Removal of Escherichia coli from saturated sand columns supplemented with hydrochar produced from maize. Journal of Environmental Quality, 43(6): 2096-2103.

Cleasby, J.L. and Woods, C.F., 1975. Intermixing of Dual Media and Multimedia Granular Filters (PDF). Journal-American Water Works Association, 67(4): 197-203.

Cook, P.G., Love, A.J., Robinson, N.I. and Simmons, C.T., 2005. Groundwater ages in fractured rock aquifers. Journal of Hydrology, 308(1): 284-301.

Cordova, A., Deserno, M., Gelbart, W.M. and Ben-Shaul, A., 2003. Osmotic shock and the strength of viral capsids. Biophysical journal, 85(1): 70-74.

Côté, P., Masini, M. and Mourato, D., 2004. Comparison of membrane options for water reuse and reclamation. Desalination, 167: 1-11.

Cui, X., Hao, H., Zhang, C., He, Z. and Yang, X., 2016. Capacity and mechanisms of ammonium and cadmium sorption on different wetland-plant derived biochars. Science of The Total Environment, 539: 566-575.

Czarnecki, J. and Warszyński, P., 1987. The evaluation of tangential forces due to surface inhomogeneties in the particle deposition process. Colloids and Surfaces, 22(2): 187-205.

Da Silva, A.K., Kavanagh, O.V., Estes, M.K. and Elimelech, M., 2011. Adsorption and aggregation properties of norovirus GI and GII virus-like particles demonstrate differing responses to solution chemistry. Environmental Science and Technology, 45(2): 520-526.

Dabroś, T. and van de Ven, T.G.M., 1983. A direct method for studying particle deposition

onto solid surfaces. Colloid & Polymer Science, 261(8): 694-707.

Dabrowski, A., Hubicki, Z., Podkościelny, P. and Robens, E., 2004. Selective removal of the heavy metal ions from waters and industrial wastewaters by ion-exchange method. Chemosphere, 56(2): 91-106.

Dalby, M.J., Riehle, M.O., Johnstone, H., Affrossman, S. and Curtis, A.S.G., 2002. In vitro reaction of endothelial cells to polymer demixed nanotopography. Biomaterials, 23(14): 2945-2954.

Davidson, M.W., 2015. Virus Structure, Molecular Expressions: Cell biology and Microscopy Structure and function of cells and viruses. The Florida State University, United States.

De Kerchove, A.J. and Elimelech, M., 2008. Calcium and magnesium cations enhance the adhesion of motile and nonmotile Pseudomonas aeruginosa on alginate films. Langmuir, 24(7): 3392-3399.

De Latour, C., 1973. Magnetic separation in water pollution control. Magnetics, IEEE Transactions on, 9(3): 314-316.

Deligianni, D.D., Katsala, N.D., Koutsoukos, P.G. and Missirlis, Y.F., 2000. Effect of surface roughness of hydroxyapatite on human bone marrow cell adhesion, proliferation, differentiation and detachment strength. Biomaterials, 22(1): 87-96.

Department of Health and Human Services, Infectious diseases. In: C.D.P.a.C.U.a.C.D.E.a.S. Unit (Editor), State Government of Victoria, Australia.

Derjaguin, B. and Landau, L., 1993. Theory of the stability of strongly charged lyophobic sols and of the adhesion of strongly charged particles in solutions of electrolytes. Progress in

Surface Science, 43(1–4): 30-59.

Derjaguin, B.V., 1941. Theory of the stability of strongly charged lyophobic sols and the adhesion of strongly charged particles in solutions of electrolytes. Acta Physicochim. USSR, 14: 633-662.

DHHS, 2016. Salmonella outbreak associated with some types of salad leaf products, Product recall: Information for consumers. Department of Health & Human Services, Victoria, Australia.

Dhont, J.K.G. and Briels, W.J., 2008. Single-particle thermal diffusion of charged colloids: Double-layer theory in a temperature gradient. The European Physical Journal E, 25(1): 61-76.

Dika, C., Duval, J.F.L., Francius, G., Perrin, A. and Gantzer, C., 2015. Isoelectric point is an inadequate descriptor of MS2, Phi X 174 and PRD1 phages adhesion on abiotic surfaces. Journal of Colloid and Interface Science, 446: 327-334.

Dillon, P., 2005. Future management of aquifer recharge. Hydrogeology Journal, 13(1): 313-316.

Dillon, P., 2015. Australian progress in managed aquifer recharge and the water banking frontier. Water: Journal of the Australian Water Association, 42(6): 53.

Dillon, P. et al., 2008. A critical evaluation of combined engineered and aquifer treatment systems in water recycling, Water Science and Technology, pp. 753-762.

Dillon, P., Pavelic, P., Page, D., Beringen, H. and Ward, J., 2009. Managed aquifer recharge: An Introduction, CSIRO, National Water Commission.

Dillon, P. et al., 2010. Managed aquifer recharge: Rediscovering nature as a leading edge

technology. Water Science and Technology, 62(10): 2338-2345.

Diop, S., M'mayi, P., Lisbjerg, D. and Johnstone, R., 2002. Vital water graphics: an overview of the state of the world's fresh and marine waters, 1. UNEP/Earthprint.

Doan, T.T., Henry-des-Tureaux, T., Rumpel, C., Janeau, J.-L. and Jouquet, P., 2015. Impact of compost, vermicompost and biochar on soil fertility, maize yield and soil erosion in Northern Vietnam: A three year mesocosm experiment. Science of The Total Environment, 514: 147-154.

Dolnicar, S. and Schäfer, A.I., 2009. Desalinated versus recycled water: Public perceptions and profiles of the accepters. Journal of Environmental Management, 90(2): 888-900.

Downie, A., Crosky, A. and Munroe, P., 2009. Physical properties of biochar. Biochar for environmental management: Science and technology: 13-32.

Drioli, E. and Giorno, L., 2010. Comprehensive membrane science and engineering, 1. Newnes.

Duan, D., 2006. From the Smallest Virus to the Biggest Gene: Marching Towards Gene Therapy for Duchenne Muscular Dystrophy. Discovery medicine, 6(33): 103-108.

Duffadar, R., Kalasin, S., Davis, J.M. and Santore, M.M., 2009. The impact of nanoscale chemical features on micron-scale adhesion: Crossover from heterogeneity-dominated to mean-field behavior. Journal of Colloid and Interface Science, 337(2): 396-407.

Duffadar, R.D. and Davis, J.M., 2007. Interaction of micrometer-scale particles with nanotextured surfaces in shear flow. Journal of Colloid and Interface Science, 308(1): 20-29.

Duffadar, R.D. and Davis, J.M., 2008. Dynamic adhesion behavior of micrometer-scale

particles flowing over patchy surfaces with nanoscale electrostatic heterogeneity. Journal of Colloid and Interface Science, 326(1): 18-27.

Earth Policy Institute, 2006. Water: Local Action For Global Challenge, Sustainability and Water Earth Policy Institute.

Elimelech, M., 1994. Effect of Particle Size on the Kinetics of Particle Deposition under Attractive Double Layer Interactions. Journal of Colloid And Interface Science, 164(1): 190-199.

Elimelech, M., Chen, J.Y. and Kuznar, Z.A., 2003. Particle deposition onto solid surfaces with micropatterned charge heterogeneity: The "hydrodynamic bump" effect. Langmuir, 19(17): 6594-6597.

Elimelech, M., Chen, W.H. and Waypa, J.J., 1994. Measuring the zeta (electrokinetic) potential of reverse osmosis membranes by a streaming potential analyzer. Desalination, 95(3): 269-286.

Elimelech, M. and Phillip, W.A., 2011. The Future of Seawater Desalination: Energy, Technology, and the Environment. Science, 333(6043): 712-717.

Emily, R. and Geoffrey, S., 2009. Bioinspiration—the solution for biofouling control? Bioinspiration & Biomimetics, 4(1): 015007.

Engelman, R., 1997. Why population matters. Population Action International: 54.

Eslamian, S., 2015. Urban Water Reuse Handbook. CRC Press

Fang, J., Xu, M.J., Wang, D.J., Wen, B. and Han, J.Y., 2013. Modeling the transport of TiO2 nanoparticle aggregates in saturated and unsaturated granular media: Effects of ionic

strength and pH. Water Research, 47(3): 1399-1408.

Fetter, C.W. and Fetter Jr, C., 1999. Contaminant hydrogeology, 500. Prentice hall New Jersey.

Fiessinger, F., Richard, Y., Montiel, A. and Musquere, P., 1981. Advantages and disadvantages of chemical oxidation and disinfection by ozone and chlorine dioxide. Science of The Total Environment, 18: 245-261.

Fleischmann, W.J., 1996. Medical Microbiology. In: B. S (Editor). University of Texas, Medical Branch at Galveston, Galveston (TX).

Flint, S., Brooks, J. and Bremer, P., 2000. Properties of the stainless steel substrate, influencing the adhesion of thermo-resistant streptococci. Journal of Food Engineering, 43(4): 235-242.

Foppen, J.W., Liem, Y. and Schijven, J., 2008. Effect of humic acid on the attachment of Escherichia coli in columns of goethite-coated sand. Water Res, 42(1-2): 211-9.

Foppen, J.W., Okletey, S. and Schijven, J.F., 2006. Effect of goethite coating and humic acid on the transport of bacteriophage PRD1 in columns of saturated sand. J Contam Hydrol, 85(3-4): 287-301.

Franchi, A. and O'Melia, C.R., 2003. Effects of natural organic matter and solution chemistry on the deposition and reentrainment of colloids in porous media. Environmental science & technology, 37(6): 1122-1129.

Freitas, C. and Müller, R.H., 1998. Effect of light and temperature on zeta potential and physical stability in solid lipid nanoparticle (SLN™) dispersions. International Journal of Pharmaceutics, 168(2): 221-229.

Fujita, Y., Ding, W.-H. and Reinhard, M., 1996. Identification of wastewater dissolved organic carbon characteristics in reclaimed wastewater and recharged groundwater. Water Environment Research, 68(5): 867-876.

Furiga, A. et al., 2010. Effects of ionic strength on bacteriophage MS2 behavior: Implications on the assessment of virus retention by ultrafiltration membranes, ASABE - 21st Century Watershed Technology: Improving Water Quality and Environment 2010, pp. 218-225.

Galisteo, F., de las Nieves López, F.J., Cabrerizo, M. and Hidalgo-Alvarez, R., 1990. Effects of particle concentration, ionic strength, pH and temperature on the microelectrophoretic mobility of cationic polystyrene latex. I. In: B. Lindman, J.B. Rosenholm and P. Stenius (Editors), Surfactants and Macromolecules: Self-Assembly at Interfaces and in Bulk. Progress in Colloid & Polymer Science. Steinkopff, pp. 313-320.

Gallardo-Moreno, A.M. et al., 2003. Influence of the growth medium, suspending liquid and measurement temperature on the physico-chemical surface properties of two enterococci strains. Journal of Adhesion Science and Technology, 17(14): 1877-1887.

García-García, S., Jonsson, M. and Wold, S., 2006. Temperature effect on the stability of bentonite colloids in water. Journal of Colloid and Interface Science, 298(2): 694-705.

García-García, S., Wold, S. and Jonsson, M., 2009. Effects of temperature on the stability of colloidal montmorillonite particles at different pH and ionic strength. Applied Clay Science, 43(1): 21-26.

Geise, G.M. et al., 2010. Water purification by membranes: the role of polymer science. Journal of Polymer Science Part B: Polymer Physics, 48(15): 1685-1718.

Chapter 9

Gelhar, L.W., Welty, C. and Rehfeldt, K.R., 1992. A critical review of data on field-scale dispersion in aquifers. Water resources research, 28(7): 1955-1974.

Genzer, J. and Marmur, A., 2008. Biological and Synthetic Self-Cleaning Surfaces. MRS Bulletin, 33(08): 742-746.

Gerba, C.P., 1984. Applied and Theoretical Aspects of Virus Adsorption to Surfaces. 30: 133-168.

Gharabaghi, B. et al., 2015. Temperature effect on the transport of bromide and *E. coli* NAR in saturated soils. Journal of Hydrology, 522: 418-427.

Glaser, B., Lehmann, J. and Zech, W., 2002. Ameliorating physical and chemical properties of highly weathered soils in the tropics with charcoal - A review. Biology and Fertility of Soils, 35(4): 219-230.

Glaze, W.H., Kang, J.-W. and Chapin, D.H., 1987. The chemistry of water treatment processes involving ozone, hydrogen peroxide and ultraviolet radiation.

Gleick, P.H., 1993. Water in crisis: a guide to the world's fresh water resources. Oxford University Press, Inc.

Gleick, P.H., 2002. Dirty-water: Estimated Deaths from Water-related Diseases 2000-2020. Pacific Institute for Studies in Development, Environment, and Security Oakland.

Goreham, R.V., Mierczynska, A., Smith, L.E., Sedev, R. and Vasilev, K., 2013. Small surface nanotopography encourages fibroblast and osteoblast cell adhesion. RSC Advances, 3(26): 10309-10317.

Grabow, W., 2004. Bacteriophages: update on application as models for viruses in water.

Chapter 9

Water Sa, 27(2): 251-268.

Grafe, A., 2012. A history of experimental virology. Springer Science & Business Media.

Grasso, D., Subramaniam, K., Butkus, M., Strevett, K. and Bergendahl, J., A review of non-DLVO interactions in environmental colloidal systems. Reviews in Environmental Science and Biotechnology, 1(1): 17-38.

Greenland, D., 1971. Interactions between humic and fulvic acids and clays. Soil Science, 111(1): 34-41.

Greenlee, L.F., Lawler, D.F., Freeman, B.D., Marrot, B. and Moulin, P., 2009. Reverse osmosis desalination: Water sources, technology, and today's challenges. Water Research, 43(9): 2317-2348.

Gregory, J., 1975. Interaction of unequal double layers at constant charge. Journal of Colloid and Interface Science, 51(1): 44-51.

Gregory, J., 1981. Approximate expressions for retarded van der waals interaction. Journal of Colloid and Interface Science, 83(1): 138-145.

Gregory, J. and Wishart, A.J., 1980. Deposition of latex particles on alumina fibers. Colloids and Surfaces, 1(3–4): 313-334.

Gutierrez, L., Mylon, S.E., Nash, B. and Nguyen, T.H., 2010. Deposition and aggregation kinetics of rotavirus in divalent cation solutions. Environmental science & technology, 44(12): 4552-4557.

Hale, L., Luth, M., Kenney, R. and Crowley, D., 2014. Evaluation of pinewood biochar as a carrier of bacterial strain Enterobacter cloacae UW5 for soil inoculation. Applied Soil

Ecology, 84: 192-199.

Han, Y. et al., 2016. Transport, retention, and long-term release behavior of ZnO nanoparticle aggregates in saturated quartz sand: Role of solution pH and biofilm coating. Water Research, 90: 247-257.

Harmand, B., Rodier, E., Sardin, M. and Dodds, J., 1996. Transport and capture of submicron particles in a natural sand: short column experiments and a linear model. Colloids and Surfaces A: Physicochemical and Engineering Aspects, 107(0): 233-244.

Harrington, N. and Cook, P.G., 2014. Groundwater in Australia.

Hartl, D.L.a.J., E. W, 2009. Genetics. Analysis of Genes and Genomes, 7. Jones and Bartlett Publishers, Inc., United Sates of America.

Harvey, R.W. and Ryan, J.N., 2004. Use of PRD1 bacteriophage in groundwater viral transport, inactivation, and attachment studies. FEMS Microbiol Ecol, 49(1): 3-16.

Hassen, A. et al., 2000. UV disinfection of treated wastewater in a large-scale pilot plant and inactivation of selected bacteria in a laboratory UV device. Bioresource Technology, 74(2): 141-150.

Havelaar, A., Pot-Hogeboom, W., Furuse, K., Pot, R. and Hormann, M., 1990. F-specific RNA bacteriophages and sensitive host strains in faeces and wastewater of human and animal origin. Journal of applied bacteriology, 69(1): 30-37.

He, F., Zhang, M., Qian, T. and Zhao, D., 2009. Transport of carboxymethyl cellulose stabilized iron nanoparticles in porous media: column experiments and modeling. J Colloid Interface Sci, 334(1): 96-102.

Chapter 9

Helfferich, F.G., 1962. Ion exchange. Dover Publications, New York.

Hem, J.D., 1985. Study and interpretation of the chemical characteristics of natural water, 2254. Department of the Interior, US Geological Survey.

Hida, T., 1980. Brownian motion. Applications of Mathematics, 11. Springer, New York.

Hijnen, W.A., Brouwer-Hanzens, A.J., Charles, K.J. and Medema, G.J., 2005. Transport of MS2 phage, *Escherichia coli*, *Clostridium perfringens, Cryptosporidium parvum*, and *Giardia intestinalis* in a gravel and a sandy soil. Environmental science & technology, 39(20): 7860-7868.

Hilbert, L.R., Bagge-Ravn, D., Kold, J. and Gram, L., 2003. Influence of surface roughness of stainless steel on microbial adhesion and corrosion resistance. International Biodeterioration & Biodegradation, 52(3): 175-185.

Hoek, E.M.V. and Agarwal, G.K., 2006. Extended DLVO interactions between spherical particles and rough surfaces. Journal of Colloid and Interface Science, 298(1): 50-58.

Hoek, E.M.V., Bhattacharjee, S. and Elimelech, M., 2003. Effect of membrane surface roughness on colloid-membrane DLVO interactions. Langmuir, 19(11): 4836-4847.

Hogg, R., Healy, T.W. and Fuerstenau, D.W., 1966. Mutual coagulation of colloidal dispersions. Transactions of the Faraday Society, 62(0): 1638-1651.

Holmes, E.C., 2007. Viral evolution in the genomic age. PLoS Biol, 5(10): e278.

Hori, K. and Matsumoto, S., 2010. Bacterial adhesion: from mechanism to control. Biochemical Engineering Journal, 48(3): 424-434.

Huang, X., Bhattacharjee, S. and Hoek, E.M.V., 2009. Is Surface Roughness a "Scapegoat"

or a Primary Factor When Defining Particle−Substrate Interactions? Langmuir, 26(4): 2528-2537.

Hughes, L., 2004. Ion exchange resins. Unique solutions to formulation problems. Pharma Technol, 28(6): 20-5.

Huiskonen, J.T., Manole, V. and Butcher, S.J., 2007. Tale of two spikes in bacteriophage PRD1. Proceedings of the National Academy of Sciences, 104(16): 6666-6671.

Huisman, L., Wood, W. and Organization, W.H., 1974. Slow sand filtration, 16. World Health Organization Geneva.

Igbal, M.Z. and Krothe, N.C., 1995. Infiltration mechanisms related to agricultural waste transport through the soil mantle to karst aquifers of southern Indiana, USA. Journal of Hydrology, 164(1): 171-192.

Ishido, T., Mizutani, H. and Baba, K., 1983. Streaming potential observations, using geothermal wells and in situ electrokinetic coupling coefficients under high temperature. Tectonophysics, 91(1): 89-104.

Israelachvili, J., 2011. Intermolecular and Surface Forces, 3. Elsevier, University of California Santa Barbara, California, USA.

Israelachvili, J.N., 1992. Intermolecular and surface forces. Academic Press, London ; San Diego.

Jaisi, D.P. and Elimelech, M., 2009. Single-walled carbon nanotubes exhibit limited transport in soil columns. Environmental Science & Technology, 43(24): 9161-9166.

Janjaroen, D., Liu, Y., Kuhlenschmidt, M.S., Kuhlenschmidt, T.B. and Nguyen, T.H., 2010.

Role of divalent cations on deposition of cryptosporidium parvum oocysts on natural organic matter surfaces. Environmental Science and Technology, 44(12): 4519-4524.

Jiang, W. et al., 2004. Elucidation of functional groups on gram-positive and gram-negative bacterial surfaces using infrared spectroscopy. Langmuir, 20(26): 11433-11442.

Jin, Y., Chu, Y. and Li, Y., 2000. Virus removal and transport in saturated and unsaturated sand columns. Journal of Contaminant Hydrology, 43(2): 111-128.

Jin, Y. and Flury, M., 2002. Fate and transport of viruses in porous media. Advances in Agronomy, 77: 39-102.

Jindo, K. et al., 2012. Biochar influences the microbial community structure during manure composting with agricultural wastes. Science of The Total Environment, 416: 476-481.

Johnson, P.R. and Elimelech, M., 1995. Dynamics of colloid deposition in porous media: Blocking based on random sequential adsorption. Langmuir, 11(3): 801-812.

Johnson, P.R., Sun, N. and Elimelech, M., 1996. Colloid transport in geochemically heterogeneous porous media: Modeling and measurements. Environmental Science and Technology, 30(11): 3284-3293.

Judd, S., 2010. The MBR book: principles and applications of membrane bioreactors for water and wastewater treatment. Elsevier.

Jullien, C., Bénézech, T., Carpentier, B., Lebret, V. and Faille, C., 2003. Identification of surface characteristics relevant to the hygienic status of stainless steel for the food industry. Journal of Food Engineering, 56(1): 77-87.

Jun-min, G., Ze-gen, Z., Yan, W. and Jun-feng, D., 2001. Application of Zeolite in Water

Treatment [J]. Journal of Chongqing Jianzhu University, 1: 023.

Kalantariasl, A. and Bedrikovetsky, P., 2013. Stabilization of External Filter Cake by Colloidal Forces in a "Well–Reservoir" System. Industrial & Engineering Chemistry Research.

Kalasin, S., Martwiset, S., Bryan Coughlin, E. and Santore, M.M., 2010. Particle capture via discrete binding elements: Systematic variations in binding energy for randomly distributed nanoscale surface features. Langmuir, 26(22): 16865-16870.

Kanade, P.S., and Bhattacharya, S.S, 2016. A Guide to Filtration with String Wound Cartridges: Influence of Winding Parameters on Filtration Behaviour of String Wound Filter Cartridges, I. Elsevier.

Kar, S. et al., 2010. Arsenic-enriched aquifers: Occurrences and mobilization of arsenic in groundwater of Ganges Delta Plain, Barasat, West Bengal, India. Applied Geochemistry, 25(12): 1805-1814.

Katz, M. and Plotkin, S.A., 1967. Minimal infective dose of attenuated poliovirus for man. American Journal of Public Health and the Nations Health, 57(10): 1837-1840.

Kavanaugh, M.C.L., James O., 1980. Particulates in Water: Characterization, Fate, Effects, and Removal, 189. American Chemical Society.

Kazumori, Y., 1981. Electron microscopic studies of bacteriophage φ X174 intact and 'eclipsing' particles, and the genome by the staining and shadowing method. Journal of virological methods, 2(3): 159-167.

Kearns, J., Wellborn, L., Summers, R. and Knappe, D., 2014. 2, 4-D adsorption to biochars: Effect of preparation conditions on equilibrium adsorption capacity and comparison with commercial activated carbon literature data. Water research, 62: 20-28.

Chapter 9

Kim, H.N., Bradford, S.A. and Walker, S.L., 2009. *Escherichia coli O157:H7* transport in saturated porous media: Role of solution chemistry and surface macromolecules. Environmental Science & Technology, 43(12): 4340-4347.

Kim, H.N. and Walker, S.L., 2009. *Escherichia coli* transport in porous media: Influence of cell strain, solution chemistry, and temperature. Colloids and Surfaces B: Biointerfaces, 71(1): 160-167.

Kim, S.-B., Park, S.-J., Lee, C.-G., Choi, N.-C. and Kim, D.-J., 2008. Bacteria transport through goethite-coated sand: Effects of solution pH and coated sand content. Colloids and Surfaces B: Biointerfaces, 63(2): 236-242.

Ko, C.H. and Elimelech, M., 2000. The 'shadow effect' in colloid transport and deposition dynamics in granular porous media: Measurements and mechanisms. Environmental Science and Technology, 34(17): 3681-3689.

Kookana, R.S., 2010. The role of biochar in modifying the environmental fate, bioavailability, and efficacy of pesticides in soils: a review. Soil Research, 48(7): 627-637.

Koonin, E.V., Senkevich, T.G. and Dolja, V.V., 2006. The ancient Virus World and evolution of cells. Biol Direct, 1(1): 29.

Krasner, S.W. et al., 2006. Occurrence of a new generation of disinfection byproducts. Environmental science & technology, 40(23): 7175-7185.

Kropinski, A.M., Mazzocco, A., Waddell, T.E., Lingohr, E. and Johnson, R.P., 2009. Enumeration of bacteriophages by double agar overlay plaque assay. Bacteriophages: Methods and Protocols, Volume 1: Isolation, Characterization, and Interactions: 69-76.

Kumar, S., 2012. Textbook of microbiology. JP Medical Ltd.

Chapter 9

Kumari, K.G.I.D. et al., 2014. Effects of biochar on air and water permeability and colloid and phosphorus leaching in soils from a natural calcium carbonate gradient. Journal of Environmental Quality, 43(2): 647-657.

Kuznar, Z.A. and Elimelech, M., 2007. Direct microscopic observation of particle deposition in porous media: Role of the secondary energy minimum. Colloids and Surfaces A: Physicochemical and Engineering Aspects, 294(1-3): 156-162.

La Scola, B. et al., 2003. A giant virus in amoebae. Science, 299(5615): 2033-2033.

Leclerc, H., Edberg, S., Pierzo, V. and Delattre, J., 2000. Bacteriophages as indicators of enteric viruses and public health risk in groundwaters. Journal of applied microbiology, 88(1): 5-21.

Lehmann, J., Gaunt, J. and Rondon, M., 2006. Bio-char sequestration in terrestrial ecosystems - A review. Mitigation and Adaptation Strategies for Global Change, 11(2): 403-427.

Lehmann, J. and Joseph, S., 2015. Biochar for Environmental Management: Science, Technology and Implementation, Routledge.

Lehmann, J. et al., 2011. Biochar effects on soil biota – A review. Soil Biology and Biochemistry, 43(9): 1812-1836.

Lenar, J., 1978. Virus envelopes and plasma membranes Annual Review of Biophysics and Bioengineering 139-165.

Levine, A.D. and Asano, T., 2004. Peer reviewed: recovering sustainable water from wastewater. Environmental science & technology, 38(11): 201A-208A.

Li, J.-h. et al., 2014. Modification and use of biochar from wheat straw (Triticum aestivum L.) for nitrate and phosphate removal from water. Desalination and Water Treatment: 1-13.

Li, Q. et al., 2008a. Antimicrobial nanomaterials for water disinfection and microbial control: potential applications and implications. Water Res, 42(18): 4591-602.

Li, X., Scheibe, T.D. and Johnson, W.P., 2004. Apparent decreases in colloid deposition rate coefficients with distance of transport under unfavorable deposition conditions: A general phenomenon. Environmental Science & Technology, 38(21): 5616-5625.

Li, Y., Wang, Y., Pennell, K.D. and Briola, L.M.A., 2008b. Investigation of the transport and deposition of fullerene (C60) nanoparticles in quartz sands under varying flow conditions. Environmental Science and Technology, 42(19): 7174-7180.

Liang, Y. et al., 2013. Retention and remobilization of stabilized silver nanoparticles in an undisturbed loamy sand soil. Environmental Science & Technology, 47(21): 12229-12237.

Lin, S. et al., 2011. Deposition of silver nanoparticles in geochemically heterogeneous porous media: predicting affinity from surface composition analysis. Environ Sci Technol, 45(12): 5209-15.

Lodish, H., Berk, A. and Zipursky, S., 2000. Molecular cell biology 4th edition.

Logan, J.D., 2001. Reaction—Advection—Dispersion Equation, Transport Modeling in Hydrogeochemical Systems. Springer, pp. 29-73.

Loveland, J.P., Ryan, J.N., Amy, G.L. and Harvey, R.W., 1996. The reversibility of virus attachment to mineral surfaces. Colloids and Surfaces A: Physicochemical and Engineering Aspects, 107: 205-221.

Lucas, W., 2001. Viral Capsids and Envelopes: Structure and Function, eLS. John Wiley & Sons, Ltd.

Ma, H., Hradisky, M. and Johnson, W.P., 2013. Extending Applicability of Correlation Equations to Predict Colloidal Retention in Porous Media at Low Fluid Velocity. Environ Sci Technol, 47(5): 2272-2278.

Macdonald, L.W., M; Oliver, D; Kookana, R, 2015. Biochar and hydrochar as low-cost sorbents for removing contaminants from water. Journal of the Australian Water Association, 42(2): 142-147.

Magal, E., Weisbrod, N., Yechieli, Y., Walker, S.L. and Yakirevich, A., 2011. Colloid transport in porous media: impact of hyper-saline solutions. Water Res, 45(11): 3521-32.

Malard, F., Reygrobellet, J.-L. and Soulie, M., 1994. Transport and retention of fecal bacteria at sewage-polluted fractured rock sites. Journal of Environmental Quality, 23(6): 1352-1363.

Malato, S. et al., 2016. Decontamination and disinfection of water by solar photocatalysis: The pilot plants of the Plataforma solar de Almeria. Materials Science in Semiconductor Processing, 42: 15-23.

Malysa, K., Dabros, T. and Van De Ven, T.G.M., 1986. The sedimentation of one sphere past a second attached to a wall. Journal of Fluid Mechanics, 162: 157-170.

Mandal, S. et al., 2015. Biochar-induced concomitant decrease in ammonia volatilization and increase in nitrogen use efficiency by wheat. Chemosphere(0).

Marsily, G.d., 1986. Quantitative hydrology: groundwater hydrology for engineers. Academic, San Diego, Calif.

Chapter 9

Martin, N.L., Bass, P. and Liss, S.N., 2015. Antibacterial Properties and Mechanism of Activity of a Novel Silver-Stabilized Hydrogen Peroxide. PloS one, 10(7): e0131345.

Massoudieh, A., Lu, N., Liang, X., Nguyen, T.H. and Ginn, T.R., 2013. Bayesian process-identification in bacteria transport in porous media. Journal of Contaminant Hydrology, 153: 78-91.

Mayer, G., 2016. Bacteriology - chapter seven bacteriophage. In: R.C. Hunt (Editor), Microbiology and Immunology On-line. University of South Carolina School of Medicine, United States.

McBeath, A.V., Wurster, C.M. and Bird, M.I., 2015. Influence of feedstock properties and pyrolysis conditions on biochar carbon stability as determined by hydrogen pyrolysis. Biomass and Bioenergy, 73: 155-173.

McCaulou, D.R., Bales, R.C. and Arnold, R.G., 1995. Effect of temperature controlled motillity on transport of bacteria and microspheres through saturated sediment. Water Resources Research, 31(2): 271-280.

McDowell-Boyer, L.M., Hunt, J.R. and Sitar, N., 1986. Particle transport through porous media. Water Resour. Res, 22(13): 1901-1921.

Meder, F. et al., 2013. The role of surface functionalization of colloidal alumina particles on their controlled interactions with viruses. Biomaterials, 34(17): 4203-4213.

Meinders, J.M. and Busscher, H.J., 1993. Influence of ionic strength and shear rate on the desorption of polystyrene particles from a glass collector as studied in a parallel-plate flow chamber. Colloids and Surfaces A: Physicochemical and Engineering Aspects, 80(2-3): 279-285.

Meinders, J.M., Noordmans, J. and Busscher, H.J., 1992. Simultaneous monitoring of the adsorption and desorption of colloidal particles during deposition in a parallel plate flow chamber. Journal of Colloid And Interface Science, 152(1): 265-280.

Meinders, J.M., van der Mei, H.C. and Busscher, H.J., 1995. Deposition Efficiency and Reversibility of Bacterial Adhesion under Flow. Journal of Colloid And Interface Science, 176(2): 329-341.

Mendonça, G., Mendonça, D.B.S., Aragão, F.J.L. and Cooper, L.F., 2008. Advancing dental implant surface technology – From micron- to nanotopography. Biomaterials, 29(28): 3822-3835.

Messina, F., Marchisio, D.L. and Sethi, R., 2015. An extended and total flux normalized correlation equation for predicting single-collector efficiency. Journal of Colloid and Interface Science, 446: 185-193.

Mohanty, S.K. and Boehm, A.B., 2014. Escherichia coli removal in biochar-augmented biofilter: Effect of infiltration rate, initial bacterial concentration, biochar particle size, and presence of compost. Environmental Science and Technology, 48(19): 11535-11542.

Mohanty, S.K., Cantrell, K.B., Nelson, K.L. and Boehm, A.B., 2014. Efficacy of biochar to remove Escherichia coli from stormwater under steady and intermittent flow. Water Research, 61: 288-296.

Molina-Sabio, M. and Rodríguez-Reinoso, F., 2004. Role of chemical activation in the development of carbon porosity. Colloids and Surfaces A: Physicochemical and Engineering Aspects, 241(1–3): 15-25.

Monteagudo, J.M. and Ortiz, M.J., 2000. Removal of inorganic mercury from mine waste

water by ion exchange. Journal of Chemical Technology and Biotechnology, 75(9): 767-772.

Morita, S. et al., 2002. Efficacy of UV Irradiation in Inactivating Cryptosporidium parvum Oocysts. Applied and Environmental Microbiology, 68(11): 5387-5393.

Mosley, L., Willson, P., Hamilton, B., Butler, G. and Seaman, R., 2015. The capacity of biochar made from common reeds to neutralise pH and remove dissolved metals in acid drainage. Environmental Science and Pollution Research: 1-10.

Muellner, M.G. et al., 2007. Haloacetonitriles vs. regulated haloacetic acids: are nitrogen-containing DBPs more toxic? Environmental science & technology, 41(2): 645-651.

Mujeriego, R. and Asano, T., 1999. The role of advanced treatment in wastewater reclamation and reuse. Water Science and Technology, 40(4–5): 1-9.

Mukherjee, A. and Lal, R., 2014. The biochar dilemma. Soil Research, 52(3): 217-230.

Mukherjee, A., Lal, R. and Zimmerman, A.R., 2014. Effects of biochar and other amendments on the physical properties and greenhouse gas emissions of an artificially degraded soil. Science of The Total Environment, 487: 26-36.

Mukherjee, A.L., R., 2013. Biochar Impacts on Soil Physical Properties and Greenhouse Gas Emissions. Agronomy Journal, 3(2): 313.

Mutsaers, D.I., 2016. Immunological Discourse in Political Philosophy. Ashgate Pub Limited.

Narsilio, G.A., Buzzi, O., Fityus, S., Yun, T.S. and Smith, D.W., 2009. Upscaling of Navier–Stokes equations in porous media: Theoretical, numerical and experimental approach. Computers and Geotechnics, 36(7): 1200-1206.

Chapter 9

Nartey, O.D. and Zhao, B., 2014. Biochar Preparation, Characterization, and Adsorptive Capacity and Its Effect on Bioavailability of Contaminants: An Overview. Advances in Materials Science and Engineering, 2014: 12.

Nelson, K.E. and Ginn, T.R., 2005. Colloid Filtration Theory and the Happel Sphere-in-Cell Model Revisited with Direct Numerical Simulation of Colloids. Langmuir, 21(6): 2173-2184.

Nelson, K.E. and Ginn, T.R., 2011. New collector efficiency equation for colloid filtration in both natural and engineered flow conditions. Water Resources Research, 47(5).

Ngo, H.H. and Vigneswaran, S., 1995. Application of floating medium filter in water and wastewater treatment with contact-flocculation filtration arrangement. Water Research, 29(9): 2211-2213.

Nguyen, T., Roddick, F.A. and Fan, L., 2012. Biofouling of water treatment membranes: a review of the underlying causes, monitoring techniques and control measures. Membranes, 2(4): 804-840.

NHMRC, N., 2011. Australian drinking water guidelines 6 National Water Quality Management Strategy. Commonwealth of Australia, Canberra., National Health and Medical Research Council, Natural Resource Management Ministerial Council.

NRC, 1980. Drinking Water and Health: Volume 2. The Disinfection of Drinking Water, 2. National Academies Press (US), Washington (DC).

NRC, 2012. Water Reuse: Potential for Expanding the Nation's Water Supply Through Reuse of Municipal Wastewater. National Research Council . Committee on the Assessment of Water Reuse as an Approach for Meeting Future Water Supply Needs. National Academies

Press.

NRMMC-EPHC-NHMRC, 2009. National Water Quality Management Strategy, Australian guidelines for water recycling: Managing health and

environmental risks (phase 2) Managed Aquifer Recharge. In: N.R.M.M. Council, E.P.a.H. Council and N.H.a.M.R. Council (Editors), National Water Quality Management Strategy, Canberra. .

NWC, 2008. Emerging trends in desalination: A review, National Water Commission, Australia.

NWQMS, 2000. Australian and New Zealand Guidelines for Fresh and Marine Water Quality National water quality management strategy. In: A.a.R.M.C.o.A.a.N.Z. Australian and New Zealand Environment and Conservation Council (Editor), The Guidelines. Australia Agriculture and Resource Management Council of Australia and New Zealand, Australia.

Orlova, E.V., 2009. How viruses infect bacteria? The EMBO Journal, 28(7): 797-798.

Page, D., Dillon, P., Vanderzalm, J., Toze, S., Sidhu, J., Barry, K., Levett, K., Kremer, S. and Regel, R., , 2010. Risk assessment of aquifer storage transfer and recovery with urban stormwater for producing water of a potable quality. Journal of environmental quality, 39(6): 2029-2039.

Page, D., Gonzalez, D. and Dillon, P., 2012. Microbiological risks of recycling urban stormwater via aquifers. Water Science and Technology, 65(9): 1692-1695.

Page, D. et al., 2015a. E. coli and turbidity attenuation during urban stormwater recycling via Aquifer Storage and Recovery in a brackish limestone aquifer. Ecological Engineering, 84: 427-434.

Chapter 9

Page, D.W. et al., 2015b. E. coli and turbidity attenuation during urban stormwater recycling via Aquifer Storage and Recovery in a brackish limestone aquifer. Ecological Engineering, 84: 427-434.

Palaniappan, M. and Gleick, P.H., 2008. Peak water. The World's Water 2008–2009. The Biennial Report on Freshwater Resources: 1-16.

Parsons, S. et al., 2012. Progress in managed aquifer recharge in Australia. National Water Commission.

Pavelic, P. et al., 2007. Water quality effects on clogging rates during reclaimed water ASR in a carbonate aquifer. Journal of Hydrology, 334(1-2): 1-16.

Pavelic, P., Ragusa, S.R., Flower, R.L., Rinck-Pfeiffer, S.M. and Dillon, P.J., 1998. Diffusion chamber method for in situ measurement of pathogen inactivation in groundwater. Water Research, 32(4): 1144-1150.

Pelley, A.J. and Tufenkji, N., 2008. Effect of particle size and natural organic matter on the migration of nano- and microscale latex particles in saturated porous media. Journal of Colloid and Interface Science, 321(1): 74-83.

Perrott, K., 2016. Salmonella in lettuce could be from faeces-laden water in washing process, expert says, ABC. ABC News, Australia, pp. 5 Feb 2016.

Petosa, A.R., Brennan, S.J., Rajput, F. and Tufenkji, N., 2012. Transport of two metal oxide nanoparticles in saturated granular porous media: role of water chemistry and particle coating. Water Res, 46(4): 1273-85.

Petosa, A.R., Jaisi, D.P., Quevedo, I.R., Elimelech, M. and Tufenkji, N., 2010. Aggregation and deposition of engineered nanomaterials in aquatic environments: Role of physicochemical

interactions. Environmental Science & Technology, 44(17): 6532-6549.

Pham, M., Mintz, E.A. and Nguyen, T.H., 2009. Deposition kinetics of bacteriophage MS2 to natural organic matter: Role of divalent cations. Journal of colloid and interface science, 338(1): 1-9.

Philibert, J., 2006. One and a half century of diffusion: Fick, Einstein, before and beyond. Diffusion Fundamentals, 4(6): 1-19.

Pi, Y.-z. and Wang, J.-l., 2006. A field study of advanced municipal wastewater treatment technology for artificial groundwater recharge. Journal of Environmental Sciences, 18(6): 1056-1060.

Prasad, B.V.V. and Schmid, M.F., 2012. Principles of Virus Structural Organization. Advances in experimental medicine and biology, 726: 17-47.

Public Health Agency of Canada, 2011. Pathogen Safety Data Sheets and Risk Assessment, Laboratory Biosafety and Biosecurity, Public Health Agency of Canada.

Pyne, R.D.G., Singer, P.C. and Miller, C.T., 1996. Aquifer storage recovery of treated drinking water. American Water Works Association.

Quevedo, I.R. and Tufenkji, N., 2009. Influence of Solution Chemistry on the Deposition and Detachment Kinetics of a CdTe Quantum Dot Examined Using a Quartz Crystal Microbalance. Environmental Science & Technology, 43(9): 3176-3182.

Raghu, H., Manju, G., Mishra, S. and Sawale, P., 2012. Beneficial face of bacteriophages: Applications in food processing. International Journal for Quality Research, 6(2).

Redman, J.A., Walker, S.L. and Elimelech, M., 2004. Bacterial Adhesion and Transport in

Porous Media: Role of the Secondary Energy Minimum. Environmental Science and Technology, 38(6): 1777-1785.

Rengaraj, S., Yeon, K.-H. and Moon, S.-H., 2001. Removal of chromium from water and wastewater by ion exchange resins. Journal of Hazardous Materials, 87(1–3): 273-287.

Reppert, P.M. and Morgan, F.D., 2003. Temperature-dependent streaming potentials: 1. Theory. Journal of Geophysical Research: Solid Earth, 108(B11): n/a-n/a.

Reynolds, K.A., Mena, K.D. and Gerba, C.P., 2008. Risk of waterborne illness via drinking water in the United States, Reviews of environmental contamination and toxicology. Springer, pp. 117-158.

Richardson, S.D. and Postigo, C., 2012. Drinking Water Disinfection By-products. In: D. Barceló (Editor), Emerging Organic Contaminants and Human Health. Springer Berlin Heidelberg, Berlin, Heidelberg, pp. 93-137.

Rivera-Utrilla, J. et al., 2011. Activated carbon modifications to enhance its water treatment applications. An overview. Journal of Hazardous Materials, 187(1–3): 1-23.

Rizwan, T. and Bhattacharjee, S., 2009. Particle deposition onto charge-heterogeneous substrates. Langmuir, 25(9): 4907-4918.

Rodriguez-Reinoso, F., Molina-Sabio, M. and Gonzalez, M., 1995. The use of steam and CO_2 as activating agents in the preparation of activated carbons. Carbon, 33(1): 15-23.

Rodríguez, K. and Araujo, M., 2006. Temperature and pressure effects on zeta potential values of reservoir minerals. Journal of Colloid and Interface Science, 300(2): 788-794.

Rowell, R.M., 2006. Removal of metal ions from contaminated water using agricultural

residues.

Roy, S.B. and Dzombak, D.A., 1996. Na+-Ca2+ exchange effects in the detachment of latex colloids deposited in glass bead porous media. Colloids and Surfaces A: Physicochemical and Engineering Aspects, 119(2-3): 133-139.

Ruckenstein, E. and Prieve, D.C., 1976. Adsorption and desorption of particles and their chromatographic separation. AIChE Journal, 22(2): 276-283.

Ryan, J.N. and Elimelech, M., 1996. Colloid mobilization and transport in groundwater. Colloids and Surfaces A: Physicochemical and Engineering Aspects, 107: 1-56.

Rybicki, E., 1990. The classification of organisms at the edge of life or problems with virus systematics. South African Journal of Science, 86(4): 182-186.

Sadeghi, G., Behrends, T., Schijven, J.F. and Hassanizadeh, S.M., 2013. Effect of dissolved calcium on the removal of bacteriophage PRD1 during soil passage: the role of double-layer interactions. J Contam Hydrol, 144(1): 78-87.

Saeb-Parsy, K., 1999. Instant pharmacology. John Wiley & Sons, England, UK.

Santore, M.M. and Kozlova, N., 2007. Micrometer scale adhesion on nanometer-scale patchy surfaces: Adhesion rates, adhesion thresholds, and curvature-based selectivity. Langmuir, 23(9): 4782-4791.

Sasidharan, S., Torkzaban, S., Bradford, S.A., Dillon, P.J. and Cook, P.G., 2014. Coupled effects of hydrodynamic and solution chemistry on long-term nanoparticle transport and deposition in saturated porous media. Colloids and Surfaces A: Physicochemical and Engineering Aspects, 457(0): 169-179.

Sasidharan, S. et al., 2016. Transport and retention of bacteria and viruses in biochar-amended sand. Science of The Total Environment, 548–549: 100-109.

Savage, N. and Diallo, M.S., 2005. Nanomaterials and water purification: opportunities and challenges. Journal of Nanoparticle research, 7(4-5): 331-342.

Schijven, J.F. and Hassanizadeh, S.M., 2000. Removal of viruses by soil passage: Overview of modeling, processes, and parameters. Critical Reviews in Environmental Science and Technology, 30(1): 49-127.

Schijven, J.F., Hassanizadeh, S.M. and De Bruin, R.H.A.M., 2002. Two-site kinetic modeling of bacteriophages transport through columns of saturated dune sand. Journal of Contaminant Hydrology, 57(3-4): 259-279.

Schmid-Hempel, P. and Frank, S.A., 2007. Pathogenesis, Virulence, and Infective Dose. PLoS Pathogens, 3(10): e147.

Schumacher, J.F. et al., 2008. Engineered nanoforce gradients for inhibition of settlement (attachment) of swimming algal spores. Langmuir, 24(9): 4931-4937.

Seth, P., 1994. Mechanism of adenovirus-mediated endosome lysis: role of the intact adenovirus capsid structure. Biochemical and biophysical research communications, 205(2): 1318-1324.

Shang, J., Liu, C. and Wang, Z., 2013. Transport and retention of engineered nanoporous particles in porous media: Effects of concentration and flow dynamics. Colloids and Surfaces A: Physicochemical and Engineering Aspects, 417: 89-98.

Shani, C., Weisbrod, N. and Yakirevich, A., 2008. Colloid transport through saturated sand columns: Influence of physical and chemical surface properties on deposition. Colloids and

Surfaces A: Physicochemical and Engineering Aspects, 316(1-3): 142-150.

Shannon, M.A. et al., 2008. Science and technology for water purification in the coming decades. Nature, 452(7185): 301-310.

Shen, C., Huang, Y., Li, B. and Jin, Y., 2010. Predicting attachment efficiency of colloid deposition under unfavorable attachment conditions. Water Resources Research, 46(11): n/a-n/a.

Shen, C., Li, B., Huang, Y. and Jin, Y., 2007. Kinetics of coupled primary- and secondary-minimum deposition of colloids under unfavorable chemical conditions. Environ Sci Technol, 41(20): 6976-82.

Shen, C. et al., 2012a. Application of DLVO energy map to evaluate interactions between spherical colloids and rough surfaces. Langmuir, 28(41): 14681-92.

Shen, C., Wang, L.-P., Li, B., Huang, Y. and Jin, Y., 2012b. Role of Surface Roughness in Chemical Detachment of Colloids Deposited at Primary Energy Minima. Vadose Zone Journal, 11(1): 0.

Shen, Y., Zhao, P. and Shao, Q., 2014. Porous silica and carbon derived materials from rice husk pyrolysis char. Microporous and Mesoporous Materials, 188(0): 46-76.

Sheng, Z., 2005. An aquifer storage and recovery system with reclaimed wastewater to preserve native groundwater resources in El Paso, Texas. Journal of Environmental Management, 75(4): 367-377.

Sidhu, J. et al., 2015. Pathogen decay during managed aquifer recharge at four sites with different geochemical characteristics and recharge water sources. Journal of Environmental Quality, 44(5): 1402-1412.

Chapter 9

Sidhu, J.P.S. et al., 2010. Pathogen inactivation during passage of stormwater through a constructed reedbed and aquifer transfer, storage and recovery. Water Science and Technology, 62(5): 1190-1197.

Silveira, L.a.U., E. J, 2009. Groundwater II. EOLSS Publications, United Kingdom.

Simmons, C., 2015. As drought looms, scientists call for national water bank. NCGRT, www.groundwater.com.au.

Simpson, D., 2009. UNEP 2008 ANNUAL REPORT, UNEP Division of Communications and Public Information, UNON/Publishing Section Services/Nairobi.

Simunek, J., Van Genuchten, M.T. and Sejna, M., 2005. The HYDRUS-1D software package for simulating the one-dimensional movement of water, heat, and multiple solutes in variably saturated media. The HYDRUS-1D Software Package for Simulating the One-dimensional Movement of Water, Heat, and Multiple Solutes in Variably-saturated Media.

Simunek, J.v.G., M.Th.; Sejna, M 2005. The HYDRUS-1D software package for simulating the one-dimensional movement of water, heat, and multiple solutes in variably-saturated media – version 3.0,, HYDRUS software series 1, Department of Environmental Sciences, University of California Riverside, Riverside, CA, 2005, pp. 270.

Sirikanchana, K., 2007. Kinetics and Mechanisms of Human Adenovirus 2 Inactivation with UV and Chlorine. ProQuest.

Smith, A. et al., 2006. Outbreaks of waterborne infectious intestinal disease in England and Wales, 1992–2003. Epidemiology and infection, 134(06): 1141-1149.

Solaiman, Z.M., Blackwell, P., Abbott, L.K. and Storer, P., 2010. Direct and residual effect of biochar application on mycorrhizal root colonisation, growth and nutrition of wheat. Soil

Research, 48(7): 546-554.

Solovitch, N. et al., 2010. Concurrent aggregation and deposition of TiO2 nanoparticles in a sandy porous media. Environmental Science & Technology, 44(13): 4897-4902.

Song, K., Mohseni, M. and Taghipour, F., 2016. Application of ultraviolet light-emitting diodes (UV-LEDs) for water disinfection: A review. Water Research, 94: 341-349.

Song, L. and Elimelech, M., 1993. Calculation of particle deposition rate under unfavourable particle-surface interactions. Journal of the Chemical Society, Faraday Transactions, 89(18): 3443-3452.

Sontheimer, H., Crittenden, J.C., Summers, R.S. and Hubele, C., 1988. Activated carbon for water treatment.

Spellman, F.R., 2013. Handbook of water and wastewater treatment plant operations. CRC Press.

Spire, B., Montagnier, L., Barré-Sinoussi, F. and Chermann, J.C., 1984. INACTIVATION OF LYMPHADENOPATHY ASSOCIATED VIRUS BY CHEMICAL DISINFECTANTS. The Lancet, 324(8408): 899-901.

Sposito, G., 2008. The chemistry of soils. Oxford university press.

Steven, A.C., Aebi, U. and Showe, M.K., 1976. Folding and capsomere morphology of the P23 surface shell of bacteriophage T4 polyheads from mutants in five different head genes. Journal of Molecular Biology, 102(3): 373-407.

Sugiyama, T., Hebert, R.R. and Hartman, K.A., 1967. Ribonucleoprotein complexes formed between bacteriophage MS2 RNA and MS2 Protein in vitro. Journal of Molecular

Biology, 25(3): 455-463.

Sulcius, S., Staniulis, J. and Paškauskas, R., 2011. Morphology and distribution of phage-like particles in a eutrophic boreal lagoon*. Oceanologia, 53(2): 587-603.

Suresh, L. and Walz, J.Y., 1997. Direct measurement of the effect of surface roughness on the colloidal forces between a particle and flat plate. Journal of Colloid and Interface Science, 196(2): 177-190.

Talbot, J. and Schaaf, P., 1989. Random sequential adsorption of mixtures. Physical Review A, 40(1): 422-427.

Tan, K.H., 2014. Humic matter in soil and the environment: principles and controversies. CRC Press.

Taylor, R., Sloan, D., Cooper, T., Morton, B. and Hunter, I., 2000. A waterborne outbreak of Salmonella Saintpaul. Communicable diseases intelligence, 24(11): 336-339.

Tazehkand, S.S., Torkzaban, S., Bradford, S.A. and Walker, S.L., 2008. Cell preparation methods influence Escherichia coli D21g surface chemistry and transport in saturated sand. J Environ Qual, 37(6): 2108-15.

Thomson, N.R., 2005. Bringing Groundwater Quality Research to the Watershed Scale. IAHS Proceedings & Reports. International Association of Hydrological Sciences, UK, 576 pp.

Tien, C., 2013. Granular Filtration of Aerosols and Hydrosols: Butterworths Series in Chemical Engineering. Butterworth-Heinemann.

Tong, M., Shen, Y., Yang, H. and Kim, H., 2012. Deposition kinetics of MS2

bacteriophages on clay mineral surfaces. Colloids and Surfaces B: Biointerfaces, 92: 340-347.

Torkzaban, S. and Bradford, S.A., 2016. Critical role of surface roughness on colloid retention and release in porous media. Water Research, 88: 274-284.

Torkzaban, S., Bradford, S.A., van Genuchten, M.T. and Walker, S.L., 2008. Colloid transport in unsaturated porous media: the role of water content and ionic strength on particle straining. J Contam Hydrol, 96(1-4): 113-27.

Torkzaban, S. et al., 2015. Colloid Release and Clogging in Porous Media: Effects of Solution Ionic Strength and Flow Velocity. Journal of Contaminant Hydrology(0).

Torkzaban, S., Bradford, S.A. and Walker, S.L., 2007. Resolving the coupled effects of hydrodynamics and DLVO forces on colloid attachment in porous media. Langmuir, 23(19): 9652-9660.

Torkzaban, S., Bradford, S.A., Wan, J., Tokunaga, T. and Masoudih, A., 2013. Release of quantum dot nanoparticles in porous media: Role of cation exchange and aging time. Environmental Science and Technology, 47(20): 11528-11536.

Torkzaban, S., Hassanizadeh, S.M., Schijven, J.F., De Bruin, H.A.M. and De Roda Husman, A.M., 2006. Virus transport in saturated and unsaturated sand columns. Vadose Zone Journal, 5(3): 877-885.

Torkzaban, S., Kim, Y., Mulvihill, M., Wan, J. and Tokunaga, T.K., 2010. Transport and deposition of functionalized CdTe nanoparticles in saturated porous media. J Contam Hydrol, 118(3-4): 208-17.

Torkzaban, S., Wan, J., Tokunaga, T.K. and Bradford, S.A., 2012. Impacts of bridging complexation on the transport of surface-modified nanoparticles in saturated sand. J Contam

Hydrol, 136-137: 86-95.

Toze, S., 2003. Pathogen survival in groundwater during artificial recharge. IAHS-AISH Publication(285): 70-84.

Trakal, L., Šigut, R., Šillerová, H., Faturíková, D. and Komárek, M., 2014. Copper removal from aqueous solution using biochar: Effect of chemical activation. Arabian Journal of Chemistry, 7(1): 43-52.

Treumann, S., Torkzaban, S., Bradford, S.A., Visalakshan, R.M. and Page, D., 2014. An explanation for differences in the process of colloid adsorption in batch and column studies. Journal of Contaminant Hydrology, 164: 219-229.

Truesdail, S.E., Lukasik, J., Farrah, S.R., Shah, D.O. and Dickinson, R.B., 1998. Analysis of bacterial deposition on metal (hydr)oxide-coated sand filter media. Journal of Colloid and Interface Science, 203(2): 369-378.

Tsai, Y.-L., Sobsey, M.D., Sangermano, L. and Palmer, C., 1993. Simple method of concentrating enteroviruses and hepatitis A virus from sewage and ocean water for rapid detection by reverse transcriptase-polymerase chain reaction. Applied and Environmental Microbiology, 59(10): 3488-3491.

Tsuneda, S., Aikawa, H., Hayashi, H., Yuasa, A. and Hirata, A., 2003. Extracellular polymeric substances responsible for bacterial adhesion onto solid surface. FEMS microbiology letters, 223(2): 287-292.

Tufenkji, N. and Elimelech, M., 2004a. Correlation Equation for Predicting Single-Collector Efficiency in Physicochemical Filtration in Saturated Porous Media. Environmental Science and Technology, 38(2): 529-536.

Tufenkji, N. and Elimelech, M., 2004b. Deviation from the classical colloid filtration theory in the presence of repulsive DLVO interactions. Langmuir, 20(25): 10818-10828.

Tufenkji, N. and Elimelech, M., 2005a. Breakdown of colloid filtration theory: Role of the secondary energy minimum and surface charge heterogeneities. Langmuir, 21(3): 841-852.

Tufenkji, N. and Elimelech, M., 2005b. Spatial distributions of Cryptosporidium oocysts in porous media: Evidence for dual mode deposition. Environmental Science & Technology, 39(10): 3620-3629.

Tully, J., Cole, R., Taylor-Robinson, D. and Rose, D., 1981. A NEWLY DISCOVERED MYCOPLASMA IN THE HUMAN UROGENITAL TRACT. The Lancet, 317(8233): 1288-1291.

USGS, 2013. General Interest Publications of the U.S. Geological Survey. U.S. Geological Survey, USGS Office of Ground Water

van de Ven, T.G.M., Warszynski, P., Wu, X. and Dabros, T., 1994. Colloidal particle scattering. A new method to measure surface forces. Langmuir, 10(9): 3046-3056.

van Loenhout, M.T.J., Stefan Kooij, E., Wormeester, H. and Poelsema, B., 2009. Hydrodynamic flow induced anisotropy in colloid adsorption. Colloids and Surfaces A: Physicochemical and Engineering Aspects, 342(1-3): 46-52.

Van Oss, C., 1993. Acid—base interfacial interactions in aqueous media. Colloids and Surfaces A: Physicochemical and Engineering Aspects, 78: 1-49.

Van Oss, C., Chaudhury, M. and Good, R., 1988. Interfacial Lifshitz-van der Waals and polar interactions in macroscopic systems. Chemical Reviews, 88(6): 927-941.

Vanderzalm, J.L., Page, D.W., Barry, K.E. and Dillon, P.J., 2010. A comparison of the geochemical response to different managed aquifer recharge operations for injection of urban stormwater in a carbonate aquifer. Applied Geochemistry, 25(9): 1350-1360.

Veerapaneni, S.V., Long, B., Freeman, S. and Bond, R., 2007. Reducing energy consumption for seawater desalination. American Water Works Association. Journal, 99(6): 95.

Verwey, E.J.W., 1947. Theory of the stability of lyophobic colloids. Journal of Physical and Colloid Chemistry, 51(3): 631-636.

Verwey, E.J.W. and Overbeek, J.T.G., 1955. Theory of the stability of lyophobic colloids. Journal of Colloid Science, 10(2): 224-225.

Virkutyte, J., Al-Abed, S.R., Choi, H. and Bennett-Stamper, C., 2014. Distinct structural behavior and transport of TiO2 nano- and nanostructured particles in sand. Colloids and Surfaces A: Physicochemical and Engineering Aspects, 443: 188-194.

Wang, C. et al., 2012. Retention and transport of silica nanoparticles in saturated porous media: effect of concentration and particle size. Environ Sci Technol, 46(13): 7151-8.

Wang, D., Zhang, W., Hao, X. and Zhou, D., 2013a. Transport of biochar particles in saturated granular media: Effects of pyrolysis temperature and particle size. Environmental Science and Technology, 47(2): 821-828.

Wang, D., Zhang, W. and Zhou, D., 2013b. Antagonistic effects of humic acid and iron oxyhydroxide grain-coating on biochar nanoparticle transport in saturated sand. Environmental Science and Technology, 47(10): 5154-5161.

Wang, N., Dykhuizen, D.E. and Slobodkin, L.B., 1996. The evolution of phage lysis timing.

Evolutionary Ecology, 10(5): 545-558.

Wang, Y. et al., 2008. Transport and retention of nanoscale C60 aggregates in water-saturated porous media. Environmental Science & Technology, 42(10): 3588-3594.

Ward, J. and Dillon, P., 2009. Robust design of managed aquifer recharge policy in Australia. Water for a healthy Country Flagship Report to National Water Commission.

Ward, R.L. et al., 1986. Human rotavirus studies in volunteers: determination of infectious dose and serological response to infection. Journal of Infectious Diseases, 154(5): 871-880.

Whitehead, K.A., Colligon, J. and Verran, J., 2005. Retention of microbial cells in substratum surface features of micrometer and sub-micrometer dimensions. Colloids and Surfaces B: Biointerfaces, 41(2): 129-138.

Whitehead, K.A. and Verran, J., 2006. The Effect of Surface Topography on the Retention of Microorganisms. Food and Bioproducts Processing, 84(4): 253-259.

WHO, 2003. Guidelines for safe recreational water environments: Volume 1, coastal and fresh waters. World Health Organization, Geneva, pp. 253.

WHO, 2008. Guidelines for drinking-water quality - Volume 1: Recommendations Third edition, incorporating first and second addenda. World Health Organization, Geneva, pp. 668.

WHO, 2011. WHO World Water Day Report. World Health Organization.

Wiencek, K.M. and Fletcher, M., 1995. Bacterial adhesion to hydroxyl- and methyl-terminated alkanethiol self- assembled monolayers. Journal of Bacteriology, 177(8): 1959-1966.

Wiesner, M.R., Lowry, G.V., Alvarez, P., Dionysiou, D. and Biswas, P., 2006. Assessing

the risks of manufactured nanomaterials. Environmental science & technology, 40(14): 4336-4345.

Williams, M., Martin, S. and Kookana, R., 2015. Sorption and plant uptake of pharmaceuticals from an artificially contaminated soil amended with biochars. Plant and Soil: 1-12.

Wimmer, E., Mueller, S., Tumpey, T.M. and Taubenberger, J.K., 2009. Synthetic viruses: a new opportunity to understand and prevent viral disease. Nature biotechnology, 27(12): 1163-1172.

Wintgens, T., Salehi, F., Hochstrat, R. and Melin, T., 2008. Emerging contaminants and treatment options in water recycling for indirect potable use. Water Science and Technology, 57(1): 99-108.

Wise, K., 2006. Preparing Spread Plates Protocols. American Society for Microbiology USA.

Wolbarsht, M.L., 1971. Laser applications in medicine and biology, 2. Springer.

Wommack, K.E., Hill, R.T., Muller, T.A. and Colwell, R.R., 1996. Effects of sunlight on bacteriophage viability and structure. Applied and Environmental Microbiology, 62(4): 1336-41.

Wong, K., Bouchard, D. and Molina, M., 2014. Relative transport of human adenovirus and MS2 in porous media. Colloids and Surfaces B: Biointerfaces.

Wong, K., Voice, T.C. and Xagoraraki, I., 2013. Effect of organic carbon on sorption of human adenovirus to soil particles and laboratory containers. Water Research, 47(10): 3339-3346.

Xu, L.C. and Logan, B.E., 2006. Adhesion forces between functionalized latex microspheres and protein-coated surfaces evaluated using colloid probe atomic force microscopy. Colloids Surf B Biointerfaces, 48(1): 84-94.

Xu, L.C., Vadillo-Rodriguez, V. and Logan, B.E., 2005. Residence time, loading force, pH, and ionic strength affect adhesion forces between colloids and biopolymer-coated surfaces. Langmuir, 21(16): 7491-7500.

Xu, P. et al., 2012. Use of iron oxide nanomaterials in wastewater treatment: a review. Science of the Total Environment, 424: 1-10.

Yan, Z., Huang, X. and Yang, C., 2015. Deposition of colloidal particles in a microchannel at elevated temperatures. Microfluidics and Nanofluidics, 18(3): 403-414.

Yao, K.-M., Habibian, M.T. and O'Melia, C.R., 1971. Water and waste water filtration. Concepts and applications. Environmental Science & Technology, 5(11): 1105-1112.

Yaron, S. and Matthews, K., 2002. A reverse transcriptase-polymerase chain reaction assay for detection of viable Escherichia coli O157: H7: investigation of specific target genes. Journal of applied microbiology, 92(4): 633-640.

Yates, M.V., Gerba, C.P. and Kelley, L.M., 1985. Virus persistence in groundwater. Applied and Environmental Microbiology, 49(4): 778-781.

Yavari, S., Malakahmad, A. and Sapari, N.B., 2014. The Effects of Feedstock Sources and Pyrolytic Temperature on Biochars Sorptive Characteristics, Applied Mechanics and Materials. Trans Tech Publ, pp. 150-154.

Yim, E.K.F., Darling, E.M., Kulangara, K., Guilak, F. and Leong, K.W., 2010. Nanotopography-induced changes in focal adhesions, cytoskeletal organization, and

mechanical properties of human mesenchymal stem cells. Biomaterials, 31(6): 1299-1306.

Yoon, R.-H., Flinn, D.H. and Rabinovich, Y.I., 1997. Hydrophobic interactions between dissimilar surfaces. Journal of colloid and interface science, 185(2): 363-370.

You, Y., Han, J., Chiu, P.C. and Jin, Y., 2005. Removal and inactivation of waterborne viruses using zerovalent iron. Environmental science & technology, 39(23): 9263-9269.

Yu, J.-G. et al., 2015. Graphene nanosheets as novel adsorbents in adsorption, preconcentration and removal of gases, organic compounds and metal ions. Science of The Total Environment, 502: 70-79.

Yuan, H. and Shapiro, A.A., 2011. A mathematical model for non-monotonic deposition profiles in deep bed filtration systems. Chemical Engineering Journal, 166(1): 105-115.

Zeng, D., Wu, J. and Kennedy, J.F., 2008. Application of a chitosan flocculant to water treatment. Carbohydrate polymers, 71(1): 135-139.

Zeng, Z. et al., 2013. Sorption of ammonium and phosphate from aqueous solution by biochar derived from phytoremediation plants. Journal of Zhejiang University SCIENCE B, 14(12): 1152-1161.

Zhang, L., Seagren, E.A., Davis, A.P. and Karns, J.S., 2012. Effects of temperature on bacterial transport and destruction in bioretention media: Field and laboratory evaluations. Water Environment Research, 84(6): 485-496.

Zhang, W. et al., 2010. Transport and retention of biochar particles in porous media: effect of pH, ionic strength, and particle size. Ecohydrology, 3(4): 497-508.

Zhang, Z., Solaiman, Z., Meney, K., Murphy, D. and Rengel, Z., 2013. Biochars

immobilize soil cadmium, but do not improve growth of emergent wetland species Juncus subsecundus in cadmium-contaminated soil. Journal of Soils and Sediments, 13(1): 140-151.

Zhou, Y. and Tol, R.S., 2005. Evaluating the costs of desalination and water transport. Water resources research, 41(3).

Zhuang, J. and Jin, Y., 2008. Interactions between viruses and goethite during saturated flow: effects of solution pH, carbonate, and phosphate. J Contam Hydrol, 98(1-2): 15-21.